Quasi-Static and Fatigue Evaluation of Pultruded Vinyl Ester/E-Glass Composites

by

Stephan P. Phifer

Thesis submitted to the Faculty of the

Virginia Polytechnic Institute and State University

In partial fulfillment of the requirements for the degree of

MASTERS OF SCIENCE

in

Engineering Science and Mechanics

APPROVED:

_____

J. Jack Lesko Chairman

_____

Rakesh Kapania

_____

David Y. Gao

December, 1998
Blacksburg, Virginia

Key Words: Pultrusion, Composite, Residual Strength, Fatigue

QUASI-STATIC AND FATIGUE EVALUATION OF PULTRUDED VINYL ESTER/E-GLASS COMPOSITES

Stephan P. Phifer

(ABSTRACT)

The quasi-static strength, stiffness, and fatigue properties of cross-ply, angle-ply, and quasi-isotropic vinyl ester/E-glass non-woven tricot stitched fabric composite laminates fabricated from the Continuous Resin Transfer Molding (CRTM) pultrusion process were the focus of this research. The tricot stitch and the 6% vinyl ester matrix cure shrinkage were found to play key roles in the quasi-static and fatigue strength and stiffness properties of these laminates. Laminates tested transverse to the pultrusion axis had greater fiber undulation and maximum of 44% quasi-static strength reduction and 8% stiffness reduction compared with axially tested specimens. While the matrix failure strain was 1.9%, failure strain of these laminates range over 1.91 to 2.08% when tested along the pultrusion axis and as low as 1.29% transverse to the pultrusion axis. Fatigue evaluation, in load control mode, evaluated laminate S-N, stiffness reduction, and residual strength. Measured S-N curves and residual strength curves compared with literature were found most like woven fabric laminates, well below aerospace grade laminates. Residual strength and life analysis using Reifsnider's methodology [43], revealed that the choice of quasi-static strength and stiffness, S-N curve, laminate stiffness reduction, and residual strength shape parameter, J, strongly affect predicted life. Predictions at high fatigue stress/low cycle were more exact than at low stress; the S-N curve was steep initially but at low stress/high cycle was nearly horizontal. The best predictions utilized separate off-axis stiffness reductions of E_2 obtained from cross-ply and G_{12} from angle-ply laminates, the quasi-static strength and stiffness of the laminate predicted, and the average S-N and residual strength curves.

Dedication

Thanks to the wealth of ingenious minds that have brought engineering science and mechanics to its present state.

Thanks to my wife, Chaemchoi, and children, Samuel and Kristina, for their forgiveness, understanding, and constant love while the toils of academia kept me from my important duties at home.

Acknowledgements

The authors would like to recognize Hexcel's support of this work through the NIST ATP program, contract number 70NANB5H1167 and the Federal Highway Administration, Office of Technology Application, through the Virginia Transportation Research Council.

Table of Contents:

Table of Figures

Chapter 1: Introduction

Development of high strength continuous fiber reinforced polymer (CFRP) composites were first introduced into low quantity production for military applications in the 1950's. The unique high strength and stiffness to weight, the fatigue and corrosion resistance and enhanced vibration damping characteristics when compared to metallic designs were the main reasons for use of fiber reinforced polymer composites in these applications. For example, a carbon fiber epoxy helicopter fin for the Bell 206L helicopter replaced metal fins which resulted in an increase in strength and stiffness to weight and higher corrosion resistance. The metal fin required repair of pitting due to the corrosive coastal environment every 18 months and replacement after 6 years of service. The carbon fiber epoxy fins required no repairs for corrosion and still remain in service in excess of 12 years without replacement [01].

These early aerospace composites for military applications were fabricated by hand lay-up technique using expensive fiber reinforced polymer preimpregnated unidirectional tape or woven fabric and were cured slowly in a pressurized and heated autoclave. This process required extensive labor in the hand lay-up process, which included a sequence of lay-up of several layers of preimpregnated tape or fabric followed by a debulk and degas of the laminate in a vacuum bag. This debulk/degas process occurred several times during the lay-up of the preimpregnated layers. It involved an application of release and breather fabric over the laminate surface with a vacuum bag of nylon or silicone used to seal the laminate. Vacuum was then applied to the sealed bag to remove gas between layers and to compact the laminate. The resulting cycle times were long and the materials were expensive; thus the initial expense for composite laminate components were higher than the metal counterparts. For military and aerospace applications, product cost was not so important since the production quantities were low and the design, development, and testing were a much higher percentage of the overall cost than the production fabrication cost. The benefits of higher strength and stiffness to weight, longer life due to higher corrosion and fatigue resistance and enhanced damping characteristics outweighed the increase in the initial expense of the composite components.

Recently, high strength continuous fiber reinforced polymer (CFRP) composites have begun to find applications in the commercial building, construction, and infrastructure markets. Competition in these commercial markets would not tolerate the greater expense of the tradition aerospace grade hand lay-up preimpregnated fiber autoclave cured composites. For these industries, composites products must compete with inexpensive plywood, solid pine studs, metal rebar, hot and cold rolled steel and extruded aluminum beams, rods, plates, sheets, and bars. The high strength and stiffness to weight, the electrical, fatigue, and corrosion resistance and the enhanced vibration damping characteristics are desired characteristics, which improve performance and increase the useful life of these commercial products. Product cost for the commercial markets is equally important, since the commercial products have a much higher volume production and are under greater competition than aerospace products. Thus, inexpensive materials and processes are required for the commercial continuous fiber reinforced polymer composite products.

The least expensive high production process for fabrication of constant cross-section CFRP composite laminated products is pultrusion. Pultrusion produces a constant cross-section shape similar to thermoplastic and aluminum extrusion, except that continuous fiber is pulled through a resin dip-bath into a heated die with the desired cross-sectional shape as shown in Figure 1. In the original pultrusion process, dry continuous unidirectional fiber bundles were

pultruded. Currently, unidirectional, woven, and stitched fabric forming cross-ply and quasi-isotropic laminates are fabricated by the pultrusion process. Another variation of the dip-bath pultrusion process is the continuous resin transfer molding (CRTM) pultrusion process where resin is injected into the dry fiber preform as its pulled through the die as shown in Figure 2.

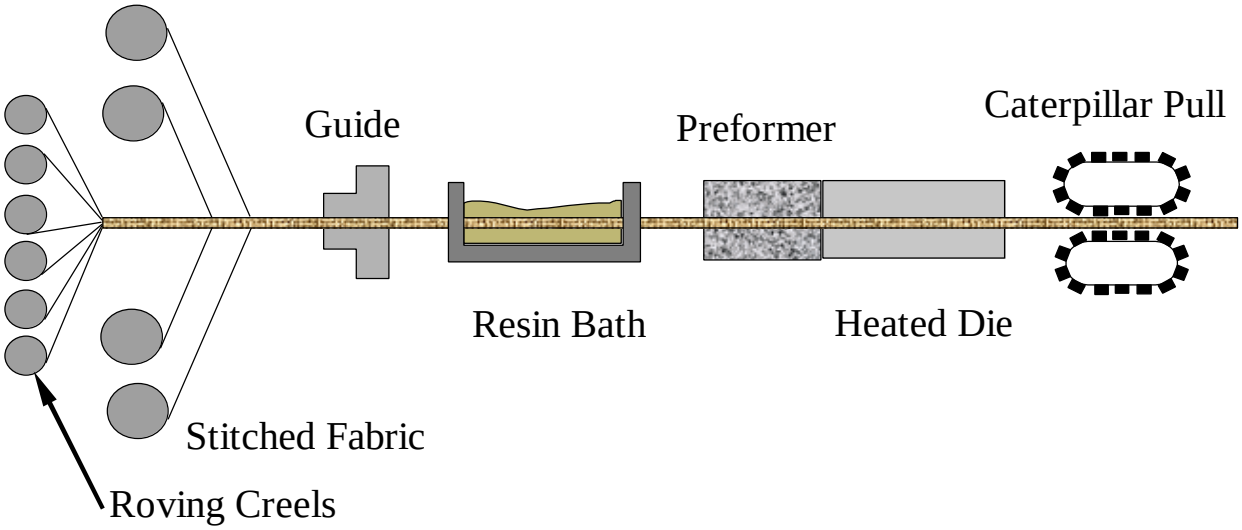

Figure 1: Resin Bath Pultrusion Process

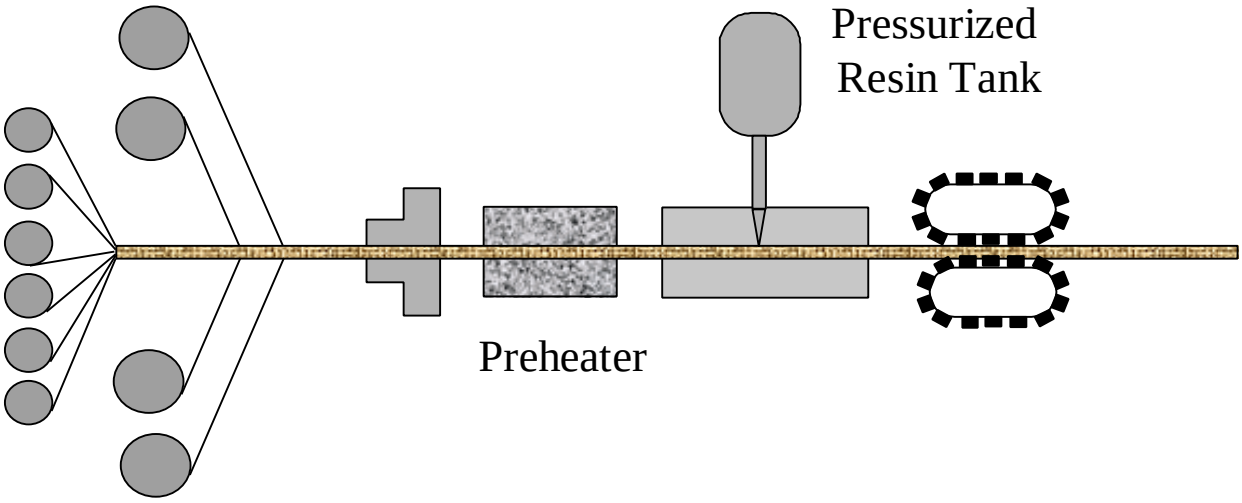

Figure 2: Continuous Resin Transfer Molding Pultrusion Process

Pultruded continuous fiber reinforced polymer (CFRP) composite products, which have been successful in the commercial markets, vary widely in purpose. Pultruded composites have found applications in the electrical equipment, transportation, construction and infrastructure industries. High strength and stiffness to weight, fatigue and corrosion resistance are key features to their success. For the electrical equipment market, fuse holders, ladders, tool handles, electrical conduits, cable trays, and power rail covers for a subway train utilized the high strength to weight ratio and the electrical insulative properties of pultruded composites as primary properties for their success. The transportation industry utilizes pultruded composite products in form of truck drive shafts, leaf springs, bumpers, frames, and cross members, transportation

container bodies, and interior structure for trains and subways [01]. The construction industry requires strength, stiffness, and corrosion and fatigue resistance for products such as gratings, stairs, guard rails, platforms, light poles and pedestrian and vehicular bridges [02] [01].

Seeking the least expensive product for commercial applications, the lowest cost fiber and matrix are utilized for pultruded products. E-glass fiber is most used in pultrusion and is the least expensive fiber but has lower strength and stiffness to weight in quasi-static and fatigue conditions than the more expensive carbon fiber. The resin most often used is polyester, which has the lowest cost at $0.50 per pound, is the most brittle in the fully cured form, has rapid cure rates, has high shrinkage to allow lower pull forces and mold abrasion, and has taylorable viscosity for flexibility in processing. Vinyl ester is the next most popular pultrusion resin very similar to polyester in chemistry and processing, which has slightly higher ductility and toughness, has higher cost of $1.50 per pound, and slightly slower cure rates. Epoxy resin are used least among these resins for pultrusion due to the higher material costs of $3 to $100 per pound, slower cure rates, and more difficult processing due to lower volumetric shrinkage. Epoxy offers the best long long-term electrical properties, highest strengths at room and elevated temperatures and best hot/wet performance. [02] With these cost-conscious material and process selections for commercial products, quasi-static and fatigue performance is sacrificed to reduce cost of these pultruded CFRP composite laminates when compared with the military and aerospace grade composites.

The quasi-static and fatigue response of composite laminates is dependent upon many factors including constituent material properties and processing related factors. Materials properties such as the fiber strength and stiffness, matrix ductility, matrix chemical shrinkage, and fiber/matrix interfacial bond strength will affect the quasi-static and fatigue response. Processing related effects such as thermally induced stress, fiber undulation, void, matrix cracking, and delamination also affect quasi-static and fatigue response of these CFRP composite laminates. Aerospace grade laminated composites using the best materials and least damaging of processes have very little of these process induced defects. On the other hand, commercial grade composites seeking the least expensive alternatives are forced to accept lower quality along with the lower cost. Pultrusion is the lowest cost continuous fiber laminating process partially because it is a rapid process utilizing inexpensive rapid reacting resins cured at elevated temperatures. These resins are most often polyester and vinyl ester which have high thermal and chemical shrinkage and have low ductility when formulated for the rapid elevated cure required for pultrusion. High residual stresses, resulting from this shrinkage, are often relieved by formation of microcracking and delamination in the as processed condition. This low ductility of the brittle resin also can reduce the ultimate strain in the laminate.

Fiber undulation, another result of the pultrusion process can reduce quasi-static and fatigue performance and when linked with a brittle resin can be even more degrading. Pultrusion requires preprocessing of the fiber to attach the off-axis plies to the plies aligned with the pultrusion axis. Only fibers aligned to the pultrusion axis can be pulled through the pultrusion die; all other off-axis fiber must be attached to the axial fiber to be carried through the pultrusion die. Stitching the most common method of attachment can create gaps between axial fiber bundles. When stacked in multiple layers and laminated, fiber undulation can result. With cost again in mind, the use of larger fiber bundles in the stitching process is an economical method to reduce processing time; although, greater fiber undulation can result from use of larger fiber bundle size. The combination of brittle matrix and fiber undulation can drastically reduce quasi-static and fatigue performance of pultruded laminates when compared with aerospace grade

laminates. When comparing cost, quasi-static and fatigue performance, what is the optimum design of resin ductility and allowable fiber undulation for the pultrusion process?

Rational for this Research

Most all quasi-static and fatigue evaluations found in literature have concentrated on military and aerospace grade CFRP composite laminates. No comprehensive quasi-static and fatigue evaluation has been found in literature for non-woven stitched cross-ply and quasi-isotropic pultruded CFRP laminates. Military and aerospace grade CFRP composite laminates in unidirectional, cross-ply, and quasi-isotropic forms have been evaluated in quasi-static, static, and cyclic fatigue modes [03]. In general, high quality aerospace grade composites have low void content, thin uniform plies, low residual stresses, and very little fiber undulation created from fabrications process such as filament winding or autoclaved curing of hand lay-up resin preimpregnated fabric or tape. The pultruded products can have much lower quasi-static and fatigue properties than the aerospace grade CFRP composite laminates. Pultruded CFRP composite laminates, in general, use a brittle type matrix with high residual stresses created due to a combination of the rapid high temperature cure process and the high thermal and chemical shrinkage of polyester or vinyl ester. These residual stresses are often relieved by formation of microcracking and delamination in the as-processed state. Fiber deformation or undulation is created by the stitch or weave geometry and is common in pultruded CFRP composite laminates.

Do these pultruded composites differ from their aerospace grade counterparts in quasi-static and fatigue performance? What are the effects of the pultrusion process, the matrix properties and the fiber architecture on the quasi-static and fatigue properties? Similar questions as these were posed at a recent Composite Durability Workshop sponsored by the Civil Engineering Research Foundation (CERF) in September of 1998. From this workshop a list of technical issues preventing the implementation of continuous fiber reinforced polymer composites into the building, construction, and infrastructure industries were formulated. These technical issues were the unknowns associated with the durability, fatigue, and creep resistance of glass fiber composites, and the environmental degradation of these composites in alkaline and wet environments. Understanding the cyclic and creep fatigue durability and environmental degradation of pultruded composite laminates is critical to the implementation of composites in the building, construction, and infrastructure industries. For these reasons, the quasi-static and fatigue evaluation of pultruded vinyl ester/ E-glass non-woven stitched composite laminates will be the topic of this research.

Goals of this Thesis

This thesis will investigate the quasi-static and fatigue performance of vinyl ester/E-glass non-woven stitched fabric composite laminates fabricated from the Continuous Resin Transfer Molding (CRTM) pultrusion process. The goal of the quasi-static research was to obtain the quasi-static strength and stiffness properties of unidirectional, cross-ply, angle-ply, and quasi-isotropic laminates and to extract the quasi-static ply level properties from the measured laminate properties. A secondary purpose was to characterize the effects of the non-woven stitched fabric, the vinyl ester matrix, and the pultrusion process on these stiffness and strength properties. The goal of the fatigue research was to obtain and analyze the fatigue response of these pultruded laminates by measurement of laminate residual strength, Fr-n, laminate stiffness reduction,

$E_{Lam}(n)$, and laminate applied fatigue stress to failure cycles, S_{Lam}-N. Correlation and predictions were performed using a residual strength and life methodology to determine the optimum technique for prediction of residual strength and life using Reifsnider's methodology [04].

Organization of this Thesis

This thesis is written in the form of two papers separated into the quasi-static and the fatigue performance of pultruded CFRP composite laminates. The first paper includes a literature review of methods to calculation strength and stiffness for continuous fiber reinforced polymer (CFRP) composite laminates. It also includes the measured quasi-static properties of pultruded CFRP vinyl ester/ E-glass non-woven stitched fabric composite laminates, the proposed methods to extract the ply level strength and stiffness from the measure laminate data, and the ply level strength and stiffness extracted. The second paper includes a literature review of fatigue performance of CFRP E-glass composite laminates, measured fatigue performance, predictions of the pultruded vinyl ester/ E-glass non-woven stitched fabric CFRP composite laminates from this research, and comparisons with literature.

Chapter 2: Pultruded Composites Overview

Process, Materials, and Advantages of Pultruded Composites

Pultrusion, related to extrusion of metals or non-reinforced plastics, involves the pulling of a combination of axial fiber roving, continuous strand mat, non-crimped non-woven stitched fabric, and/or woven fabric through a resin bath into a heated die. The composite cures as it is continuously pulled through the die. The advantages of the pultrusion process are continuous production, low labor costs, low materials scrap rate, and elimination of process support materials such as bagging and breather materials for pressure bag molding.

Continuous resin transfer molding (CRTM) pultrusion injects resin into the die rather than pulling reinforcement through a resin bath. This reduces the fiber distortion caused by fiber lubricity and hydraulic pressures at die entrance which squeezes excess resin from the composite, but prevents addition of fillers, since the compressed fiber reinforcement acts as a highly dense filter which hinders resin penetration. [05]

The constituents for pultruded composites are predominately fiberglass/polyester both being the lowest cost of their fiber and matrix classes. Low viscosity to penetrate and wet the fibers and rapid cure are the two major processing advantages for polyester. Vinyl ester similar to polyester in chemistry and processing is the next highest volume in use. Higher raw material costs and slower cure behavior is contrasted by higher toughness, corrosion resistance, and heat distortion properties. Epoxy resins are used least among these resins for pultrusion due the higher material costs, slower cure rates, and more difficult processing due to lower volumetric shrinkage. Epoxies offer the best long-term electrical properties, highest strengths at room and elevated temperatures, and best hot/wet performance. [05]

Applications and Properties of Pultruded Composites

Pultrusion, being the lowest cost, moderate to high production process available for continuous fiber composites, has found applications in the sporting, electrical equipment, transportation, construction and infrastructure industries. In the sporting industry, pultruded produces such as fishing rods, archery bows and arrows, hockey sticks, playground equipment,

fence posts, and baseball bats have gained a strong share of the market. The high strength and stiffness to density, and fatigue resistance are key characteristics to there success. For the electrical equipment market, fuse holders, ladders, tool handles, electrical conduits, cable trays, and power rail covers for a subway train utilized strength and electrical insulation of pultruded composites as primary properties for their success. The transportation industry utilizes pultruded composite products in form of truck drive shafts, leaf springs, bumpers, frames, and cross members, transportation container bodies, interior structure for trains and subways. [01] The construction industry requires strength, stiffness, and corrosion resistance for products such as gratings, stairs, guard rails, platforms, light poles and pedestrian and automotive bridges. [01]

Other properties making pultruded composite desirable are thermal conductivity or resistivity, acoustic, and mechanical damping, radar transparency, and moldability into complex geometries allowing subcomponent consolidation and reduction of assembly costs.

Chapter 3: Literature Review of E-Glass Composite Quasi-Static Material Properties:

A composite stiffness and strength literature review will present common methods to predict stiffness and strength of unidirectional, cross-ply and quasi-isotropic composites laminates. It will be shown through comparison of these methods with the measured quasi-static properties of the pultruded vinyl ester/E-glass non-woven composite laminates, that these predicted values in all cases are non-conservative and will greatly effect the fatigue predictions if used. Therefore, the ply level stiffness and strength properties will be extracted from the measured laminate properties by assuming elastic-fully-plastic response of transverse properties and shear response from the measured ±45° laminate testing.

Stiffness Literature Review

Lamina/Laminate Ultimate Axial Stiffness

Unidirectional composite stiffness can usually be modeled accurately with rule-of – mixture (ROM) mechanics approach. [06]

Equation 1

$$E_1 = V_f * E_f + (1 - V_f) * E_m$$

This is the upper limit of lamina stiffness from which fiber undulation, voids, delamination, etc. can cause a reduction in stiffness. To approximate the stiffness of the 0° lamina, E_1, near ultimate failure in cross-ply laminates, $E_C/a_{0°}$ may be used, where $a_{0°}$ is the percentage of fibers in the 0° direction and E_C is the composite stiffness at failure. This assumes that the transverse plies offer negligible stiffness, which is not in great error for cross-ply laminates at ultimate failure, but is in error when considering quasi-isotropic laminates. In most cases, quasi-isotropic laminates near ultimate failure offer higher stiffness than that can be obtained by the 0° laminae alone. The angle-ply laminae offer substantial stiffness at failure strains [07].

Lamina Transverse & Shear Stiffness

Transverse and shear stiffness have been shown to be poorly modeled by simple mechanics-of-materials approach in the inverse rule-of-mixtures where $C_i = E_2$ and G_{12}.

Equation 2

$$\frac{1}{C_i} = \frac{V_f}{C_{if}} + \frac{(1-V_f)}{C_{im}}$$

"Simplified Micromechanics Equations" (SME) by Chamis, are an improved mechanics of materials model which compare well with 3D finite element models for $C_i = E_2$ and G_{12} [08] [09]

Equation 3

$$C_i = C_{im} \cdot \left[\left(1-\sqrt{V_f}\right) + \frac{\sqrt{V_f}}{1-\sqrt{V_f} \cdot \left(1-C_{im}/C_{if}\right)} \right]$$

A modification from SME above is based upon division of unit cell differently as shown below which separates the representative volume element into a rule-of-mixture type arrangement rather than the inverse rule-of-mixture that Chamis and Gibson show [10].

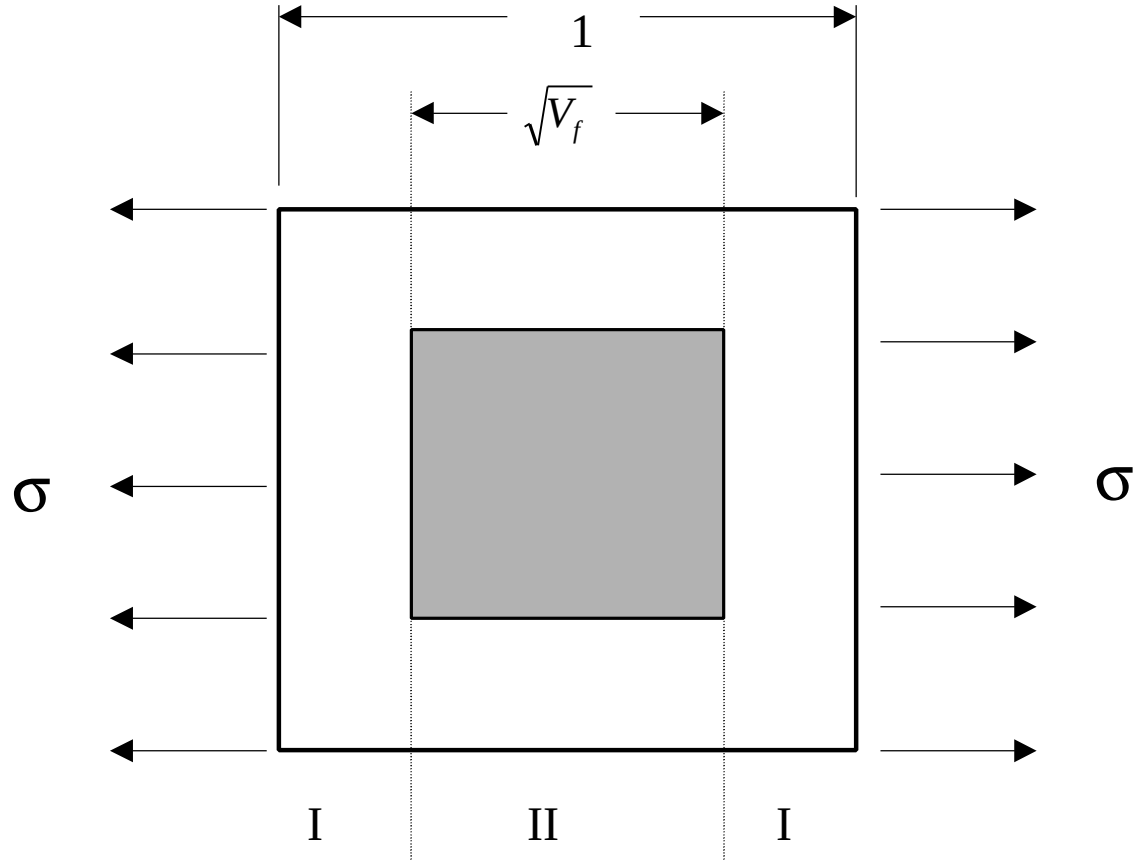

Figure 3: Mechanics-of-Materials Approach to Transverse Stiffness

This results in transverse and shear ply level modulus, designated SME-2, as shown below.

Equation 4

$$C_i = \frac{E_{if} \cdot \sqrt{V_f} + \left(1 - \sqrt{V_f}\right) \cdot E_{im}}{1 - \sqrt{V_f} + V_f + \left(\sqrt{V_f} - V_f\right) \cdot \frac{E_{if}}{E_{im}}}$$

Semi-empirical models for transverse and shear such as Halpin-Tsai are more widely accepted. For C_i=E_2 and G_{12}, this has been found to fit unidirectional data well with ξ = 1 and 2 respectively.

Equation 5

$$\frac{C_i}{C_{im}} = \frac{1 + x \cdot h \cdot V_f}{1 - h \cdot V_f}$$

$$h = \frac{(C_{if} / C_{im}) - 1}{(C_{if} / C_{im}) + x}$$

Strength and Failure Modes Literature Review:

Polymer

Stress strain curves for polymers are generally nonlinear and are dependent upon the type of test. For a brittle polymer, tension is dependent upon processing flaws, submicroscopic cracks, and added fillers, which may have low adhesion strength to the polymer. Flexible polymers are less affected by these influences in tension. Compression reflects more the pure polymer, since cracks close under compression. Under uniaxial tension, the tensile strength should be twice the shear, but it is usually less than two exhibiting the flaw reduction mechanism. Polymers act in a more brittle manner, in a biaxial or triaxial stress state when compared to a uniaxial stress state. Under hydrostatic pressure, the brittle polymer generally decreases in strength and failure strain while the ductile polymer increases in strength and failure strain [11].

Unidirectional Axial Strength

A simplistic view of uniaxial strength can suffice for most engineering purposes. Two cases need to be considered.

When the matrix has a higher failure strain than the fiber ($\varepsilon_{mu} > \varepsilon_{fu}$), the fibers will fail shifting the total load onto the matrix; which, unable to withstand the load increase, the matrix and laminate fails immediately. The rule-of-mixture (ROM) approach is used [12].

Equation 6

$$X_{TC} = V_f \cdot X_{Tf} + (1 - V_f) \cdot s_{m@Tf}$$

$\sigma_{m@Tf}$ is the matrix stress at fiber failure.

When the matrix has a low failure strain than the fiber ($\varepsilon_{mu} < \varepsilon_{fu}$), the composite stress below the matrix failure is the simple rule-of-mixtures [13].

Equation 7

$$s_1 = V_f \cdot s_f + (1 - V_f) \cdot s_m$$

Above the matrix failure strain, the matrix begins to microcrack. As load increases in quasi-static manner, microcracking continues, the load shifts to the fibers. If the matrix fails completely to carry load, the strength will be

Equation 8

$$X_{TC} = V_f \cdot X_{Tf} \ .$$

Dry Fiber & Impregnated Fiber Bundle Axial Strength

Ultimate fiber Strength, X_{Tf}, in the above rule-of-mixture strength approach is an in-situ fiber strength based upon the composite strength, a synergistic effect between fiber and matrix, not the dry fiber bundle strength. Manders and Chou have shown that epoxy impregnated fiber bundles are 2.7 and 2.4 times greater strength than dry fiber bundles for carbon and glass of the same length and bundle size [13].

The individual fibers follow Weibull statistics, a theory of weakest link based upon the brittle nature of the fiber, which have a distribution of flaws along its length. The longer the length or larger the volume, the more likely that a flaw of such size exists that failure will occur at a lower stress. If it is a single fiber, one failure along the length renders the fiber unable to carry load. If this weaker fiber is a member of a bundle, the remaining non-fractured fibers accept the increase in load until each in turn exceeds its strength and ultimate failure results.

For impregnated fiber bundles, if the failure strain of the fiber is lower than that of the matrix, the fiber failure results in load redistribution through shear through the matrix to adjacent non-fractured fibers. Moving away from the break along the fiber axis, the stress is shifted back from adjacent fibers to the broken fiber eventually back to full stress. The ineffective length is measured from the fiber break to the point where full stress level is re-attained. Through a shear lag analysis, this ineffective length may be estimated. Shear lag analysis is a mechanics of materials approach to stress analysis of a broken fiber in continuous matrix, broken matrix surrounding a continuous fiber, transverse microcracking in cross-ply laminates, and even stress distribution in an adhesive joint. Shear lag analysis assumes the fibers are infinitely stiff in shear carrying only axial tensile stress; the matrix is assumed to have negligible axial stiffness transmitting load only through shear. Radial stress, σ_{rr}, is considered constant, and angular stress, $\sigma_{\theta\theta}$, is not considered in this one dimensional analysis [07]. Fiber fracture can occur in numerous locations along the length and width of the specimen wherever a fiber flaw exists. As the load is increased, the fibers fracture to smaller and smaller lengths, the load is continually shifted through shear of the matrix to adjacent fibers. This has been modeled as a shift either equally to all unbroken adjacent fibers or in some distributed manner to only adjacent unbroken fiber segments. Only when the adjacent fibers cannot accept the load transfer will there be a catastrophic failure [07].

In another case, Chou [07] page 135, discussed the case when the failure strain of the fiber is greater than the matrix, matrix cracks first appear and load is shifted to the fibers as bridging develops in the case of ceramics. Aveston, Kelly, and others developed energy methods for the development of multiple matrix cracking in a unidirectional lamina subject to axial tensile loading.

Weibull statistics based upon weakest link predicts well single fiber strength of length L_0 to longer length L or to a bundle of dry fibers, and for different lengths of impregnated bundles

with use of shear lag. High numbers of tests at many fiber gage lengths are needed to obtain the Weibull modulus and stress, m and σ_o.

Swanson [14] has discussed two cases for the use of Weibull statistics prediction of the effect of size on tensile strength. Zweben [15] discussed size effect on large composite structures, noting with a 5% coefficient of variation (COV) and an approximate modulus of 1.2/COV that a 25-40% reduction in strength was predicted. Experimental references confirmed this reduction. On the other hand, Cohern [16] has reported a modest 3% reduction in strength of a filament wound rocket motor structure that was 10^7 greater volume than the tow size test specimen. Therefore tensile strength prediction using Weibull statistics from specimen to product size may prove unrealistic.

Unidirectional Axial Lamina Strength: Matrix and Interface Effects

The rule-of-mixtures view of uniaxial strength, Equation 7, ignores or masks various failure mechanisms, caused by processing imperfections, by using in-situ values for fiber and matrix strength. Fiber strength in a laminate is a function of statistical fiber bundle strength distribution, nonlinear matrix stress strain, fiber/sizing/matrix interface properties, and residual strains due to cure and shrinkage. Other factors deviating from ideal are void content, fiber waviness or undulation, interfacial debond, and microcracking. If fiber failure strain is lower than matrix failure strain, failure can initiate as fiber breakage leading to either transverse matrix failure or debonding along the matrix/fiber interface. The weaker of the matrix failure strain and the interfacial bond strength will determine whether matrix cracking or debonding occurs. In either case, load is shifted to adjacent fibers, which statistically are probably stronger than the broken fiber. Alternately, if the fiber has higher failure strain than does the matrix, matrix cracking occurs which either penetrates the fiber causing fiber failure or debonding along matrix/fiber interface. Figure 4 shows the effect of interface variations and size effects on ultimate fiber strength and strain. From short pristine glass filament, to production sized filament, to impregnated fiber bundle, to unidirectional lamina, the strength is reduced following Weibull statistics. The ranges over each type show the effects that various sizings have on the same fiber. Table 1 is a summary from [17] [18].

Table 1: Sizing Effects on Ultimate Tensile and Shear Strengths

Specimen	% of Pristine Filament UTS (500 Ksi)	Source
15 Various Sizings on Filament	66-84%	17
15 Various Sizings on Strand with Flexible Polyester	53-68%	17
15 Various Sizings on Strand with Rigid Polyester	45-56%	17
15 Various Sizings on Unidirectional Glass in Rigid Polyester	34-49%	17
6 Various Sizings on Unidirectional Glass in Vinyl Ester	40-56%	18
Specimen	**Interlaminar Shear Strength (% Improvement)**	**Source**
Interlaminar Shear Strengths for15 Various Sizings on Unidirectional Glass in Rigid Polyester	48%	17
Interlaminar Shear Strengths for 6 Various Sizings on Unidirectional Glass in Vinyl Ester	34%	18

Figure 5 [19] [20] [21] [22] shows the effect of matrix type on the ultimate strength of unidirectional, cross-ply, and quasi-isotropic laminates. The epoxies, in general, have the greatest interfacial bond strength and highest elongation for pultrusion grade resins. Epoxies have a much lower chemical shrinkage during cure, which reduces the residual strains. Polyesters have the most rigid molecular structure thus in general are the most brittle. Research has shown that polyesters have approximately 2.5 times lower interfacial bond strength to glass fibers than epoxy [13]. Vinyl esters behave similarly to polyesters with slightly more flexibility but similar shrinkage upon cure. Because of this lower bond strength, interfacial debonding, microcracking, and delamination more readily occur with vinyl ester and polyesters. This has been noted by Bailey, [21] as the white appearance of polyesters verses epoxies to be result of debonding of the matrix/fiber interface, resulting from thermal and chemical shrinkage induced by cure [23]. The lowest strain-to-failure epoxy laminate reported in Figure 3, with a fiber volume fraction of 60%, had very low 0.2% offset shear strength at 3.1 Ksi and transverse ultimate strength and strain of 1.1 Ksi and 0.064% respectively [22].

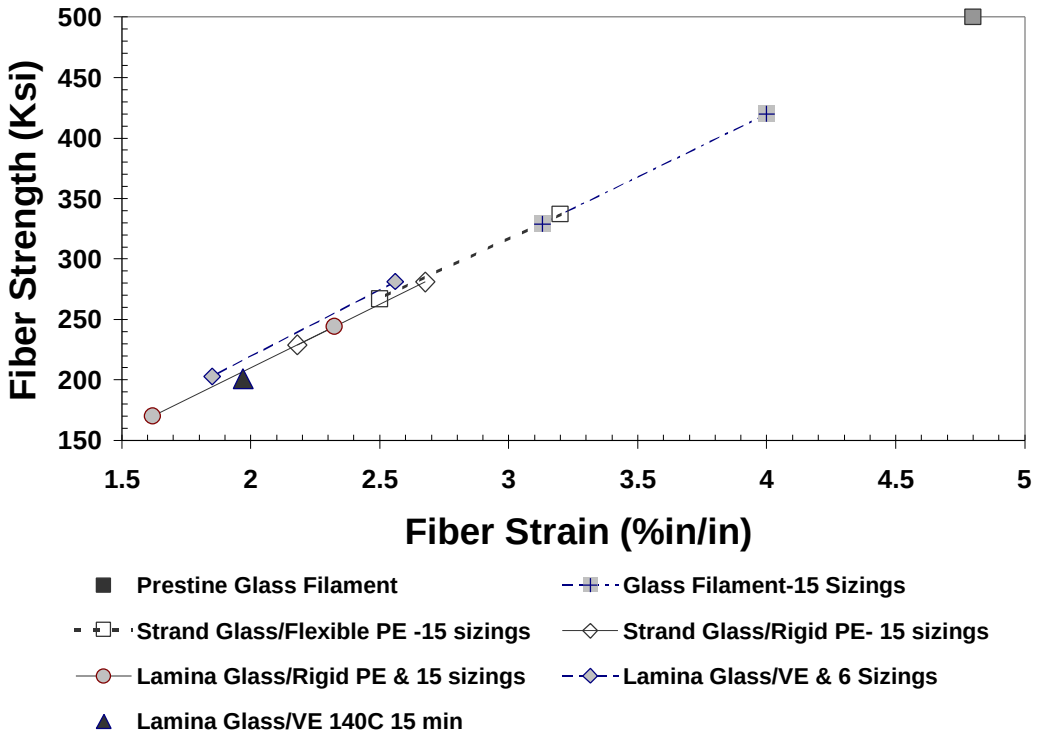

Figure 4: Interface Effects on Filament, Fiber Bundle & Unidirectional Fiber Strength

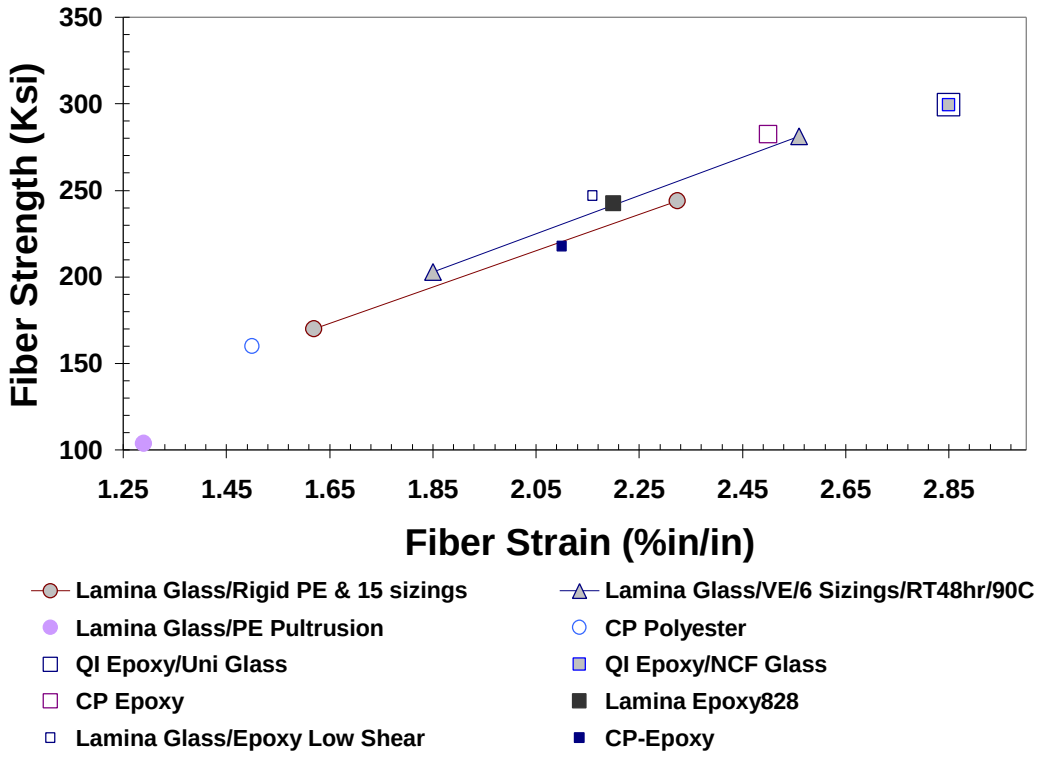

Figure 5: Matrix Effects on Fiber Strength

Uniaxial Transverse Strengths

It has been shown by Keis with a simple mechanics of materials approach that for square array packed fibers that there is a transverse strain magnification factor (SMF) [06] [12].

Equation 9

$$K_e = SMF = \frac{e_m}{e_C} = \frac{1}{\frac{d_f}{s} \cdot \left(\frac{E_m}{E_f} - 1 \right) + 1}$$

ε_m and ε_C refer to strain in the matrix between the fibers and strain of the composite. For a square array

$$\frac{d_f}{s} = \sqrt{\frac{4}{p} \cdot V_f}$$

For a nested or triangular array

$$\frac{d_f}{s} = \sqrt{\frac{2 \cdot \sqrt{3}}{p} \cdot V_f}$$

Assuming linear elastic and simple maximum strain failure criteria, the transverse strength, Y_T, is the following function of composite strength, X_{TC}.

Equation 10

$$Y_T = \frac{E_2 \cdot X_{TC}}{E_m \cdot K_e}$$

Adams performed finite element analysis of the square array for transverse stress concentration factor (SCF) [24].

Equation 11

$$K_s = \frac{s_m}{s_C} = \frac{E_m}{E_C} \cdot \frac{e_m}{e_C} = \frac{E_m}{E_C} \cdot K_e$$

For vinyl ester/glass composites at 60 fiber volume with E_m/E_f = 21, both Keis and Adams yielded K_ε = 1.87.

When the fibers are in contact, the fiber volume is 93 % in the Keis model, the strain magnification factor, K_ε, is 8.56. Adams' analysis of 78% fiber volume yields a strain magnification factor, K_ε equal to 9.2. Thus, if fibers are irregularly spaced and in random contact with other adjacent fibers, the matrix can result in nearly 10 times higher strain than the overall composite strain. If the matrix is brittle as is the case for this vinyl ester, there is little likelihood of stress redistribution thus the transverse strength will be reduced based upon the existing flaws and fiber spacing.

These approaches have not considered thermal and chemical shrink due to the cure process, which can add substantial strain to the composite and matrix. Naik and Crews [25] evaluated fiber matrix interface stresses using finite element analysis and an Airy's stress function elasticity approach for square and diamond fiber arrays. For AS4/3501-6 carbon/epoxy, the maximum thermal hoop and radial stress was 9 and -18 Psi/°C. With a cure of 140°C, matrix hoop strain is at minimum 1000 Psi. For a matrix such as polyester and vinyl ester which also have high chemical shrinkage, the stresses must be much higher and should be accounted for if other than in-situ strengths are to be used in failure theories. As conformation, Mooney and McGarry [25] found that epoxy, having lower cure shrinkage, has a 2.5 times greater bond strength than polyester.

Laminate Transverse Strengths from Literature

In transitioning from lamina to laminate, the transverse strength and stiffness are further effected by constraints from adjacent lamina in the form of ply and angle of adjacent plies. Processing parameters such as cure temperature and resin shrinkage affect the residual as processed transverse strain. Interfacial adhesion fiber and matrix strength and stiffness affect the ultimate failure as in the lamina case.

Jones, Wheatley, and Bailey [26] showed that increasing the cure temperature, from room temperature to 130° C for polyester/glass cross–ply laminates, reduced the transverse failure strain from 0.59 to 0.13%, and increased the thermal induced curvature strain of $(0,90)_T$ laminate from 0 to 0.45%. [12] [23] When all shrinkage, including 0.01% of room temperature cure shrinkage, was accounted for each laminate had a total transverse failure strain of 0.60%. For completeness, the thermal strain of a cross-ply laminate $(0,90)_T$ is shown below [12] [23].

Equation 12

$$e_{tl}^{th} = \frac{E_1 b(a_t - a_1)(T_1 - T_2)}{(E_1 b + E_t d)}$$

$(\alpha_t-\alpha_1)(T_1-T_2)$ can be obtained from the curvature of a $(0,90)_T$ laminate

$$(a_t - a_1)(T_1 - T_2) = (b+d)/2r + \frac{E_1 b^3 + E_t d^3}{6r(b+d)}\left[1/E_1 b + 1/E_t d\right]$$

The radius of curvature ρ is related to chord height δ by

$$\frac{1}{r} = \frac{2}{L} Cos^{-1}\left[1 - \frac{d}{r}\right]$$

Total transverse ply strain is then considered where ε_{tlu} is applied mechanical strain at failure.

$$e_{tu} = e_{tlu} + e_{tl}^{th}$$

Comparison between epoxy and polyester glass composites show that epoxies with higher interfacial bond strengths and lower thermal curing strains yield higher in-situ transverse strength of cross-ply laminates [20]. While the epoxy had a volume fraction of 55-60%, the polyester was restricted by high viscosity to only 37-43%. Considering Keis' mechanics of material solution to strain magnification factor (SMF), the higher fiber volume would have

higher SMF and should have higher strain state. But, the failure strain of the polyester ranged from 0.13 to 0.6 %, and the epoxy ranged from 0.55 to 0.60 %.

Bailey and others have shown that transverse failure strain in the 90° plies decreases with increasing 90° ply thickness for cross-ply laminates [27]. With very thin 90° ply thickness, the transverse failure strain was raised above the fiber failure strain thus eliminating entirely the knee in the stress-strain curve.

Cross-Ply Transverse Stress/Strain Predictions

There has been considerable research performed on microcracking of symmetric cross-ply laminates. Shear lag is the earliest approach to utilize crack spacing in the transverse plies to estimate the stiffness reduction due to microcracking which is based upon measured crack spacing and usually a shear ratio term G/b where b is thickness that shear acts over. Garret and Bailey [27] used b as the full width of the transverse ply. Highsmith used Moire interferometry to determine G/b=100 Msi/in for glass composite and 400 Msi/in for graphite/epoxy [28]. Shear lag analysis assumes that the transverse laminae accept only shear and can carry no tensile stresses. This is no longer a valid assumption for angled ply laminae which can carry substantial load in tension. Thus shear lag can only been used for determination of stress/strain response for cracks in the transverse laminae, not for the angled laminae. Therefore, the full microcracking history of quasi-isotropic laminates cannot be modeled; only, the initial microcracking, occurring in the transverse laminae, can be predicted. Shear lag also requires complete history of transverse crack density, which requires testing, and to be accurate, it must be based upon the in-situ transverse strength property dependent upon thickness and adjacent ply constraints of that particular laminate. Therefore, shear lag is not a universal solution but a solution only for that specific laminate based upon measured crack densities and in-situ ply properties [29].

A variational approach by Hashin followed by Nairn for $(0,90)_S$ and $(90,0)_S$ addresses the in-situ strength problem by using a fracture mechanics failure criteria base upon the microcracking fracture toughness measured on a unidirectional specimen. This predicts better the transverse failure strain being now a function of ply thickness, but again only the transverse plies were considered [29]. Because neither variational/fracture mechanics or shear lag/maximum strength approaches can be applied to quasi-isotropic laminates, an in-situ transverse failure strength and strain will be obtained through testing.

Laminate Ultimate Axial Strengths/Strains

Ultimate axial failure strains for cross-ply and quasi-isotropic laminates are in general the same as the failure strain for the unidirectional lamina of similar materials, which are processed in the same manner.

For laminates which have little or no fiber positioned in the direction of the load, the laminate strength can be greatly affected by the interlaminar stresses. Interlaminar stresses can cause edge delamination and are primarily affected by the stacking sequence. Ultimate strength and strain have be shown to be reduced due to delamination [30]. In addition, the stiffness and strength, offered by the off-axis lamina at ultimate axial failure, is greatly affected by delamination

Failure Criterions

Swanson has compared brittle to toughen epoxies in quasi-isotropic laminates in biaxial loading and found that laminate failure could be directly correlated to maximum fiber direction

strain over the entire range of biaxial normal loading and laminates tested [31]. Swanson has discussed and tested biaxial failure theories for matrix failure in composite laminates. He has tested epoxy/AS4 carbon in combined torsion and transverse normal loading. The matrix failure stresses and strains correlate well to Tsai-Wu failure criteria and to Hashin [14] [32].
Hart-Smith has reviewed past literature and found 30 years ago that Grumman proposed a modified matrix failure criteria including the matrix stress in the fiber direction as well as Hashin and Rotem, and Puck. He proposed separate failure criteria for each failure mode [33]. Hart-Smith proposes a modified shear stress failure criteria in terms of strain, which is almost identical with the maximum strain failure model in the tension-tension and compression-compression quadrants, but is truncated in the shear quadrants [34] [35].

Chapter 4: Quasi-Static Properties & Analysis of CRTM Pultruded Vinyl Ester/E-Glass Composite Laminates

Research Goals and Significance: Quasi-static Testing and Analysis of Pultruded Composites

The primary purpose of this research was to obtain the quasi-static strength and stiffness properties of unidirectional, cross-ply, angle-ply, and quasi-isotropic vinyl ester/E-glass composite laminates fabricated from the Continuous Resin Transfer Molding (CRTM) pultrusion process. Accurate determination of ply level quasi-static properties was vital to fatigue correlation and prediction analysis. The secondary purpose was to characterize the effects of the non-woven stitched non-crimp fabric, the vinyl ester matrix, and the pultrusion process on these stiffness and strength properties. Various methods of prediction of quasi-static properties have been discussed in the literature review; these will be compared with experimental data, and conclusions will be made as to the validity of these predictions and the physical reasons behind the deviations from predicted values. As discussed earlier, the in-situ approach to strength/failure strain will be used rather than the methods of prediction. This limits the application to predictions of similar laminates but allows simplification of future analysis.

Description of Composite Materials for Quasi-static Evaluation

Matrix, Fiber, & Stitch

The materials investigated were pultruded laminates fabricated by Hexcel, Kent Washington, using Dow Chemical's Derakane 441-400 vinyl-ester modified epoxy with PPG Hybon 2002 E-glass. Both resin and fiber components were selected for cost and compatibility with the pultrusion process. To aid in the continuous resin transfer molding (CRTM) process, resin viscosity was reduced by the addition of styrene at 28% by resin volume. The vinyl ester cure process causes high shrinkage when compared with epoxies; a 6% shrinkage in a pure resin specimen was measured when cured with the pultrusion cure cycle. For handling purposes, the unidirectional glass was pre-stitched, 0° stitched to 90° and +45° stitched to -45° ply. The 90° transverse plies were actually stitched with fiber bundles at 86° and 94° by non-woven, non-crimped fabric (NCF) stitch fabrication process. Polyester at 70 denier in a tricot stitch was arranged parallel to the 0° for 0/90°, and a chain stitch was used for the ±45° with the stitch direction at 45° to the ±45° fiber. The stitch was arranged at 7 stitches per inch transverse to the stitch direction and a penetration along the length of stitching direction of approximately 1/10

inch. The stitch by weight composed 1 % of the glass fiber weight. The tricot stitch, appearing as a zigzag stitch loops around the 0° and 90° fiber bundles and passes under a carrier thread then looping back over the 0° and 90° fiber bundles farther down the length of the 0° fiber bundle. This tricot stitch gathered each axial 0° fiber bundle into a regular pattern of fiber bundle with a gap between fiber bundles of approximately 25-33% of the fiber bundle width shown in Figure 6a and Figure 9. The 90° fiber bundles aligned transversely to the pultrusion axis were rounded by the tricot stitch looping around the carrier stitch. A slight gap between bundles is shown in Figure 6a and Figure 14. The chain stitch used for the ±45° plies is shown in Figure 6b.

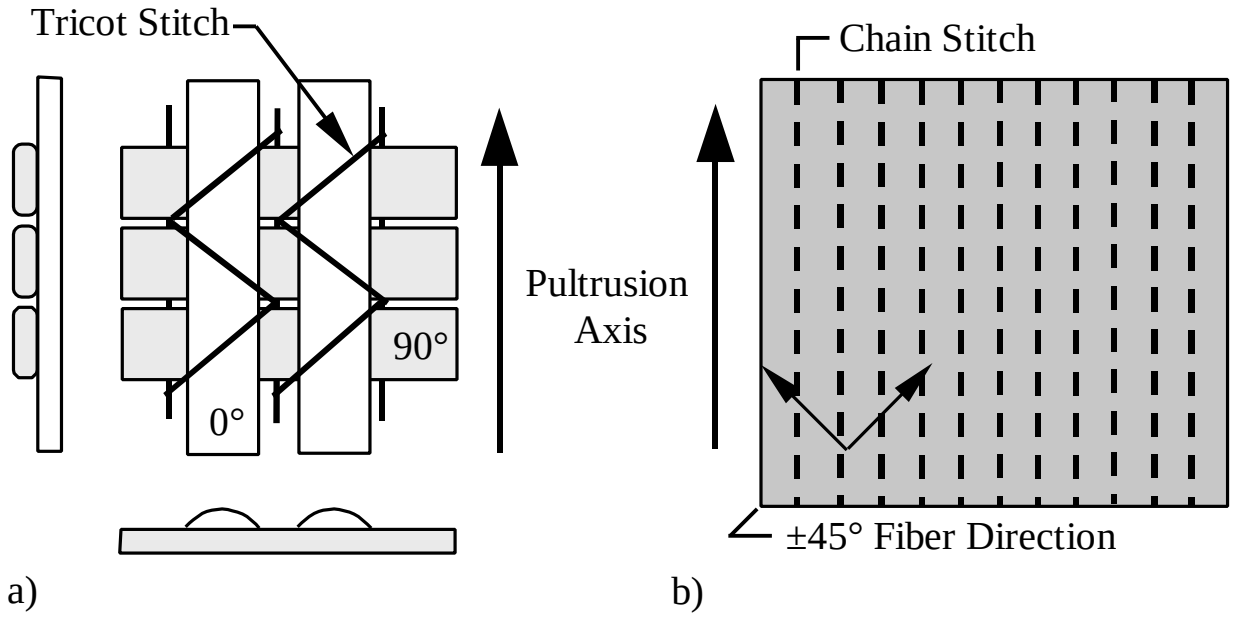

Figure 6: a) Non-woven Tricot Stitch Geometry for 0/90 Fabric, Stitch not shown for clarity in front and side views, b) Non-woven Chain Stitch Geometry for ±45° Fabric

Lamina & Laminates

Cross-ply $(0/90)_{5T}$ and $(0/90)_{3S}$, and quasi-isotropic laminates $(0/90/\pm45/0/90)_{2T}$, $(90/0/(\pm45)_2/0/90)_{2T}$ as shown in Table 2 were tested. The $(0/90)_{5T}$ cross-ply laminate was balance but non-symmetric and $(0/90)_{3S}$ was symmetric but unbalanced. Balanced is defined to have equal areal weighting of the 0° to 90°. The $(0/90)_{3S}$ cross-ply laminate had a 1.5 to 1 ratio of 90° to 0° ply thickness or areal weight. The $(0/90/\pm45/0/90)_{2T}$ was non-symmetric and balanced. The quasi-isotropic laminate $(90/0/(\pm45)_2/0/90)_{2T}$ was nearly symmetric with the ±45 plies being non-symmetric and 0/90 plies symmetric, but was unbalanced similar to $(0/90)_{3S}$. Thickness ratios are based on areal weights shown in Table 2. The angle-ply laminate, $(\pm45)_{3S}$, was cut from the cross-ply $(0/90)_{3S}$; thus, the laminate was unbalanced since the +45° was 9.6 oz/yd^2 and the -45° was 15.1oz/yd^2 fabric. The ±45 plies in the quasi-isotropic laminates above are balanced as shown in Table 2, but a purely ±45 laminate cannot be pultruded since there is no axial fiber to pull through the die. Unidirectional E-glass pultrusion stock was fabricated in 1 and 6 inch widths. Unidirectional AS4 carbon pultrusion stock was fabricated in a 1 inch width.

Table 2: Designation, Thickness, Fiber Volume, and Fiber Areal Weight

Lami-nate	Fiber Configuration	Desig-nation	Lami-nate Thick-ness	% Fiber Volume Fraction	Fiber 0 °	Areal Oz/ Yd^2 90 °	Weight +45 & -45 Separately
1	0° E glass	U1	0.078	71	-	-	-
2	0° E glass	U2	0.156	66	-	-	-
3	0°Carbon	U3	0.079	66	-	-	-
4	$(0,90)_{5T}$	CP1	0.119	56	10.2	10.5	0
5	$(0,90)_{3S}$	CP2	0.139	57	9.6	15.1	0
6	$(90,0, (\pm45)_2, 0,90)_{2T}$	QI1	0.188	56	10.1	15.3	12.3
7	$(0,90, \pm45,0,90)_{2T}$	QI2	0.143	56	12.65	12.65	12.85
8	$(\pm45,0,90, \pm45)_{2T}$	QI2@ 45°	0.143	56	12.85	12.85	12.65
9	$(\pm45)_{3S}$	AP	0.139	57	0	0	9.0/15.1 12.4 Ave.

Physical Description of As-Pultruded Laminates

A general discussion of the physical description of all the laminates will first be discussed followed by a description of each laminate associate with microscopic photographs shown in Figure 9 through 25. These CRTM pultruded glass/vinyl ester composites had a variety of as-pultruded imperfections including warp of the specimens, local fiber volume variations, pure resin rich region, microcracking, delaminations, voids, and fiber undulation. The unidirectional lamina possessed local fiber volume variations noticeable as light and dark streaks. The six-inch wide unidirectional E-glass pultrusion possessed high curvature in the transverse direction. The chord height of this curvature was 0.017 inch over the six-inch width; this curvature when straightened in the grips of the Instron strained the specimens to a maximum of 37% of its ultimate transverse failure strain. Matrix shrinkage, seen as surface sink marks in low fiber areas gave the unidirectional and laminate specimens a rough textured appearance. Matrix shrinkage interior to the laminates in low fiber volume areas often exceeded the ultimate axial tensile strain; thus to relieve the strain, debonding and microcracking resulted parallel to the fiber. A statistical analysis of microcracking and delamination densities was not conducted at this point; rather a qualitative analysis was performed. Microcracking was seen in both the axial and transverse views always occurring in a resin rich region between fiber bundles. In the axial view aligned to the pultrusion axis, microcracking occurred more often when the 0° fiber bundles were in the aligned configuration as shown in Figure 7 where a larger resin rich region existed between the 0° fiber bundles than in the nested configuration as shown in Figure 8.

Fiber undulation was apparent in all laminates tested. The tricot stitch from the non-woven fabric forced the fiber into a non-uniform fiber pattern in both the axial and transverse directions to the pultrusion axis. The axial 0° fiber bundles aligned with the pultrusion axis were gathered by the tricot stitch into a bundle, which created gaps between axial fiber bundles of width approximately 25-33% of the axial fiber bundle width. The off-axis plies to the pultrusion axis were forced into an undulating pattern in one of two geometries. The 0° fiber bundles of one ply could either be nested or aligned with the 0° fiber bundles of adjacent plies. When the 0° fiber bundles of one ply were aligned to the 0° fiber bundles of an adjacent ply as seen in Figure 7, a pure resin pocket filled the gap between the 0° fiber bundles. Because the off-axis plies have no applied tensile forces as do the axial plies to the pultrusion axis during the pultrusion process, the off-axis plies may bulge in this resin rich pocket. This produce slight undulation of the off-axis plies, but a matrix crack often occurred spaced in the gap between the 0° fiber bundles, which implied excessive processing shrinkage. The nested configuration of adjacent 0° fiber bundles as shown in Figure 8 resulted in the greatest fiber undulation of the transverse plies to the pultrusion axis. Axial fiber undulation, in the direction of pultrusion, also occurred but was much less than that of the transverse plies since the tricot stitch of the fabric created only a slight gap in the transverse. The laminates with the thicker transverse plies appeared to possess greater fiber undulation in the axial fiber, which is reasonable since there is greater undulation possible with thicker than thinner transverse and angle plies. Quasi-isotropic plies tend to have less fiber undulation than the cross-ply laminates since there is fewer 0° plies and additional angle plies to diffuse the undulation created by the 0° fiber bundle and gap pattern. In many of these photographs the full stacking sequence cannot be seen; this is due to the cut cross-section falling on the gap between plies as shown as section AA in both Figure 7 and Figure 8.

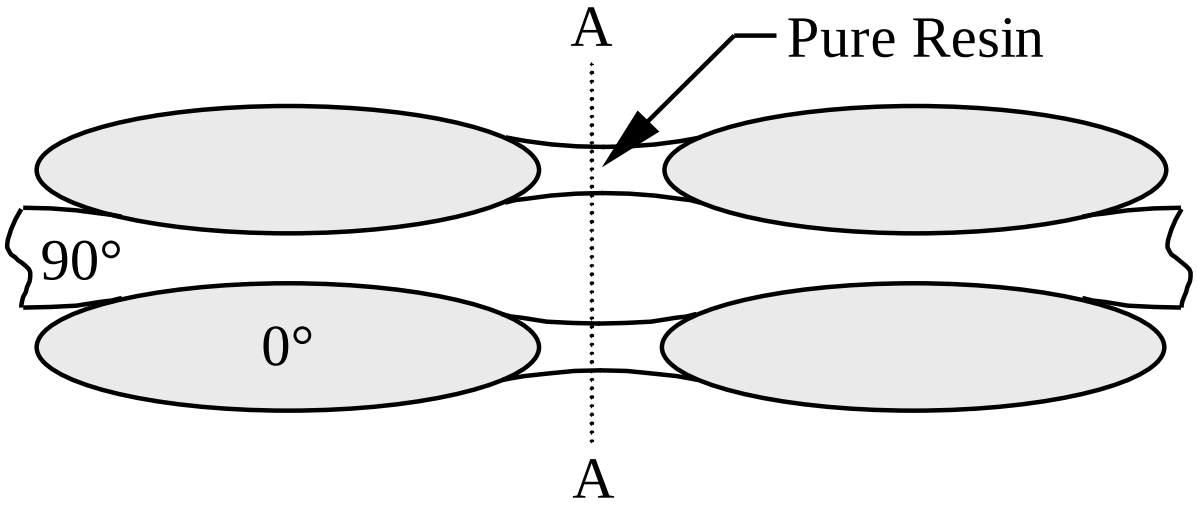

Figure 7: Align Adjacent 0 ° Fiber Bundles of the Non-woven Stitched Fabric with Pure Resin Area between the 0 ° Fiber Bundles

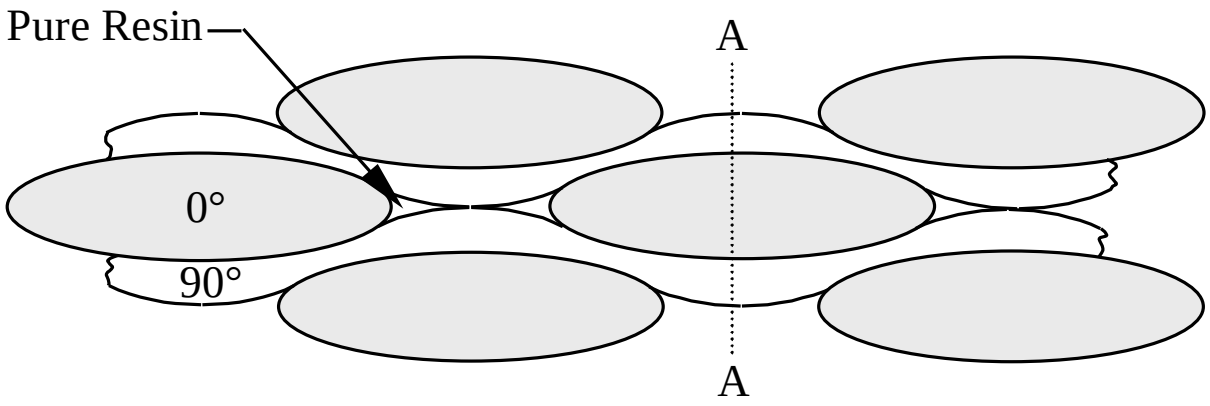

Figure 8: Nested Adjacent 0 ° Fiber Bundles of the Non-woven Stitched Fabric Forces High Fiber Undulation in 90 ° Plies Aligned Transverse to Pultrusion Axis

The cross-ply laminate, designated CP1 in Table 2, a balanced non-symmetric laminate of $(0/90)_{5T}$, is pictured in Figure 9 through 14. Views aligned along the pultrusion axis are shown in Figure 9 through 12. Both nesting and aligned 0° fiber bundles and the undulation of the fiber transverse to the pultrusion axis are seen in Figure 9 and 10. Fiber undulation, pure resin rich regions, and the stitch shown in the view aligned with the pultrusion axis are shown in Figure 10 and 11. Voids in the fiber aligned transverse to the pultrusion axis are shown in Figure 11 as a dark streak parallel to the 90° plies. Since the CRTM pultrusion process is an injection process rather than a resin dip bath process, wherever high fiber volume exists the fiber may be too densely packed to allow penetration of resin; this may cause voids. Views of CP1 laminate aligned transverse to the pultrusion axis are shown in Figure 13 and 14. Very little fiber undulation of the 0° plies was apparent in these transverse views. As shown in Figure 14, microcracking in the transverse views occurred where resin rich regions were seen.

The cross-ply laminate, designated CP2 in Table 2, is unbalanced with 0° to 90° volumetric ratio of 2/3 and is symmetric in form of $(0/90)_{3S}$; CP2 is pictured in Figure 15 through 18. Views aligned along the pultrusion axis are shown in Figure 15 and 16. The full range from aligned to nested 0° fiber bundle configurations are seen in Figure 15; fiber undulation of the plies transverse to the pultrusion axis, pure resin pockets, and stitch are shown in Figure 16. Views of CP2 laminate aligned transverse to the pultrusion axis are shown in Figure 17 and 19. Very slight fiber undulation and the stitch geometry are seen in both Figure 17 and 19. A resin rich area with associated microcrack is shown in Figure 18.

The quasi-isotropic laminate, designated QI1 in Table 2, is unbalanced with 0°, 90°, and 45° volumetric ratio of 2/3/2.5 similar to CP2 cross-ply laminate, and is the most nearly symmetric laminate with stacking sequence of $(90/0/(\pm45)_2/0/90)_{2T}$ with only the ±45 plies being non-symmetric; QI1 is pictured in Figure 19 through 22. Views aligned along the pultrusion axis are shown in Figure 19 and 20, which reveal slight fiber undulation of the plies running transverse to the pultrusion direction. Microcracking between 0° fiber bundles and delamination adjacent to the resin rich region initiating from the stitch between the 0° and 90° plies are shown in Figure 20. Views of QI1 laminate aligned transverse to the pultrusion axis are shown in Figure 21 and 22. The stitch is shown as white lines in Figure 21. A resin rich area and stitch wrapping around the 90° plies are seen in Figure 22.

The quasi-isotropic laminate, designated QI2 in Table 2, is balanced with 0°, 90°, and 45° volumetric ratio of 1/1/1 similar to CP1 but non-symmetric in the form of $(0/90/\pm45/0/90)_{2T}$. QI2 is pictured in Figure 23 through 27. Views aligned with the pultrusion axis, shown in Figure 23 and 24, reveal fiber undulation of the plies transverse, 90°, and angled, ±45°, to the pultrusion direction. Microcracking between 0° fiber bundles within the resin rich is shown in Figure 23 and in a closer view in Figure 24. Views of QI2 laminate aligned transverse to the pultrusion axis are shown in Figure 25 and 27. The stitch is shown as white lines in Figure 25. A slight resin rich area and dark appearing stitch wrapping around the 90° plies are seen in Figure 26. A resin rich area between 90° fiber bundles with a microcrack extending into an adjacent 90° ply is shown in Figure 27.

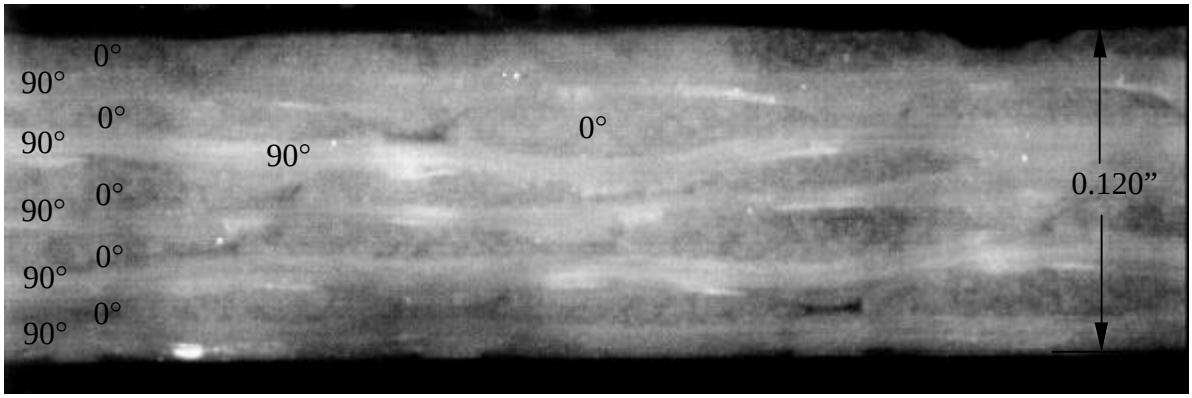

Figure 9: CP1 View Aligned with Pultrusion Axis, Full Thickness

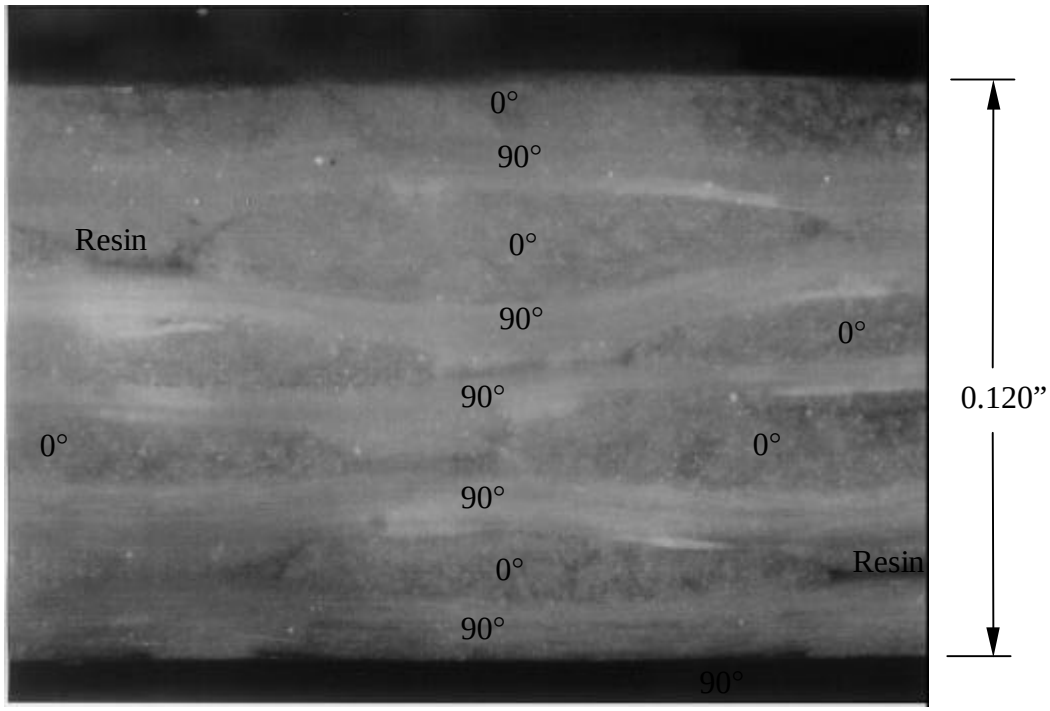

Figure 10: CP1 View Aligned with Pultrusion Axis, Full Thickness, Fiber Undulation and 0 ° Fiber Bundle Nesting

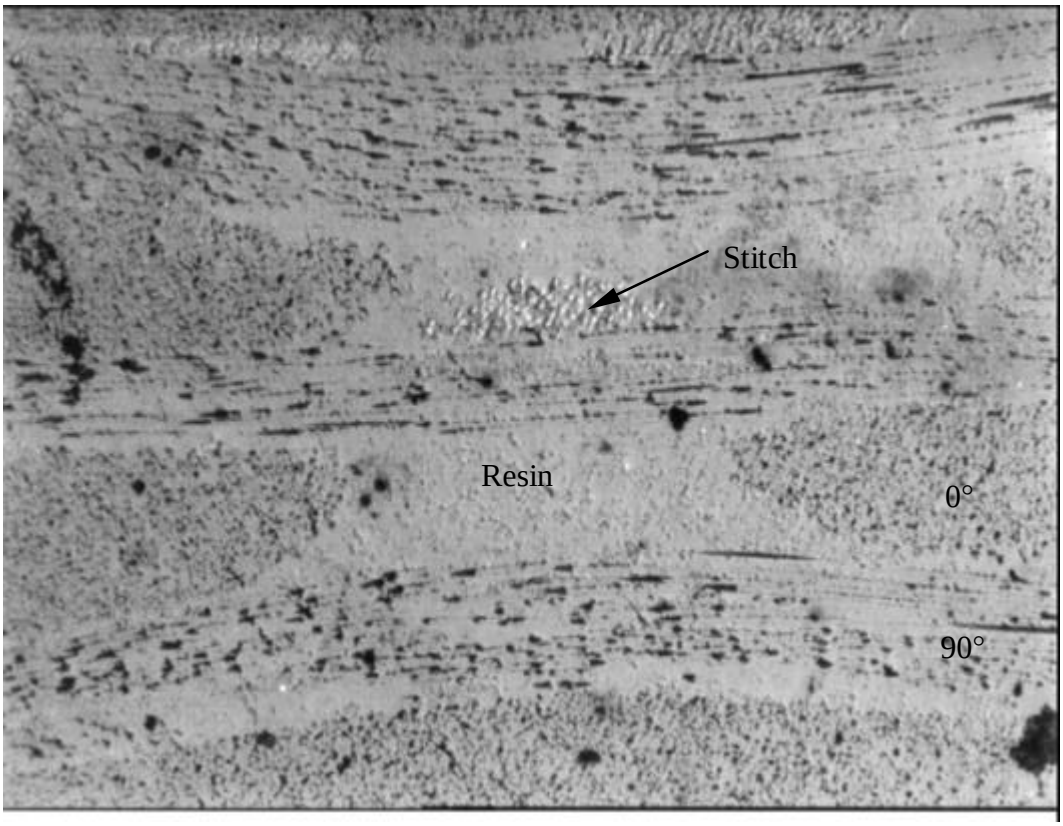

Figure 11: CP1 View Aligned with Pultrusion Axis, Pure Resin Area between 0 °Fiber Bundles and 70 Denier Polyester Stitch, and Fiber Undulation of the 90 °Plies.

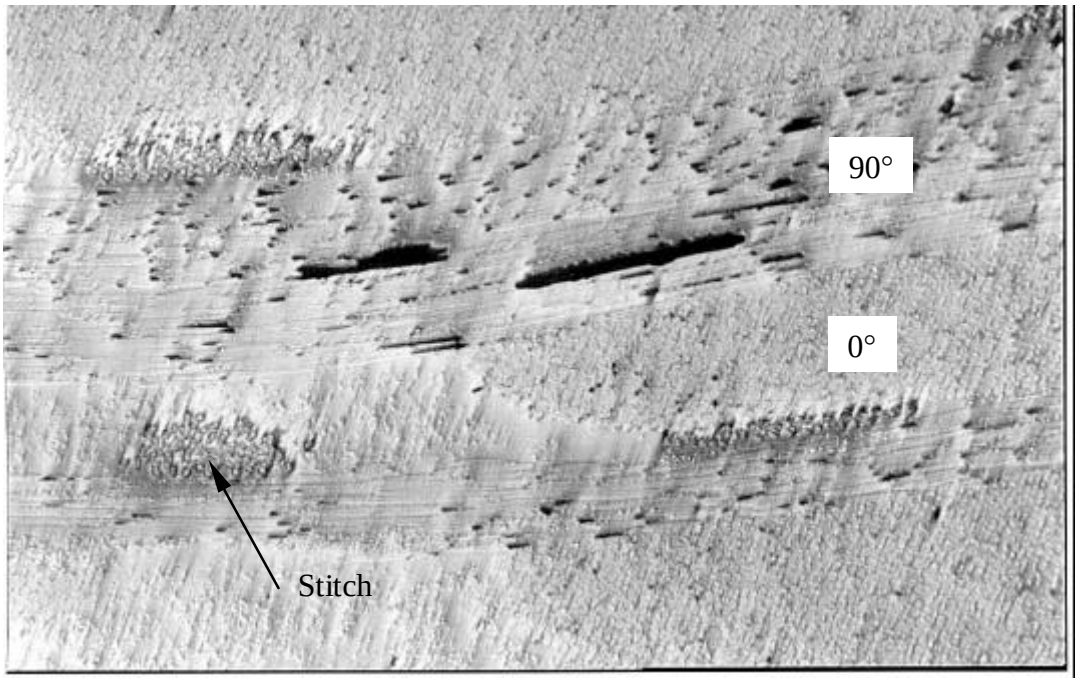

Figure 12: CP1 View aligned with Pultrusion Axis, Fiber Undulation, 70 Denier Polyester Stitch, and Void in 90 °Ply

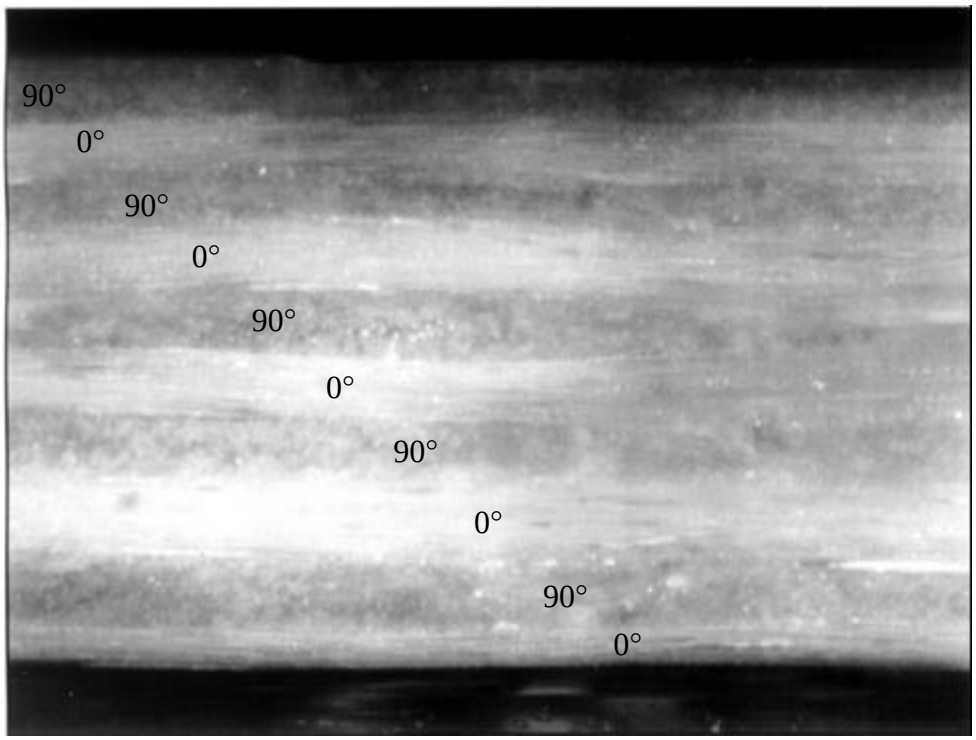

Figure 13: CP1 View Transverse to the Pultrusion Axis, Full Thickness, and Fiber Undulation of 0° Plies

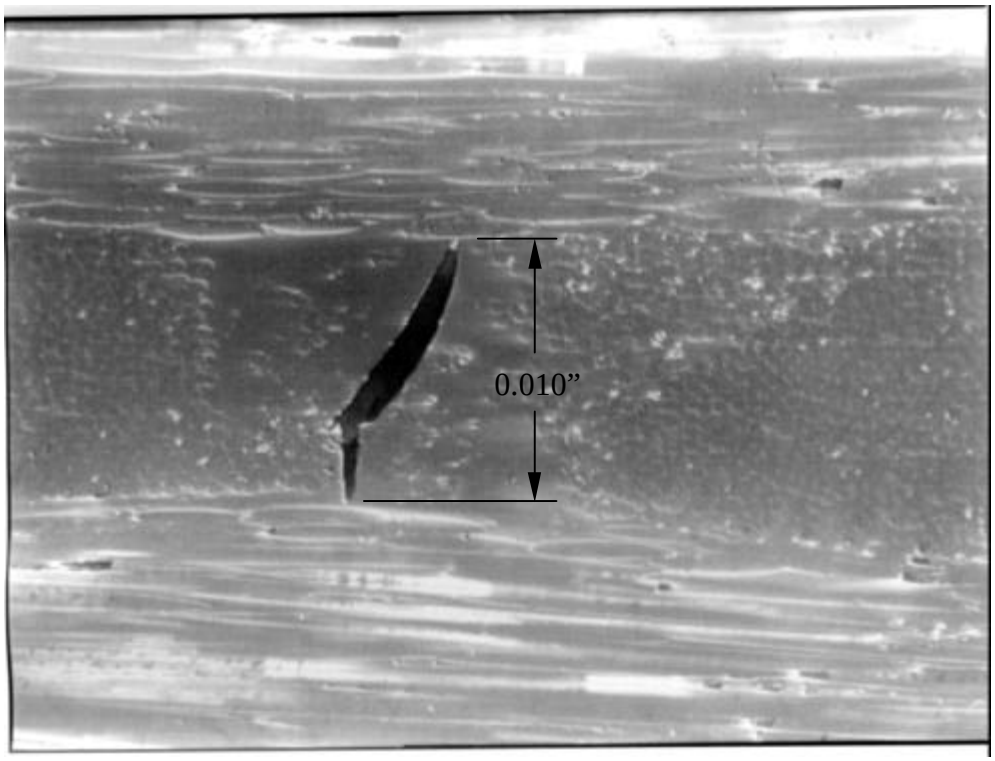

Figure 14: CP1 View Transverse to the Pultrusion Axis, Microcrack in Pure Matrix Region between 90° Fiber Bundles

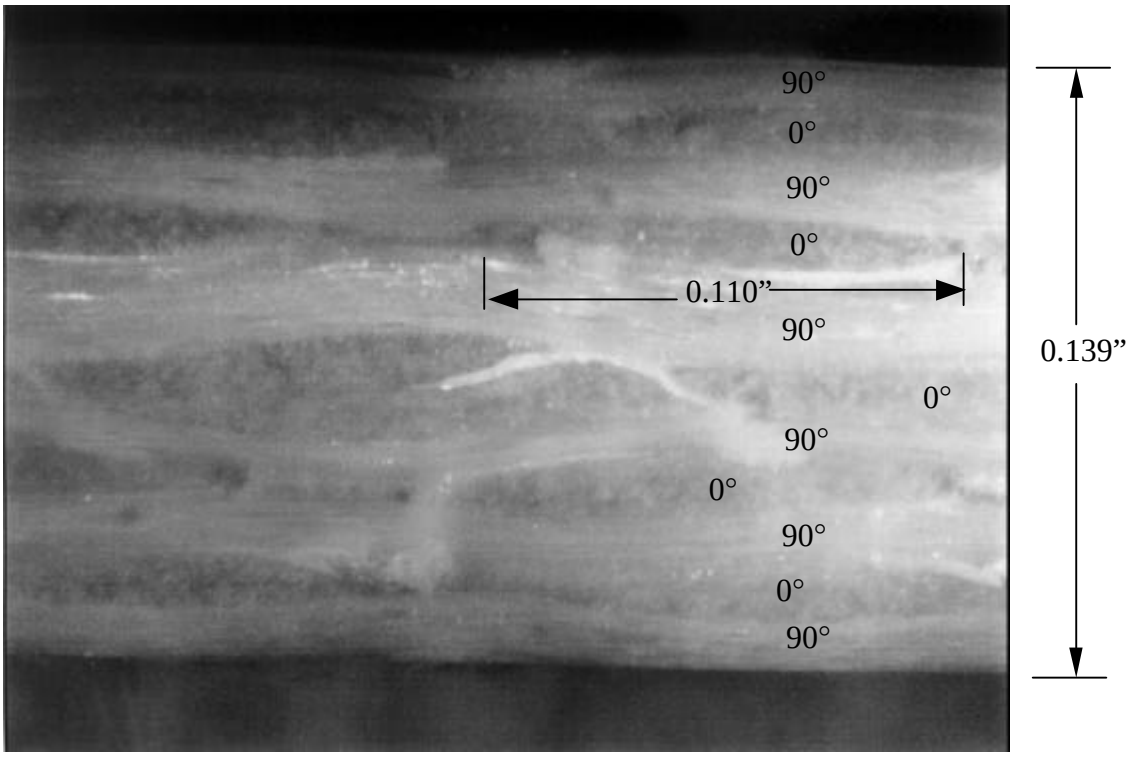

Figure 15: CP2 View Aligned with Pultrusion Axis, Nested Configuration of Adjacent 0 ° Fiber Bundles, Fiber Undulation in 90 ° Plies Transverse to the Pultrusion Axis

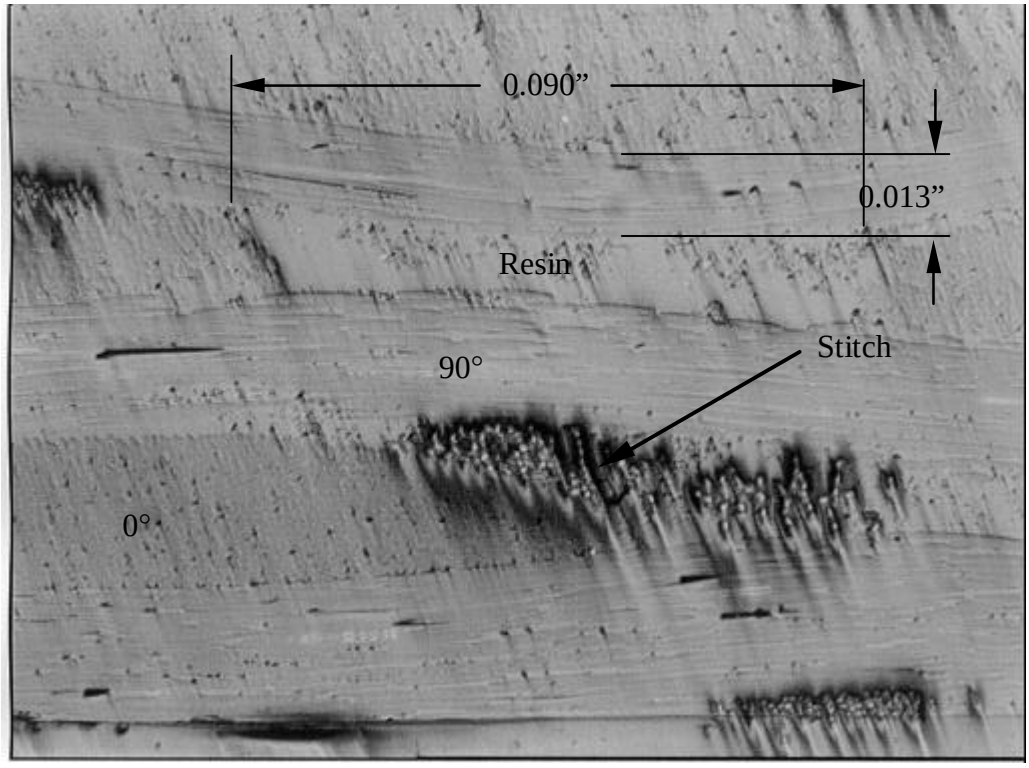

Figure 16: CP2 Axial View Aligned with Pultrusion Axis, Fiber Undulation of 90 ° Plies, Resin Rich Area between 0 Fibers, and 70 Denier Polyester Stitch

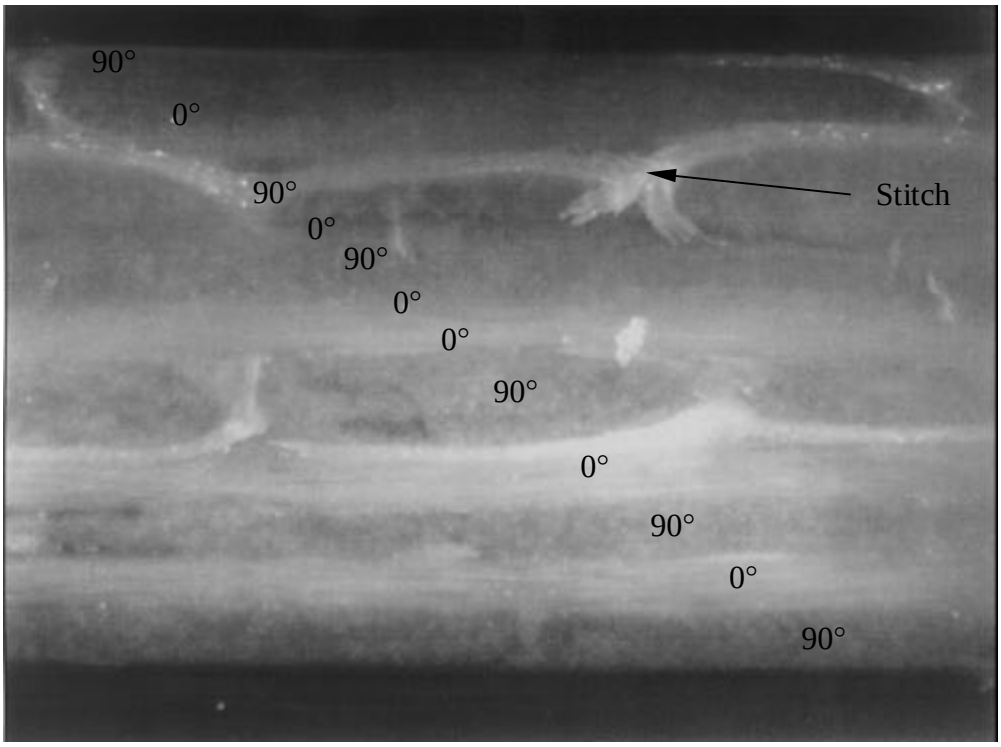

Figure 17: CP2 Transverse View, Full Thickness, and Stitch Surrounding the 90 ° Fiber Bundles

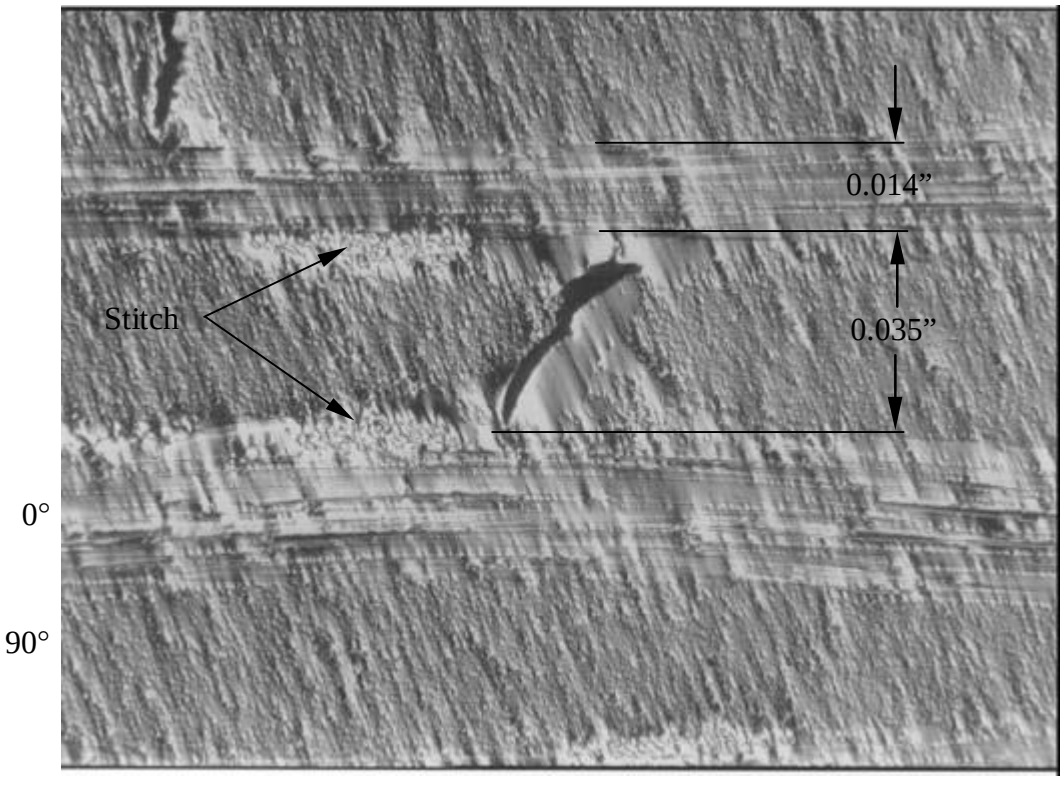

Figure 18: CP2 Transverse View, Resin Rich Area with Thermally Induced Crack between 0 Fibers, and 70 Denier Polyester Stitch

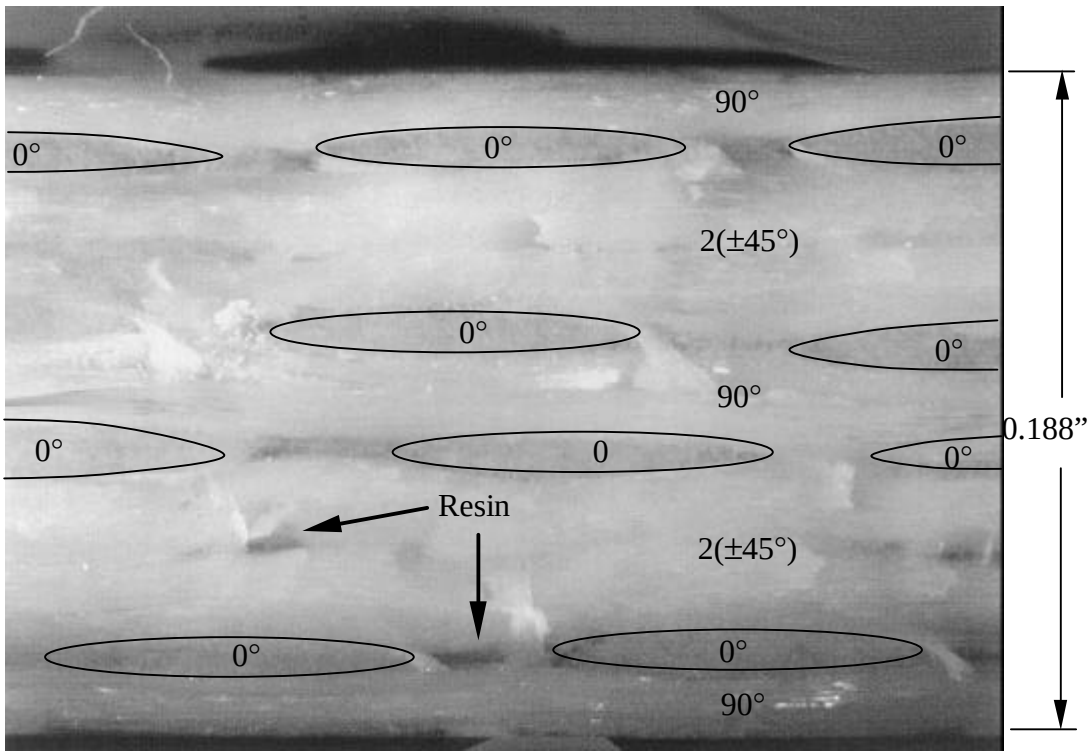

Figure 19: QI1 Axial View Aligned with Pultrusion Axis, Full Thickness, Resin Rich Regions Appear as Dark Regions

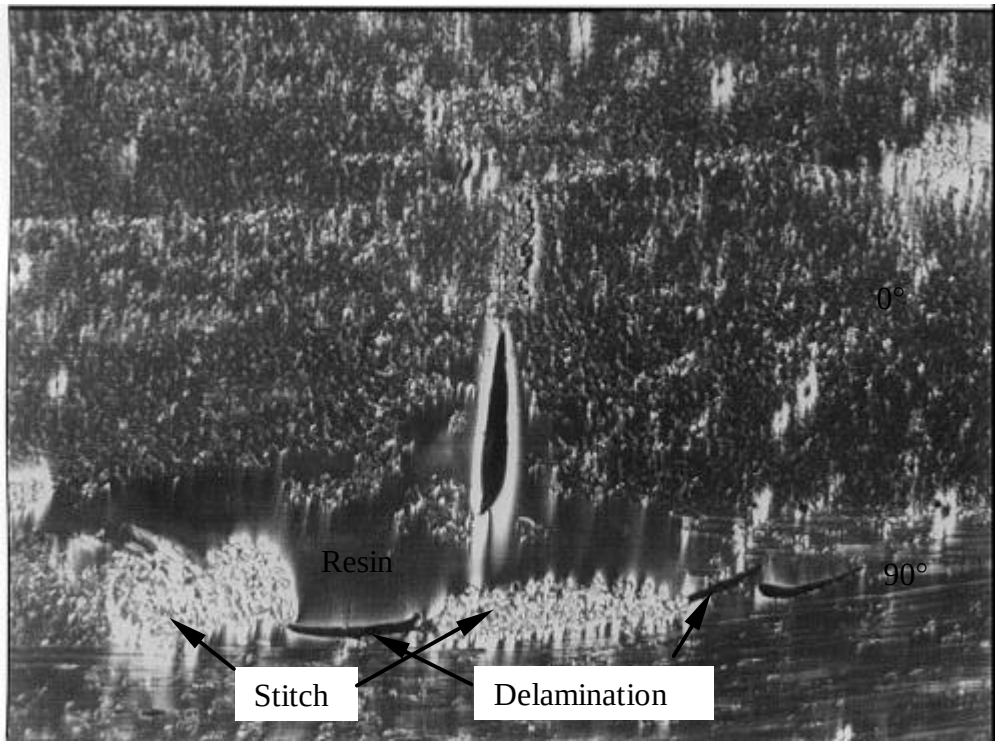

Figure 20: QI1 Axial View Aligned with Pultrusion Axis, Resin Rich Region, Stitch, and Matrix cracks and Delamination in Resin Rich Region between 0 Fiber Bundles

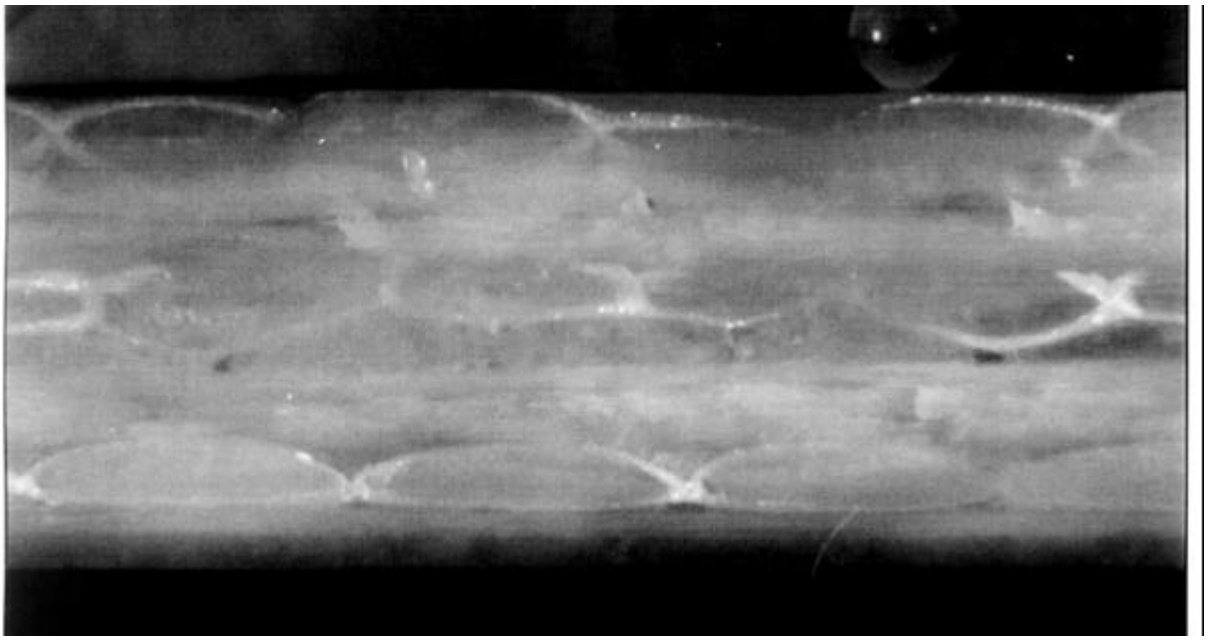

Figure 21: QI1 View aligned Transverse to Pultrusion Axis, Full Thickness

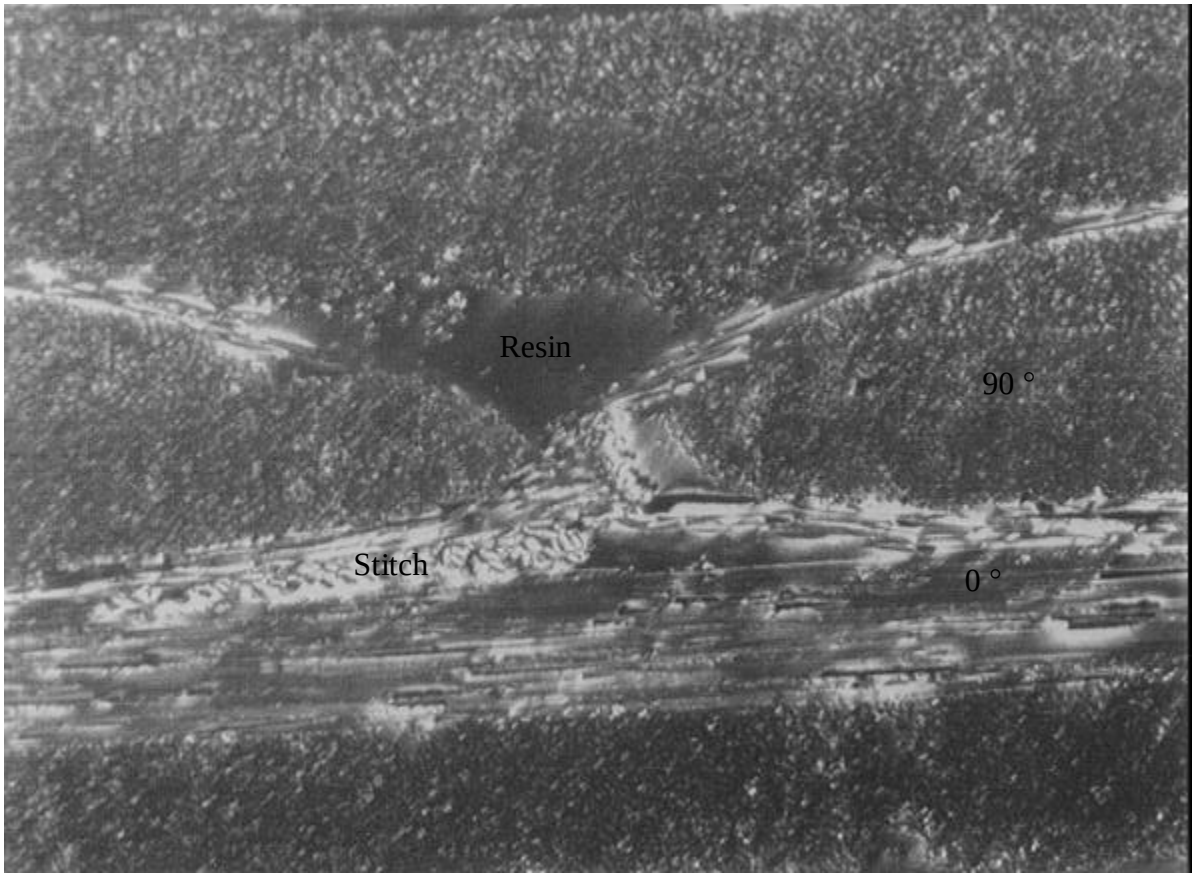

Figure 22: QI1 View aligned Transverse to Pultrusion Axis, Resin Rich Region between 90 ° Fiber Bundles

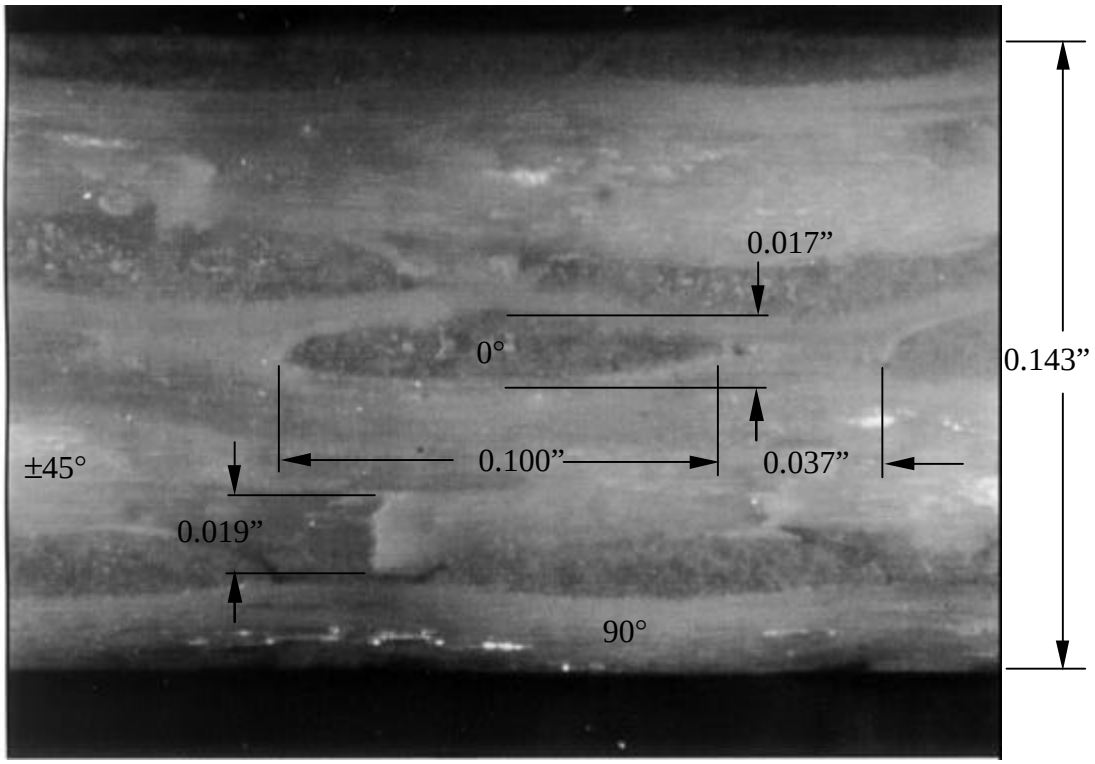

Figure 23: QI2 Axial View Aligned with Pultrusion Axis, Full Thickness, 90 ° Fiber Undulation, Matrix crack within 0 ° Fiber Bundle.

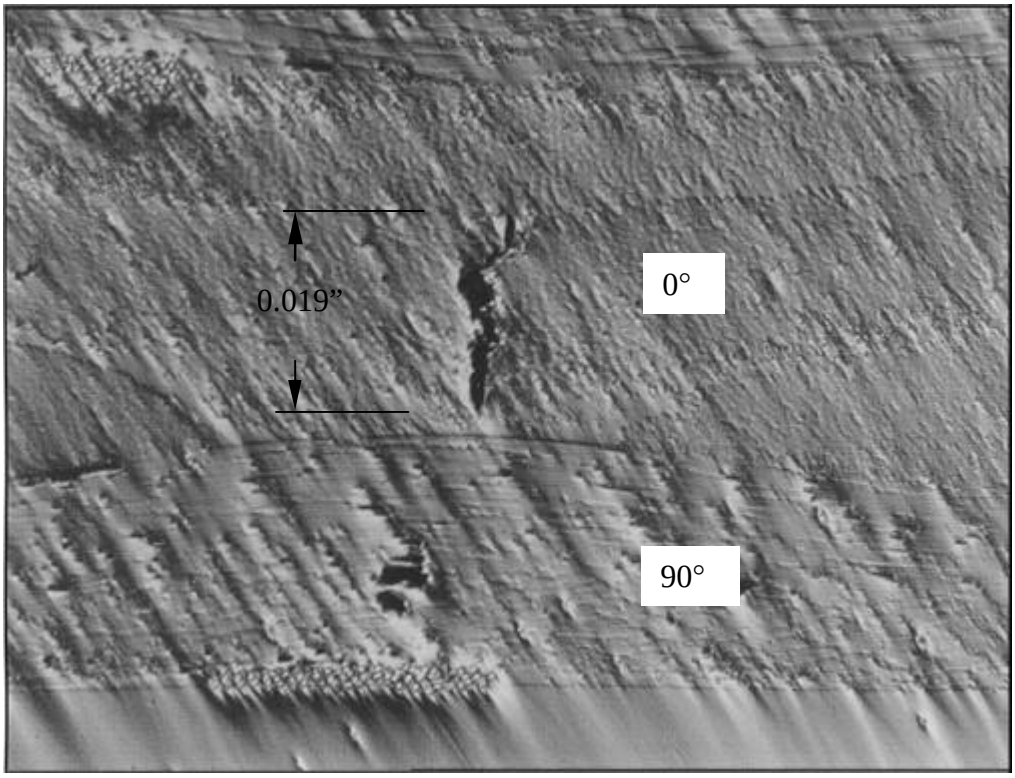

Figure 24: QI2 Axial View Aligned with Pultrusion Axis, Microcrack in Resin Rich Region within a 0 ° Fiber Bundle also Seen in Figure 21

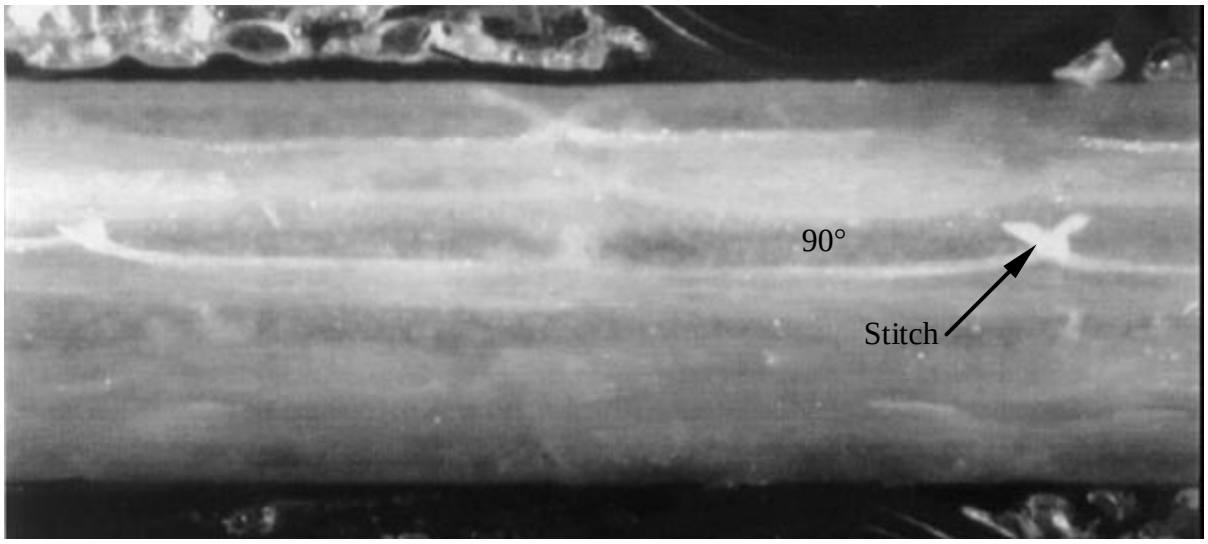

Figure 25: QI2 View Aligned Transverse to Pultrusion Axis, and Full Thickness, Stitch shown in White

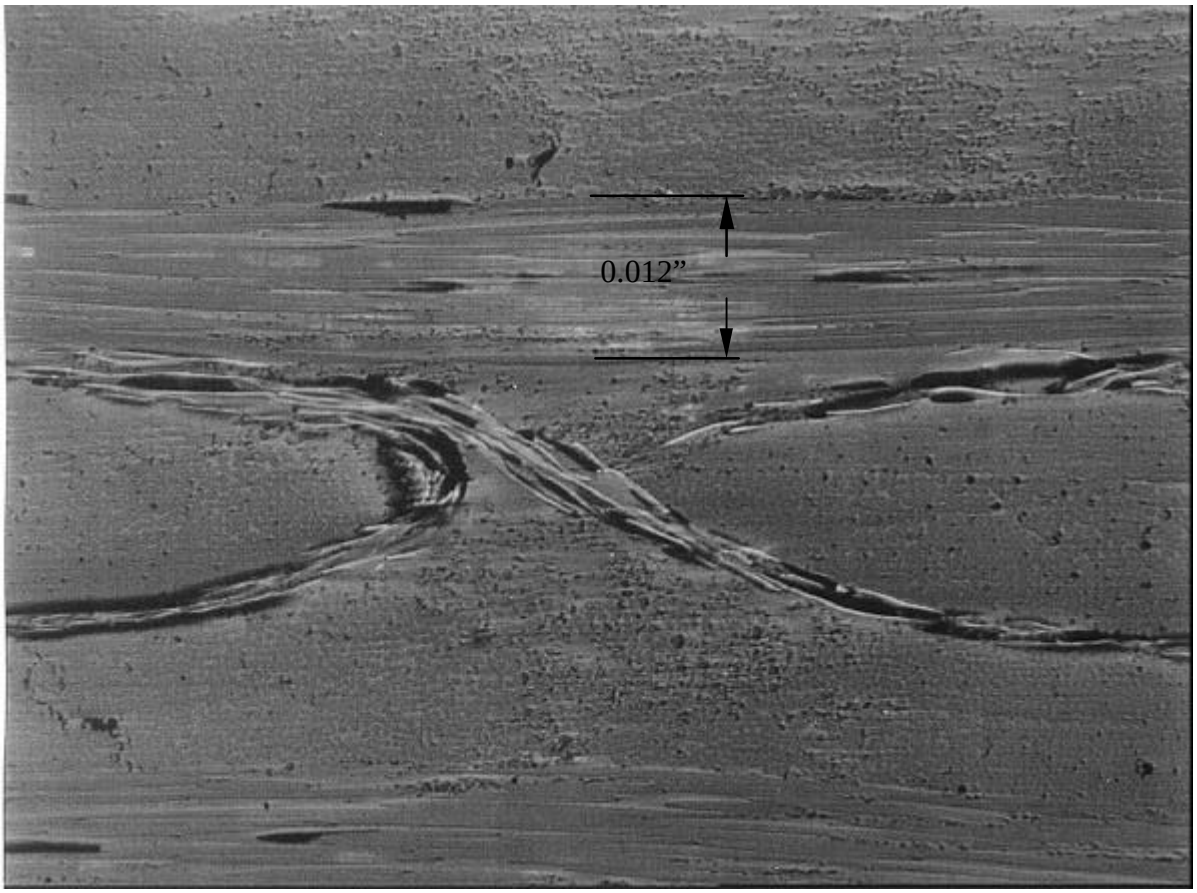

Figure 26: QI2 View Aligned Transverse to Pultrusion Axis, Stitch Wrapping around 90 ° Fiber Bundles

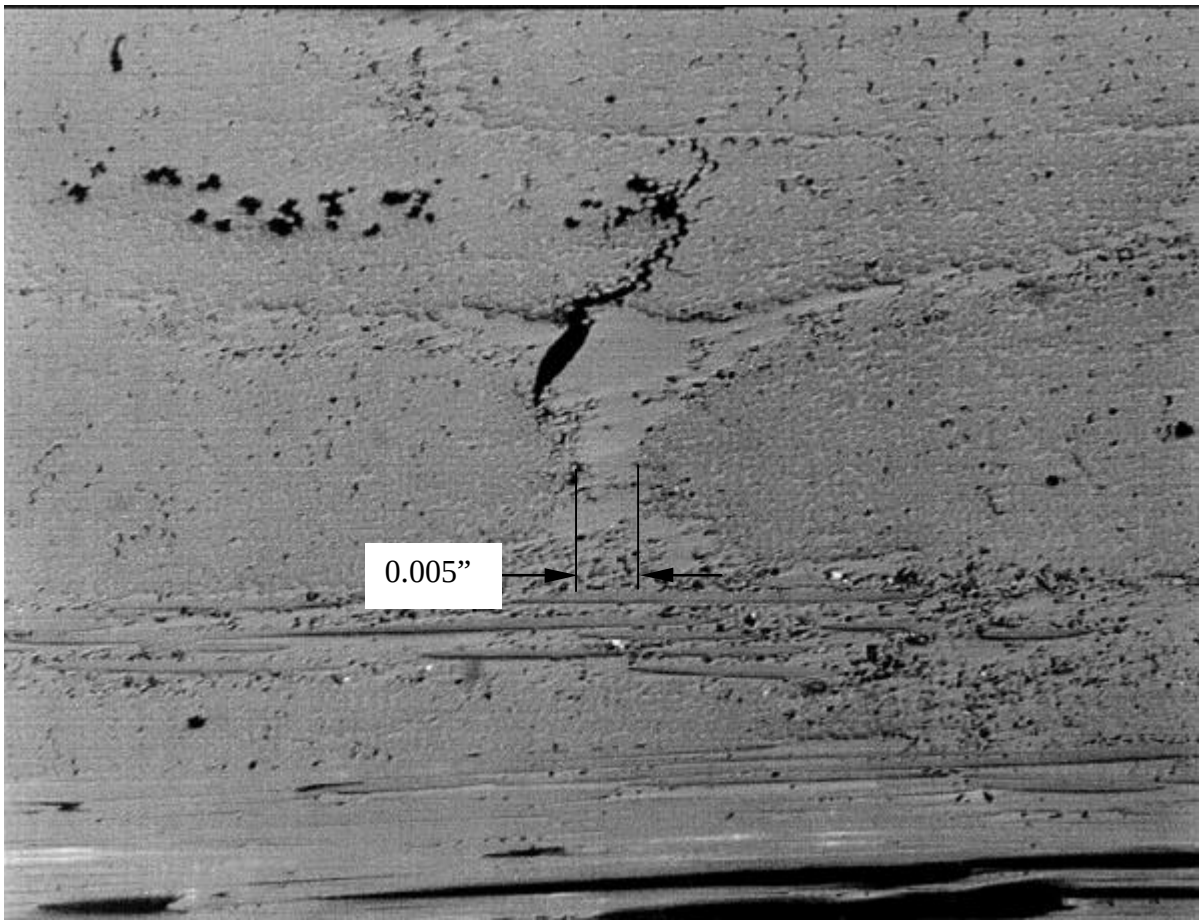

Figure 27: QI2 View Aligned Transverse to Pultrusion Axis, Resin Rich Region between 90 ° Fiber Bundle Extending into Adjacent 90 ° Ply.

Description of Testing for Quasi-static Evaluation

Quasi-static strength and stiffness data for the above unidirectional, cross-ply and quasi-isotropic laminates were obtained from tests performed on an Instron screw driven load frame. Length and width of laminated specimens were 8 by 1 inches. Unidirectional specimens were slightly less than 0.5 inch wide to allow 2 specimens produced, when cut from 1 inch wide stock. Non-tapered G-10, woven E-glass epoxy laminate, end tabs were bonded to the unidirectional specimens. Edges were cut, ground, and polished. Gripping length was 2 inches with 100 grit sandpaper for gripping facing specimen. One extensometer and two to four strain gages were used to measure strain/elongation for quasi-static testing. Minimum of 10 specimens for axial direction and 3 specimens for transverse were tested as shown in Table 3 and Table 4. ASTM Standards D3039-95a, D3410-95, and D3518-94 were followed for tension, compression, and shear tests respectively.

Results and Discussion: Quasi-static Evaluation for Matrix, Unidirectional, Cross-ply, Angle-ply and Quasi-isotropic CRTM Pultruded Laminates

Matrix Tensile Performance

Other researchers have studied unfilled Derakane 441-400 vinyl ester matrix with 1.1% of low temperature initiator, Benzoyl Peroxide (BPO), and 28% styrene, under various cure profiles [36]. Due to the high thermal and chemical shrink that occurs during cure, the neat resin specimen under the exact CRTM pultrusion process cure was impossible to reproduce without complete fracture of the net resin specimen. The pultrusion process cure profile was 5 minutes at 150° C in the heated pultrusion die. The cure profile most similar to the pultrusion process and able to successfully process the intact net resin specimens included a ramp from 20° C to 150° C at 6.5° C/min, a 20 minute hold at 150° C, followed by -2° C/min ramped to room temperature. The tensile strength and stiffness of these net resin specimens were 8 Ksi and 0.5 Msi, respectively. The failure strain was 1.9 %in/in as shown in Table 3.

Unidirectional Tensile and Compression Performance

Unidirectional tests included tension and compression on vinyl ester/E-glass and tension on vinyl ester/AS4 carbon unidirectional composites and are summarized in Table 3. Failure of the unidirectional composites for both carbon and glass were a brittle matrix/ductile fiber failure where the failure initiated in the matrix as longitudinal splitting due the combination of transverse compression and longitudinal extension in the matrix. A premature failure of a tow near the surface or corner of the specimen often occurred before final failure. Ultimate failure both in tension and compression occurred in a burst of transverse ply splitting as glass composites have been reported [24]. The compression failure strain, for the E-glass composite, was 1.74%, 12% lower than the tensile failure strain. Kinking failure was not observed in the compression tests. The calculated fiber modulus, E_T/V_f, in compression was actually higher at 11.75 Msi for the compressive test verses 10.5 Msi for tensile modulus; therefore, the ultimate strength for both tension and compression were equivalent. A possible explanation is that the matrix, the weaker link, is under tension in the two transverse axes due to the compressive applied load and associated Possion effect. In addition, tensile failure of the matrix occurs at lower strain than in compression; therefore, failure would occur at a lower compressive than tensile strain. Using a triaxial failure theory such as Tsai-Wu, and Hart-Smith's[34], the failure would occur earlier than the comparable tensile test. Due to the low failure strain of the matrix and high thermal strains of the composites, the unidirectional carbon composites failed in the same manner.

As mentioned in the Physical Description of As-Pultruded Laminates section, attempts at transverse tension measurements in unidirectional specimens were unsuccessful due to large curvature in the unidirectional panels induced during cure. Therefore the only transverse strength and stiffness measurements were obtain from in-situ measurements from off-axis ply failure of cross-ply and quasi-isotropic laminates as discussed in section entitled Extraction of Ply Level Quasi-static Properties from Measured Laminate Data.

Table 3: Matrix & Unidirectional Quasi-static Properties with Standard Deviation "nonbiased" or "n-1" method

					V_f	E_T ($<\varepsilon_{90f}$)	X_T	ε_{xf}	$E_S(\varepsilon_{xf})$	$\nu 12$
Designation	Fiber Type	Ply Orientation Degree	# of Specimens Tested	Test	% Fiber Volume	Tangent Tensile Modulus $\varepsilon_x>\varepsilon_{90f}$	Ultimate Strength	Failure Strain	Secant Modulus at failure	Poisson's Ratio
						Msi	Ksi	%in/in	Msi	
Matrix	Vinyl Ester	None	3	Tension	none	0.499	8.0	1.9	.421	NA
U1	E-glass	0°	10	Tension	71	7.467 ± 0.145	142.8 ± 7.40	1.966 ± 0.102	7.171 ± 0.249	0.283
U2	E-glass	0°	10	Compression	66	7.761 ± 0.145	140.0 ± 12.2	1.735 ± 0.135	NA	NA
U3	Carbon	0°	10	Tension	66	19.14 ± 0.72	209.6 ± 13.5	1.085 ± 0.053	19.57 ± 1.404	0.329

Cross-Ply Laminates Pultrusion Axis Tensile Performance

Considering laminates tested parallel to the pultrusion axis, cross-ply laminates $(0/90)_{5T}$ designated CP1 in Table 2, and $(90/0)_{3S}$ designated CP2 in Table 2 were seen to have differing off-axis ply failure strains shown in Figure 28 as ε_{90f}. Average and typical stress/strain curves of all the laminates are shown in Figure 29 and Figure 30; average and standard deviation laminate strength and stiffness values are shown in Table 4. Cross-ply laminate CP1 having balanced 0° and 90° plies, $t_{90°}= t_{0°}$, had a higher off-axis ply failure strain of 0.32% whereas cross-ply laminate, CP2, having thicker transverse plies, $t_{90°}=1.5 \times t_{0°}$, had lower off-axis ply failure strain at 0.22%. The ultimate failure strain, designated ε_{ult} in Figure 28, followed a similar pattern as the off-axis ply failure strain; CP1 being slightly higher at 2.08% than CP2 at 1.91% but within the standard deviation of each other.

Microcracking, delamination, and fiber fracture are the main damage mechanisms that occur in laminated composites. It is peculiar but not unusual that both cross-ply laminates have bilinear stress/strain curves with quasi-isotropic laminates being just slightly less linear than the cross-ply laminates. For CP1 laminate, both sections of the bilinear stress/strain curves were linear to $R^2 > 0.999$, for all specimens tested. The range over which microcracking occurred was qualitatively analyzed by viewing the derivative of the stress with respect to strain of the quasi-static stress strain curve, which is the instantaneous tangent modulus. Non-symmetric CP1 laminate, Figure 31, revealed a continuous drop in stiffness until 1.0% strain at which the tangent stiffness leveled off until 1.5% strain. Beyond 1.5% strain, the non-symmetric laminate began to change gradually; the damage incurred on the non-symmetric laminate is pictured as an increase in stiffness on the top side of the specimen while the bottom side revealed a decrease. The dashed curve in Figure 31 is the average of the top and bottom tangent modulus and reveals a slight decrease beyond 1.5% strain. Symmetric CP2 laminate was shown in Figure 32 to have

two flat sections; a very slight flat section below 0.1% and a longer flat section between 0.4 to 1.9%. In both cases, this nonexistent or very short constant stiffness section occurring at the beginning was reanalyzed with a polynomial fit over only the section below 0.32% and 0.2% for CP1 and CP2 respectively with no change in the result.

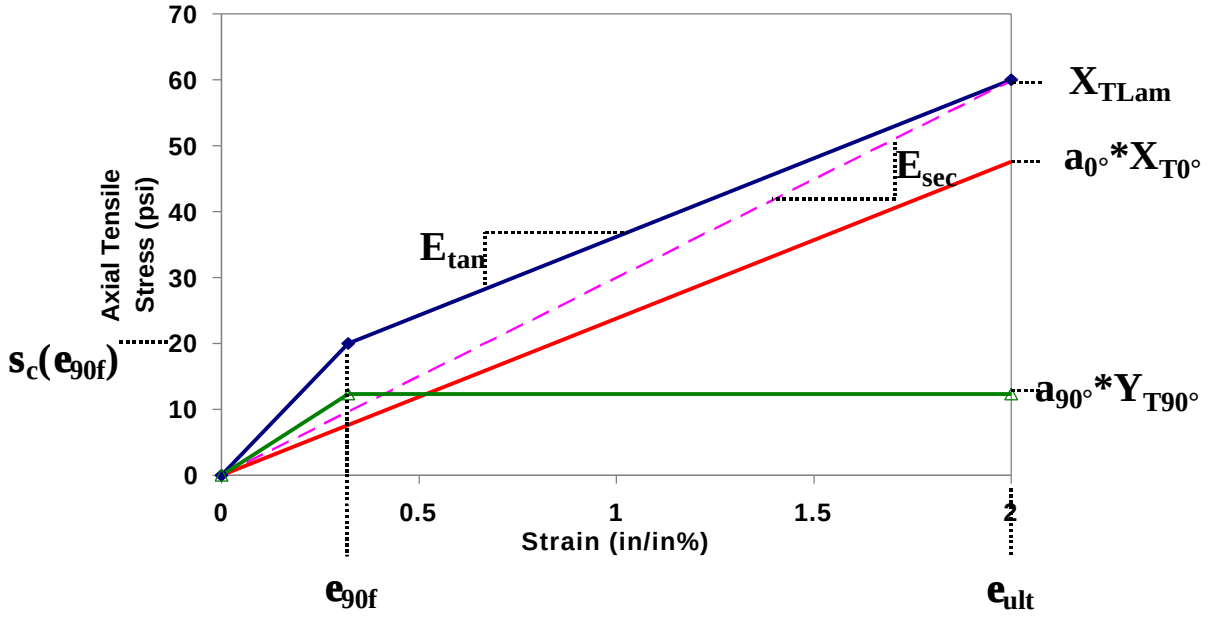

Figure 28: Designation for Extraction of Ply Level Strength and Stiffness

Cross-Ply Laminates Off-Pultrusion-Axis Tensile Performance

Testing of the CP1 cross-ply laminate, transverse to the pultrusion direction, revealed lower off-axis ply failure strain, lower ultimate failure strain, and slightly lower tensile stiffness compared with testing along the pultrusion axis. For CP1 laminate tested transverse to the pultrusion axis, the transverse failure strain of the off-axis plies was reduced from 0.032% to 0.023%. The average ultimate failure strain for CP1 tested transverse to the pultrusion axis was reduced from the axial value of 0.0208% to 0.0129%. Both these reductions are a direct result of the greater fiber undulation in the direction transverse to the pultrusion axis. The fiber undulation creates a bending strain in the fiber bundle which when bonded well to the matrix exerts an equal strain in the matrix. Both fiber and matrix will result in lower laminate failure strength/strain as a result of this higher strain concentration. The average and typical stress/strain curve of CP1 laminate tested transverse to the pultrusion axis is shown in Figure 29 and Figure 30. Short delaminations were seen to propagate from the matrix cracks for the nonsymmetric CP1 laminate but were not seen in the symmetric CP2 laminate.

Quasi-Isotropic Laminates- Axial Tensile Performance

Considering quasi-isotropic laminate, $(0,90,\pm45,0,90)_{2T}$ designated QI2 in Table 2, tested along the pultrusion axis was similar to CP1, both having balanced 0°, 90°, ±45° plies, as seen in Table 2. In turn, QI1 was similar to CP2, both having same ratio of 0° to 90° plies as CP2. In both cases, off-axis ply failure strains were similar also. Off-axis ply failure strain of QI2 was 0.37% similar to 0.32% of CP1, and the off-axis ply failure strain of QI1 was 0.22%, the same as CP2. The ultimate failure strains of QI2 and QI1 being 2.06% and 2.00%, respectively, were

within the standard deviation of each other, the cross-ply and the unidirectional laminates. Little fiber undulation was apparent for any of the cross-ply or quasi-isotropic laminates when tested along the pultrusion axis. These similarities were not surprising. The ultimate failure strain is dependent upon the fiber undulation, and the fiber undulation, in turn, is dependent upon the ply thickness, fiber bundle thickness, and the gap between fiber bundles which is the same for CP1 and QI2 and for CP2 and QI1. The off-axis failure strain is dependent upon the fiber undulation and the off-axis ply thickness which again are the same for these composites.

The microcracking and delamination histories of these quasi-isotropic laminates were not studied quantitatively. In general, the microcracking initiated in the 90° transverse plies to the load direction at low strains, followed quickly by microcracking in the ±45° plies, and finally slight edge delamination initiating from the intersection of adjacent 90° and ±45° ply microcracks. The microcracking in the 90° plies saturated quickly but the ±45° plies continued to develop more microcracks until fracture. The range over which microcracking and delamination occurred can be qualitatively measured by the derivative of the stress with respect to strain. The derivative of the stress/strain curve is the instantaneous tangent modulus. The instantaneous tangent modulus of QI2 laminate plotted as a function of strain level, as seen in Figure 33 is seen to most closely match the CP1 Tangent modulus curve. This is reasonable since QI2 and CP1 are composed of the same stitched fabric. For quasi-isotropic laminates, QI1 and QI2, bilinear stress/strain curves existed but were not as linear as the cross-ply laminates due to the more gradual degradation of the ±45° plies. Average and typical stress/strain curves for these laminates are shown in Figure 29 and Figure 30.

Quasi-Isotropic Laminates- Off-Pultrusion-Axis Tensile Performance

Testing transverse to the pultrusion direction revealed a much lower, transverse and ultimate failure strain and slightly lower stiffness than the same laminate tested transverse or at angle to the pultrusion axis. For QI2 laminate, tested at 0°, 45° and 90° to the pultrusion axis, the off-axis failure strain was reduced from 0.037 to 0.021 to 0.019%. The ultimate failure strain for QI2, tested at 0°, 45° and 90° to the pultrusion axis, was reduced from axial value of 0.0206% to 0.0193% to 0.0159%. This reduction in failure strain was attributed to the fiber undulation of the off-axis plies caused by the wide spacing of the axial fiber bundles. Average and typical stress/strain curves for quasi-isotropic laminate QI2 tested off-axis to the pultrusion direction are shown in Figure 29 and Figure 30.

Table 4: Glass/Vinyl Ester Laminate Measured Quasi-Static Tensile Strength, Stiffness, & Failure Strain and Standard Deviations

		#	V_f	e_{90f}	$E_T(<e_{90f})$	$E_T(>e_{90f})$	X_T	e_{xf}	$E_S(e_{xf})$
Desig-nation	**Ply Orienta-tion**	**of Speci-mens**	**% Fiber**	**90 °**	**Tangent**	**Tangent**	**Ultimate**	**Failure**	**Secant**
	Degree	**Tested**	**Volume**	**Failure Strain**	**Tensile Modulus**	**Tensile Modulus**	**Strength**	**Strain**	**Modulus**
					$\varepsilon_x < \varepsilon_{90f}$	$\varepsilon_x > \varepsilon_{90f}$			
				%in/in	Msi	Msi	Ksi	%in/in	Msi
CP1	$(0,90)_{5T}$	9	56.2	0.32 ± 0.05	3.961 ± 0.172	2.919 ± 0.123	62.4 ± 1.9	2.077 ± 0.203	3.030
CP1at 90°	$(90,0)_{5T}$	3	56.2	0.23 ± 0.03	3.749 ± 0.285	2.907 ± 0.138	36.4 ± 10.7	1.290 ± 0.521	2.820
CP2	$(0,90)_{3s}$	13	57.3	0.22 ± 0.02	3.503 ± 0.146	2.235 ± 0.156	45.7 ± 3.4	1.907 ± 0.147	2.394
QI1	$(90,0,(\pm45)_2,0,90)_{2T}$	10	56	0.22 ± 0.03	2.800 ± 0.087	1.576	34.8 ± 0.8	2.003 ± 0.074	1.740
QI2	$(0,90,\pm45,0,90)_{2T}$	10	56.3	0.37 ± 0.08	3.499 ± 0.294	2.382 ± 0.129	51.9 ± 2.0	2.060 ± 0.155	2.550
QI2 at 45°	$(\pm45,90,0,\pm45)_{2T}$	10	57.6	0.21 ± 0.02	2.736 ± 0.151	1.393 ± 0.102	31.3 ± 1.4	1.933 ± 0.174	1.620
QI2 at 90°	$(0,90,\pm45,0,90)_{2T}$	3	56.3	0.19 ± 0.02	3.423 ± 0.108	2.100 ± 0.136	35.4 ± 1.6	1.588 ± 0.12	2.230

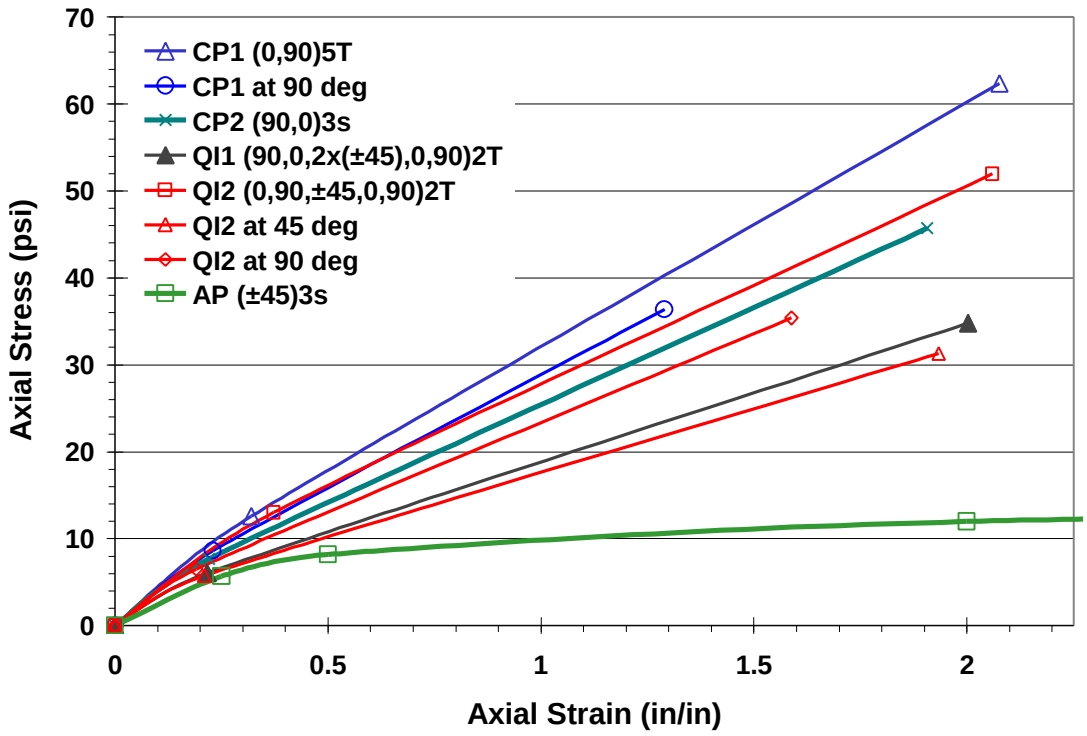

Figure 29: Average Quasi-Static Laminate Stress/Strain Response

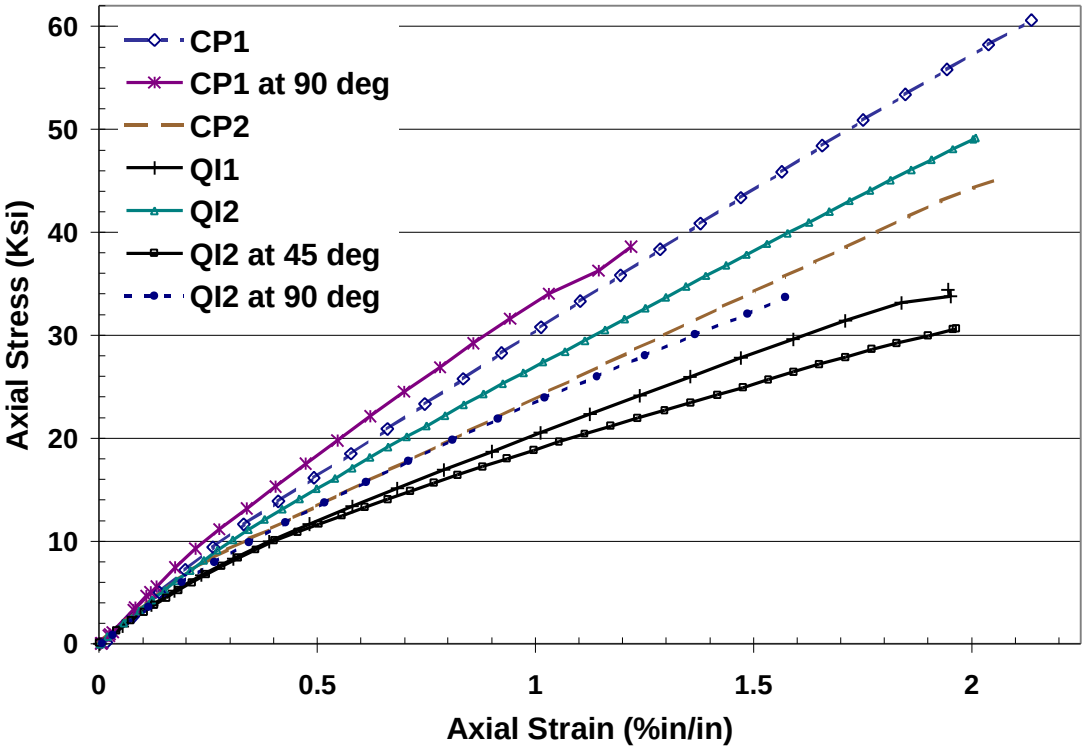

Figure 30: Typical Quasi-Static Laminate Stress/Strain Response

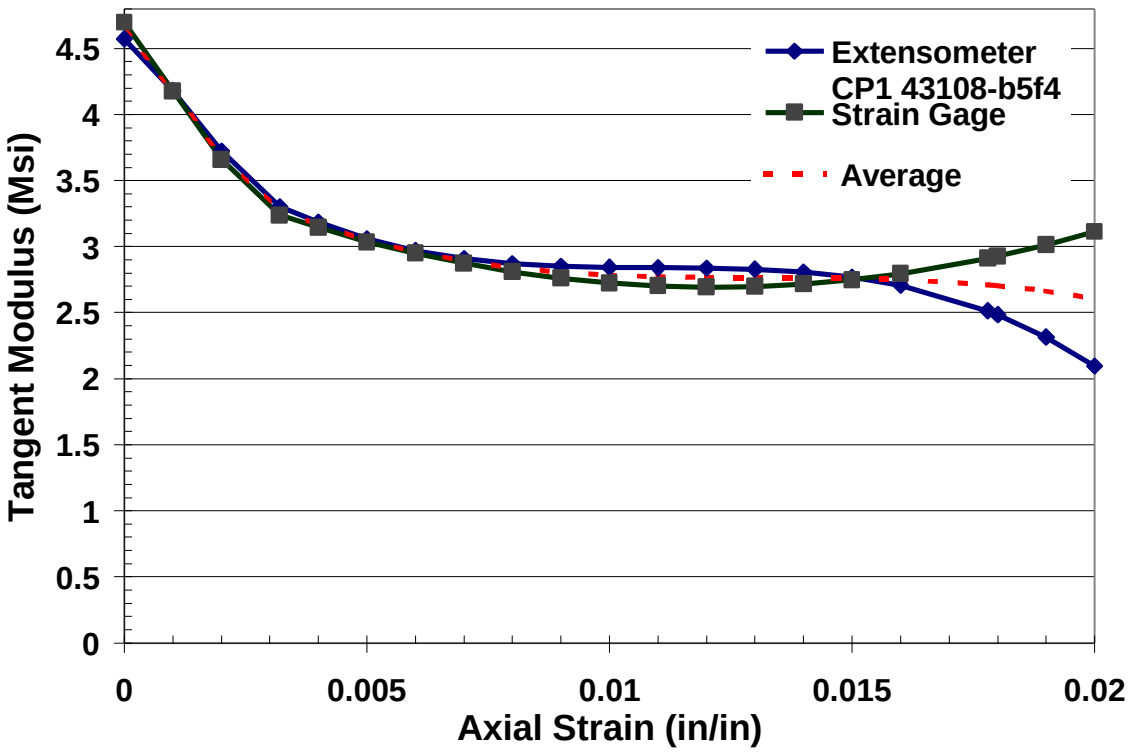

Figure 31: CP1Tangent Modulus from Derivative of Quasi-Static Stress Strain Curve

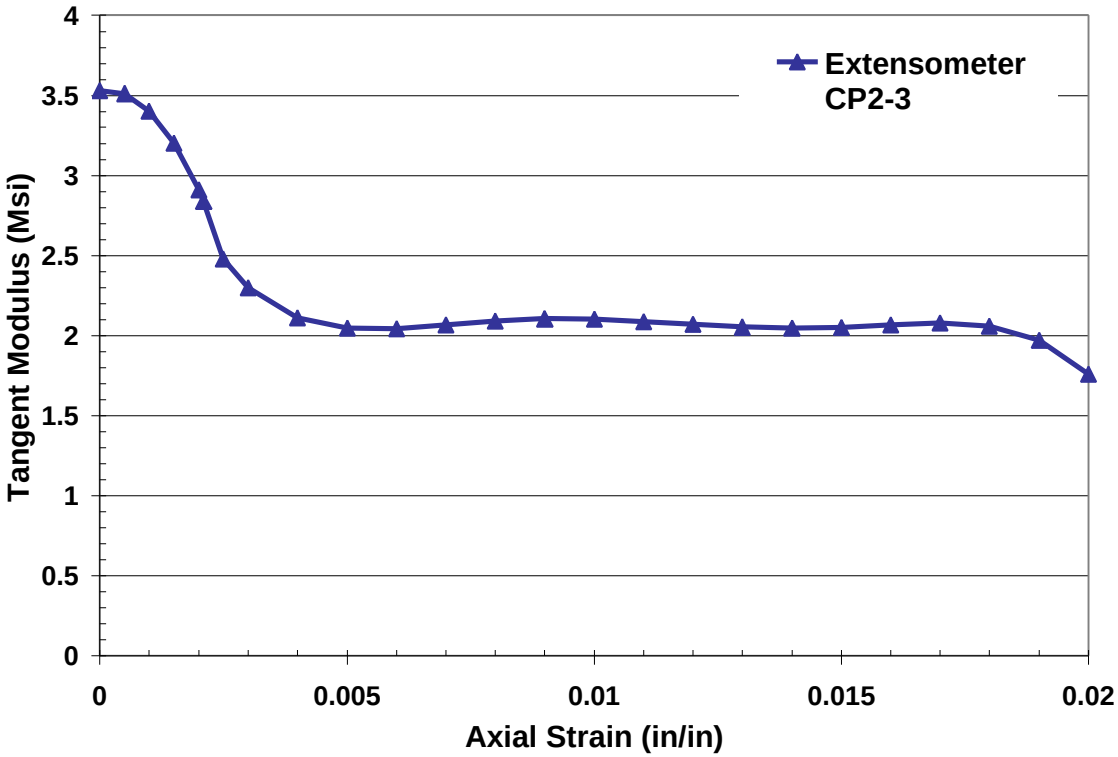

Figure 32: CP2Tangent Modulus from Derivative of Quasi-Static Stress Strain Curve

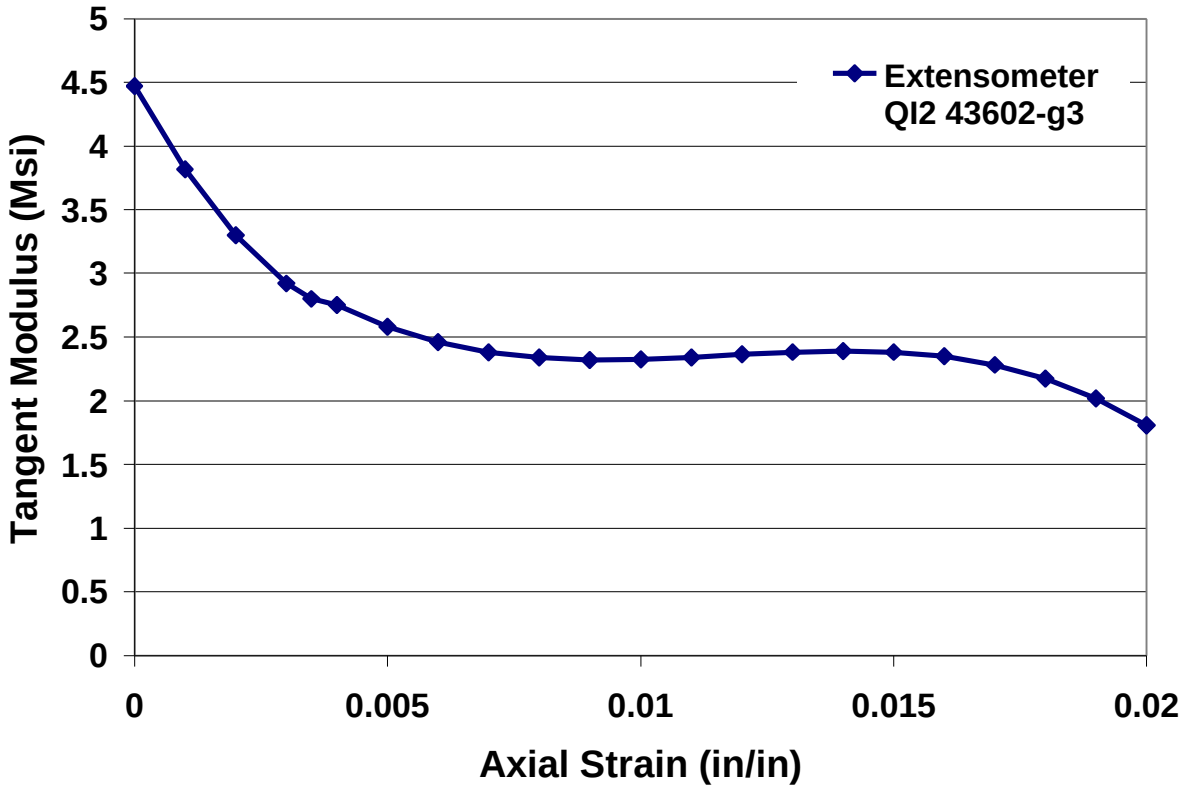

Figure 33: QI2 Tangent Modulus from Derivative of Quasi-Static Stress Strain Curve

Angle-Ply Laminate Shear Performance

Angle-ply laminates average behavior is seen in Figure 34. The angle-ply laminate was fabricated from the (90,0)3s CP2 laminate cut at 45°; therefore, the stitch was a tricot stitch rather than the blind stitch of the ±45° plies. With the Tricot stitch holding each ±45° ply together, the laminate in quasi-static tension never fully separated but reduced to 10-20% of original stiffness. The knee in the stress/strain curve indicating that microcracking began at 0.25% axial strain or 0.4% shear strain. Microcracking progressed steadily until necking occurred rapidly in a localized region across the entire width of the specimen.

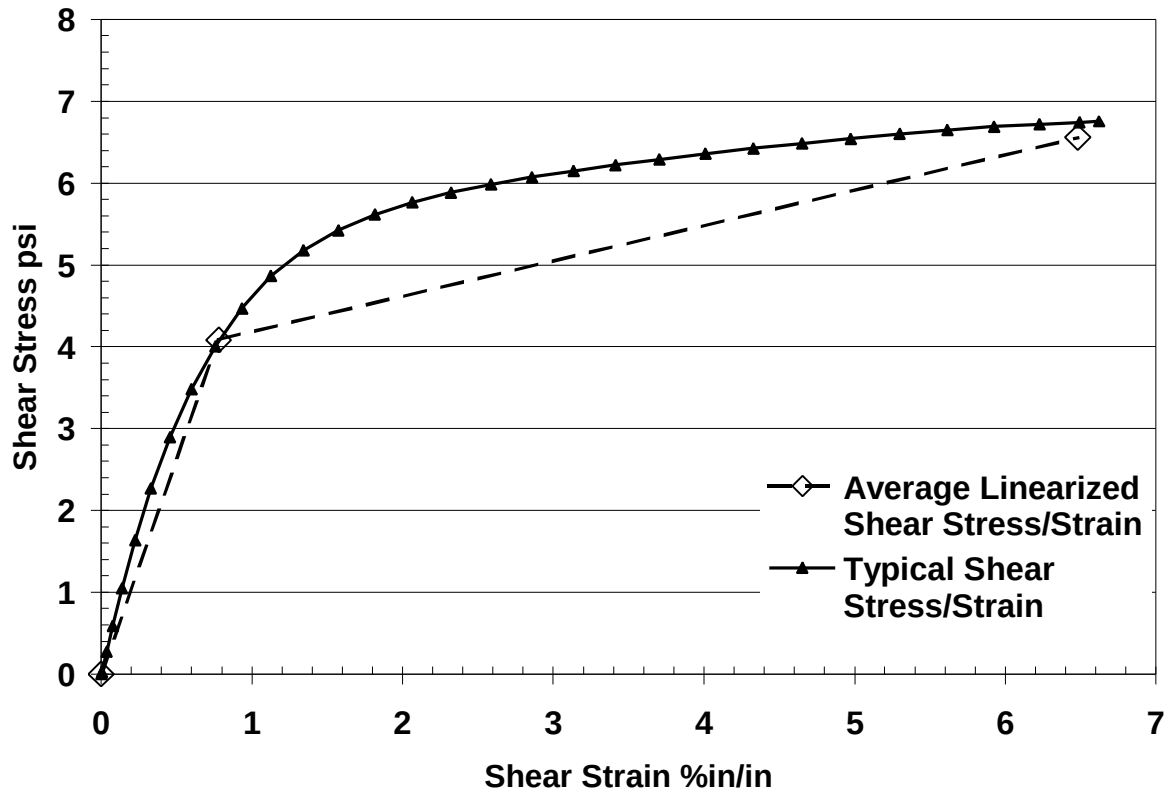

Figure 34: Typical and Average Shear Stress/Strain Response from ±45 ºTensile Test

Summary of Quasi-Static Laminate Properties

The ultimate failure strain and the transverse failure strain of off-axis plies for these CRTM pultruded cross-ply and quasi-isotropic laminates are the laminate properties which can be directly compared with values found in literature. Ultimate laminate strain is equal to the ultimate fiber strain in the direction of loading, but strength is dependent upon the tensile, shear, and transverse ply level properties of each ply in the laminate, all of which may vary the ultimate strength greatly. Off-axis ply failure strain of cross-ply and quasi-isotropic laminates, result when the fiber, matrix or fiber/matrix interfacial fail in the plies perpendicular to the applied load. This off-axis ply failure strain is dependent upon the residual cure stresses, the thickness of the transverse plies, and the properties of the fiber, matrix, and interface. Thus by comparison relative strength of the matrix and fiber/matrix interface can be studied.

Off-axis ply failure strain of polyester/E-glass cross-ply laminates, reported by Bailey, ranged from 0.13 to 0.60% [26], for cure temperatures ranging from 130° C to room temperature respectively. The off-axis ply failure strain of 0.5 to 0.63% [20] for an epoxy/E-glass cured at 100° C with 150° C post cure was also reported. Bailey proved through experimentation that the off-axis failure strain of cross-ply laminates was dependent upon thickness of the off-axis plies [20,21,26,27]. In general, epoxies are tougher and have low thermal and chemical shrinkage during cure than both vinyl ester and polyester; therefore, epoxy laminates have lower residual stress after cure. This translates into higher off-axis ply failure strains. Current testing shows transverse failure strain ranging from 0.22-0.37% for CRTM pultruded vinyl ester/E-glass

laminates. This is lower than Bailey's epoxy range and within the polyester range. Off-axis ply failure strains were reduced when tested transverse to the pultrusion axis. For CP1, transverse failure strain was 0.32% for laminate tested in the pultrusion direction but 0.23% for the laminate tested transverse to pultrusion direction. For quasi-isotropic laminate QI2, transverse failure strain was 0.37% for laminate tested in the pultrusion direction, 0°, but 0.21% for tests performed 45° to the pultrusion axis, and 0.19% for tests performed 90° to the pultrusion axis. The off-axis ply failure strain and the ultimate axial fiber failure strain are substantially reduced when these CRTM pultruded laminates are loaded off-axis to the pultrusion direction. This is due to the higher fiber undulation induced in these off-axis plies due to the axial fiber bundle and gap of the non-woven fabric geometry created by the tricot stitch as seen in Figure 6 and Figure 9.

Ultimate in-situ fiber failure strain and strength comparisons are shown in Table 4, Figure 29, and Figure 30. These pultruded vinyl ester/E glass laminates fall near the bottom of the vinyl ester range, in the middle of the polyester/E-glass range, and below the lowest performing of the epoxy/E-glass laminates. The pultruded vinyl ester/E-glass laminates tested in this research had a range of failure strains from 1.29 to 2.08%. The failure strain of the vinyl ester matrix was estimated at 1.9% using a cure process and ratio of low accelerator and styrene most similar to the pultrusion process, which would not fracture the neat resin specimen upon cool down. Failure strains of laminates tested transverse to pultrusion axis show great reductions in failure strains compared with the laminates tested aligned to pultrusion axis. This was due to greater fiber undulation in the off-axis plies. The axial fiber bundle aligned with the pultrusion axis was gathered by the tricot stitch of the non-crimp fabric leaving gaps between bundles of approximately one quarter to one half the bundle width. The off-axis plies adjacent to the axial fiber bundles were forced into this undulating pattern of fiber bundle and gap. For cross-ply laminate CP1, the strain to failure dropped from 2.08 to 1.29 %, greater than 37% reduction which approaches brittle resin woven fabric properties. For quasi-isotropic laminate QI2, the strain to failure dropped from 2.06% at 0°, to 1.93% at 45°, to 1.59% at 90° to the pultrusion axis or, a total of 23% reduction in failure strain. In addition, reductions can be seen when fiber bundle size, transverse to the pultrusion axis, was increased. Laminate CP2 with a 0°-90° ply ratio of 40-60, compared to CP1, with a 0°-90° ply ratio of 50-50, had a 8% reduction in axial ply strength, $X_{T0°}$, and 2% reduction in axial ply stiffness, E_1 when tested along the pultrusion axis. The geometry of thicker fiber bundles transverse to the pultrusion axis created higher axial fiber undulation, thus reducing the strength and stiffness.

Extraction of Ply Level Quasi-static Properties from Measured Laminate Data

Extracted Method from Cross-Ply Laminates

Ultimate laminate strength, strain, and transverse ply failure strength and strain (knee in stress/strain curve) were averaged and a generic stress strain curve was obtained.

From this average laminate stress/strain curve, constituents' stiffness and strength were obtained by a simple mechanics of materials approach in which Possion effect was accounted for. Assuming elastic-fully plastic lamina behavior of the transverse plies, a force balance of the cross-ply laminate can be converted to stress and stiffness if linearly elastic stress/strain relations are assumed,

Equation 13

$$F_C = F_0 + F_{90}$$
$$s_C = a_0 \cdot s_0 + a_{90} \cdot s_{90}$$

From the laminate stress/strain curve, there are two distinct strains, transverse failure strain and ultimate failure strain of which the laminate stresses are known. From these two points and the assumption that stress in the transverse plies are linearly elastic/fully plastic, that E_0 is constant, the force balance can be solved as shown below.

Equation 14

$$s_C(e_{90f}) = a_0 \cdot E_0 \cdot e_{90f} + a_{90} \cdot E_{90}(e_{90f}) \cdot e_{90f}$$
$$s_C(e_{ult}) = a_0 \cdot E_0 \cdot e_{ult} + a_{90} \cdot E_{90}(e_{ult}) \cdot e_{ult}$$
$$E_{90}(e_{ult}) = \frac{Y_T}{e_{ult}}$$
$$E_{90}(e_{90f}) = \frac{Y_T}{e_{90f}}$$

Four equations and four unknowns E_0, $E_{90}(\varepsilon_{ult})$, $E_{90}(\varepsilon_{90f})$, and Y_T, now may be solved. These terms are defined in Figure 28. Solution without Possion effect is;

Equation 15

$$E_1 = E_{0^\circ} = \frac{s_C(e_{ult}) - s_C(e_{90f})}{a_0 \cdot \left(e_{ult} - e_{90f}\right)}$$
$$Y_T = \frac{s_C(e_{90f}) - a_0 \cdot E_0 \cdot e_{90f}}{a_{90}}$$
$$E_2(e_{90f}) = E_{90}(e_{90f}) = \frac{Y_T}{e_{90f}}$$
$$E_2(e_{ult}) = E_{90}(e_{ult}) = \frac{Y_T}{e_{ult}}$$
$$X_{T0^\circ} = E_0 \cdot e_{ult}$$

Extraction Method for Quasi-Isotropic Laminates (Elastic Plastic Assumption for Transverse Stress and Use of Shear Stress Strain Curve)

For quasi-isotropic laminates, the angle plies must also be considered as shown in the force balance below.

Equation 16

$$F_C = F_0 + F_{90} + F_{\pm 45}$$
$$s_C = a_0 \cdot s_0 + a_{90} \cdot s_{90} + a_{\pm 45} \cdot s_{\pm 45}$$
$$s_C(e_{90f}) = a_0 \cdot E_0(e_{90f}) \cdot e_{90f} + a_{90} \cdot E_{90}(e_{90f}) \cdot e_{90f} + a_{\pm 45} \cdot E_{\pm 45}(e_{90f}) \cdot e_{90f}$$
$$s_C(e_{ult}) = a_0 \cdot E_0(e_{ult}) \cdot e_{ult} + a_{90} \cdot E_{90}(e_{ult}) \cdot e_{ult} + a_{\pm 45} \cdot E_{\pm 45}(e_{ult}) \cdot e_{ult}$$

There are six unknowns and two equations. Assumptions to obtain additional equations or reduce the number of unknowns must be made. The first is to assume that E_0 is constant. The second is to assume that the transverse plies act as similar cross-ply laminates behaved, $E_{90°}$ = E_2(quasi-isotropic) = E_2(cross-ply), and that the elastic plastic assumption also holds. Lastly, the elastic semi-plastic assumption is used for the $E_{\pm 45}$, or G_{12}, by using the quasi-static stress-strain curve obtained from the ±45° tensile test as shown in Figure 24 and 30. The ultimate axial failure strain was used to determine the $E_{\pm 45°}(\varepsilon_{ult})$ for each laminate. It should be noted that the Average curve is based upon 0.2% Offset and Ultimate Shear Stress to conform to standard methods. A 0.4% Offset Shear Stress, approximately 5 Ksi, would be a better fit to match the second portion of the stress/strain curve.

To include Possion effect, the above E_1 was used in a classical laminate theory (CLT) program and E_2 was fit to obtain the effective laminate stiffness $E_C^T(e_{90f})$ and $E_C^T(e_{ult})$ at ε_{90f} and ε_{ult}. Thus the elastic fully plastic was relaxed slightly.

Tables & Figures of Extracted Quasi-static Lamina Properties

Table 5: <u>Ply Level</u> Stiffness, Initial (e_x<e_{90f}) and Final (e_x<e_{xf}), <u>Extracted</u> from Quasi-Static Laminate Tests

Designa-tion	Stacking Sequence	E1	E1	E2	E2	G12	G12	v12
		Initial	Final	Initial	Final	Initial	Final	
		Msi	Msi	Msi	Msi	Msi	Msi	
CP1	(0,90)5T	5.71	5.71	2.21	0.367	NA	NA	0.283
CP1at 90deg	(90,0)5T	5.23	5.23	2.27	0.405	NA	NA	0.283
CP2	(0,90)3S	5.60	5.60	2.06	0.158	NA	NA	0.283
QI1	(90,0,2(+-45),0,90)2T	5.60	5.60	1.8	0.211	0.65	0.08	0.283
QI2	(0,90,+-45,0,90)2T	5.843	5.843	2.12	0.384	0.71	0.187	0.283
QI2 at 45deg	(+-45,0,90,+-45)2T	5.3	5.3	2	0.228	0.71	0.187	0.283
QI2 at 90deg	(0,90,+-45,0,90)2T	5.55	5.07	2.2	0.224	0.71	0.276	0.283

Table 6: Ply Level Strength Extracted from Quasi-Static Laminate Tests

Designa-tion	Stacking Sequence	Xt=E1*e_{xf}	Xt (CLT)	Yt=E2*ef90	Yt (CLT)	S(e_{f90})	S(e_{xf})
		Ksi	Ksi	Ksi	Ksi	Ksi	Ksi
CP1	(0,90)5T	117.6	117	7	8.8	NA	NA
CP1at 90deg	(90,0)5T	67.5	65.2	5.20	7.51	NA	NA
CP2	(0,90)3S	106.3	106.9	4.38	4.38	NA	NA
QI1	(90,0,2(+-45),0,90)2T	111.9	113.6	4.86	4.64	2.28	1.99
QI2	(0,90,+-45,0,90)2T	118.7	119.3	7.844	7.68	3.34	4.70
QI2 at 45deg	(+-45,0,90,+-45)2T	-	97.4	-	4.4	3.7	5.9
QI2 at 90deg	(0,90,+-45,0,90)2T	-	81.5	-	4.40	1.87	5.28

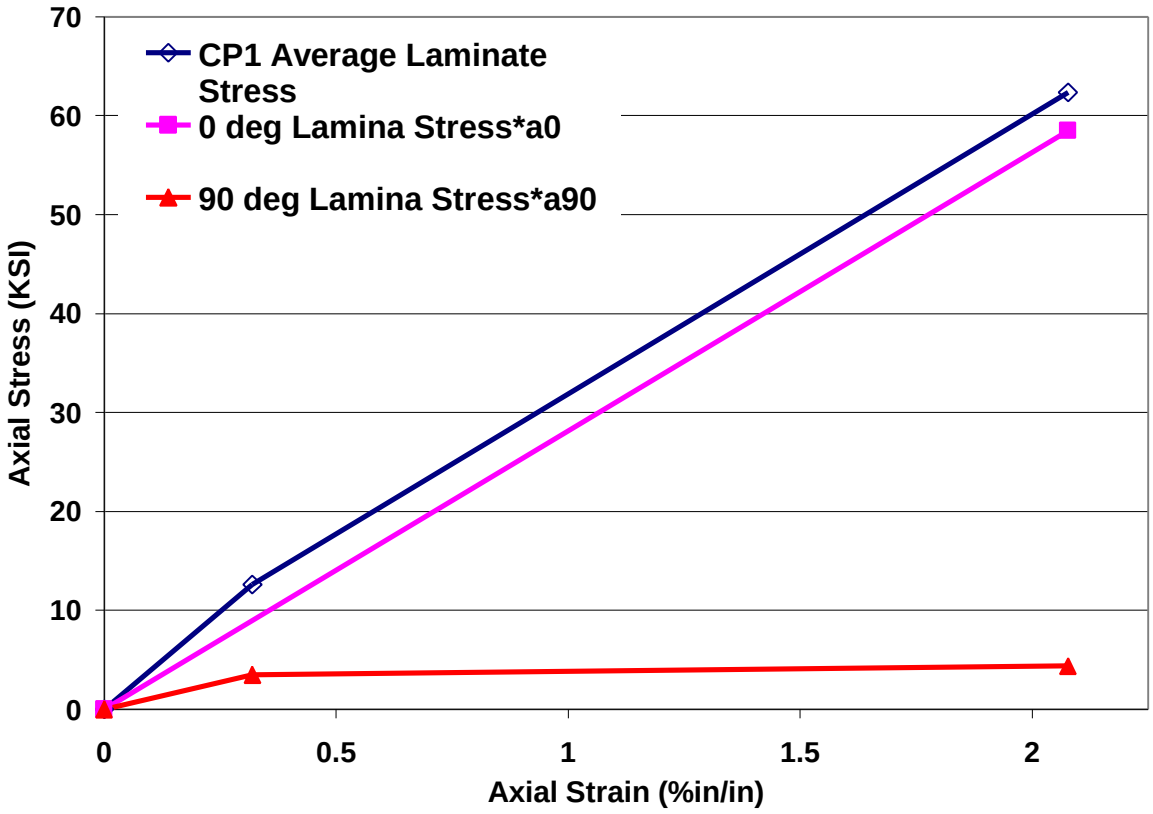

Figure 35: Cross-Ply Laminate CP1 at 0°

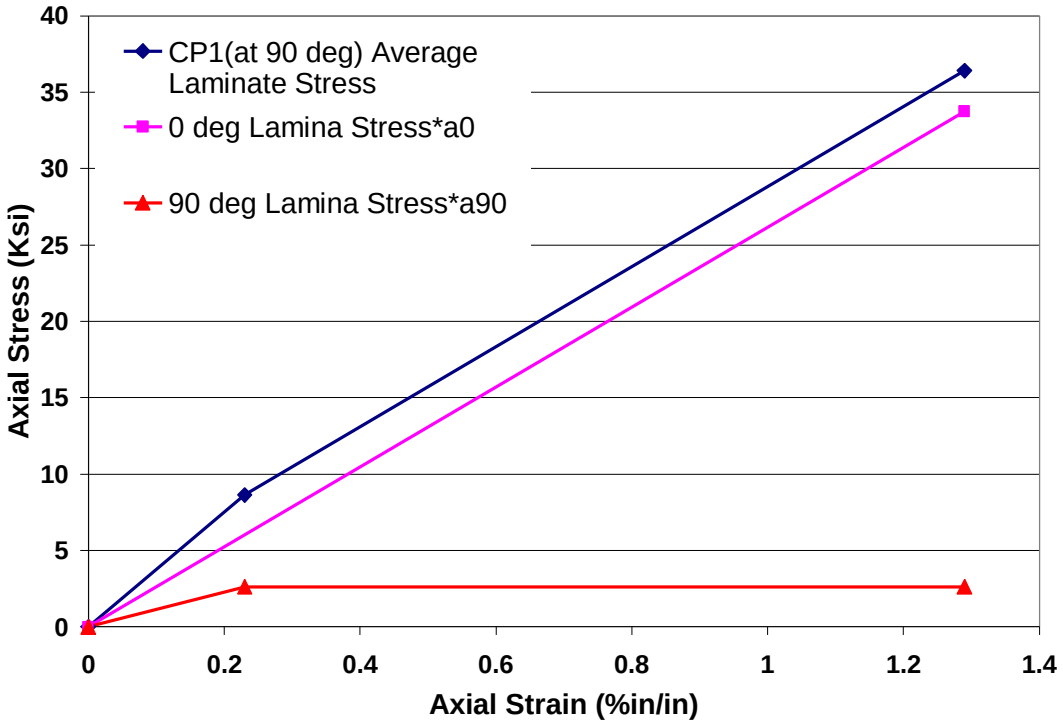

Figure 36: Cross-Ply Laminate CP1 at 90 °

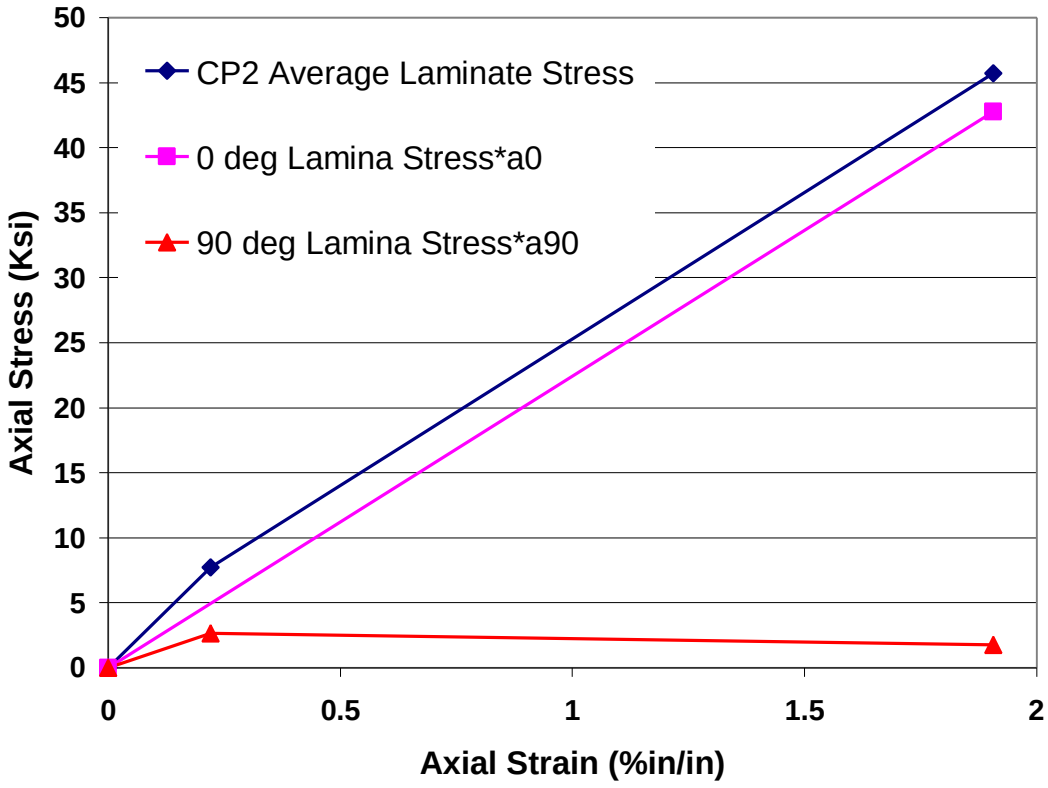

Figure 37: Cross-ply Laminate CP2 at 0 °

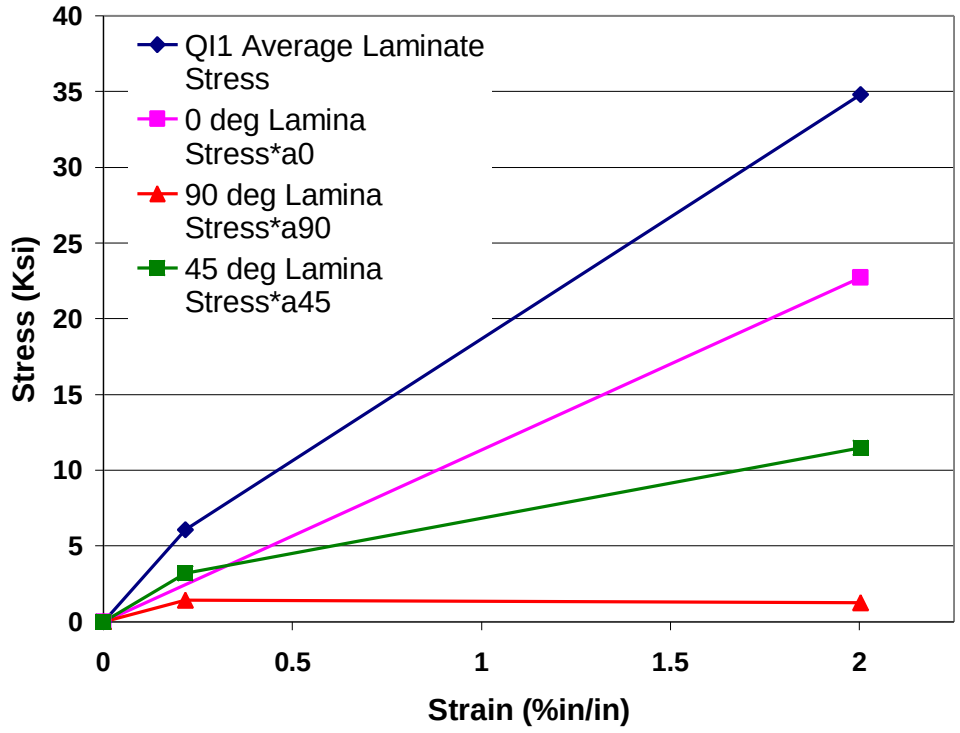

Figure 38: Quasi-Isotropic Laminate QI1 at 0 °

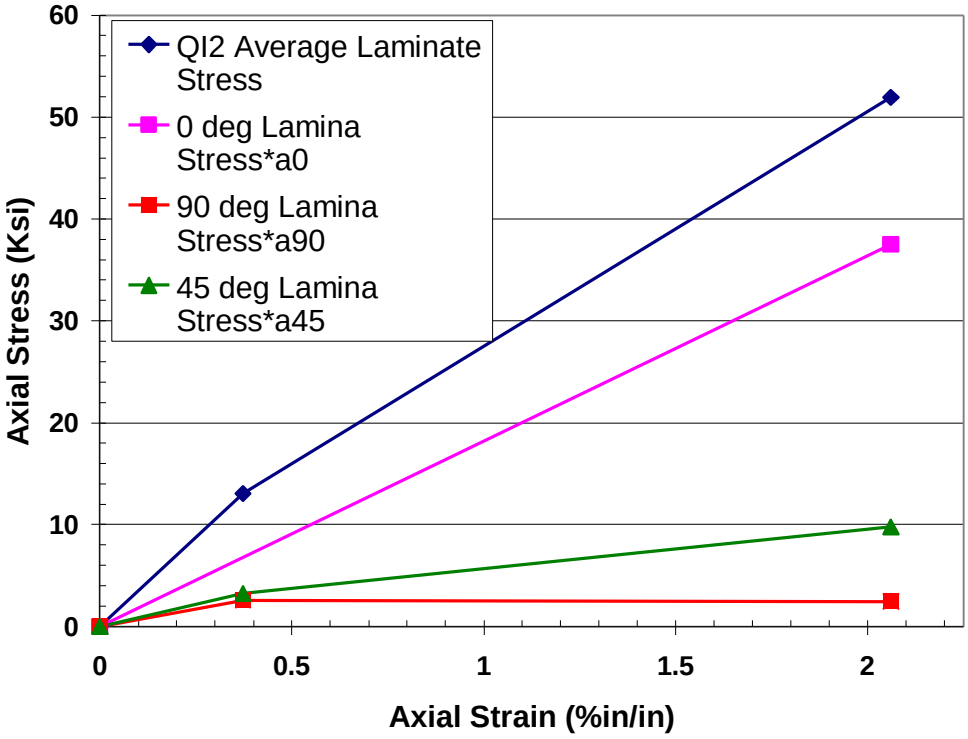

Figure 39: Quasi-Isotropic Laminate QI2 at 0 °

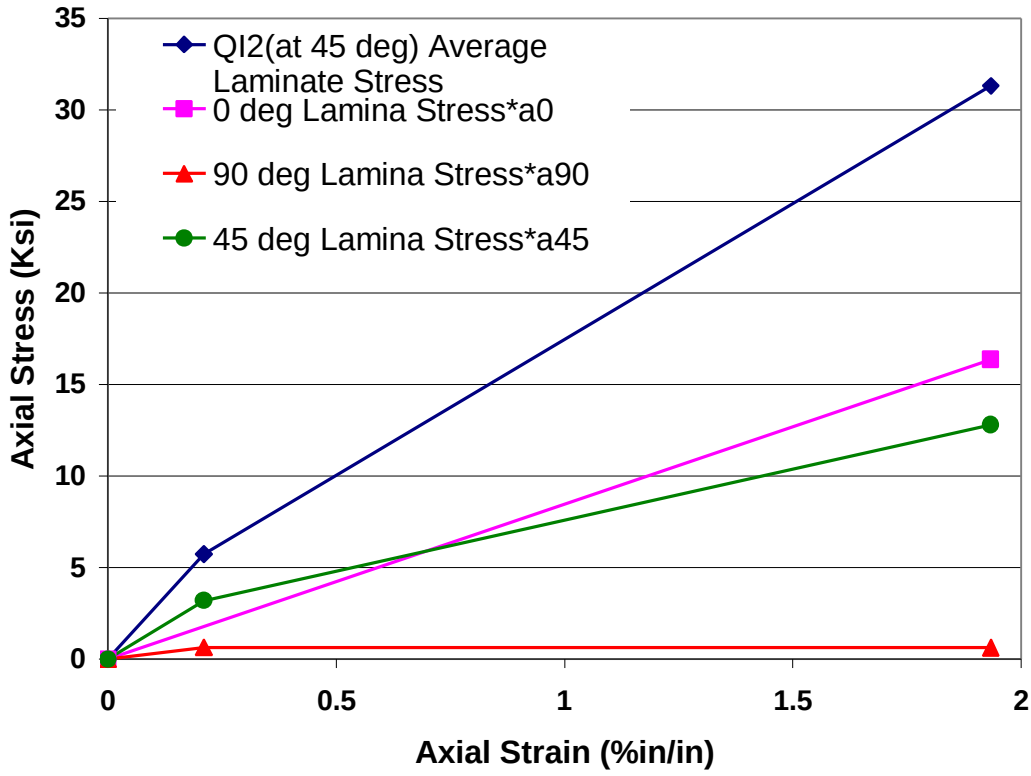

Figure 40: Quasi-Isotropic Laminate QI2 at 45°

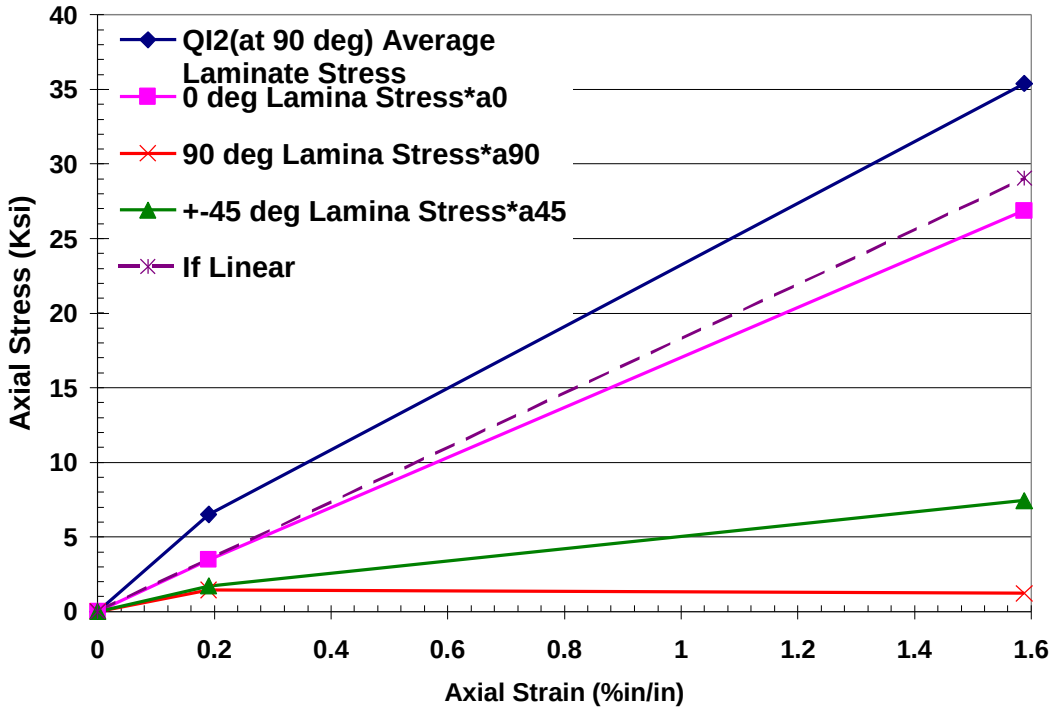

Figure 41: Quasi-Isotropic QI2 at 90°

Extracted Ply Properties Compared to Literature Predictions

Axial stiffness, E_1, of unidirectional CFRP composites is most often predicted by the rule-of-mixture (ROM) equation. For 71% fiber volume, the unidirectional composite axial stiffness is estimated by the ROM as shown in Equation 17. The CRTM pultruded vinyl ester/E-glass composite designated U1 in Table 3 has a stiffness $E_1=E_x$ of 7.47 Msi, which is 98% of the ROM prediction.

Equation 17

$$E_1(Vf) = Vf \cdot E_f + Vm \cdot E_m = 0.71 \cdot 10.5 + 0.29 \cdot 0.5 = 7.6 Msi$$

The 0° ply stiffness, E_1, extracted from the measured stiffness of the CRTM pultruded vinyl ester/E-glass non-woven stitched composite laminates, are 92-96% of the ROM calculation when applied load is parallel with the pultrusion direction. When applied load is transverse to the pultrusion axis, the extracted 0° ply stiffness, E_1, is 86-91% of the ROM calculation. The difference between the 0° ply stiffness, E_1, between loading along the axial and transverse to pultrusion axis is a 5 to 9% reduction in the transverse direction to pultrusion. The tricot stitch of the non-woven fabric forces the fiber into an undulating pattern, which was slight in the axial pultrusion direction but substantial in the transverse direction.

The transverse ply stiffness, E2, extracted from the measured stiffness of the CRTM pultruded vinyl ester/E-glass non-woven stitched composite laminates ranged from 1.8 to 2.2 Msi. The inverse rule-of-mixtures, Chamis' improved mechanics of materials, alternate improved mechanics, and Halpin Tsai Equations 2-6 for 56% fiber volume are 1.1, 1.4, 1.7, and 1.5 Msi, respectively. These predictions range from 50 to 94% of the extracted transverse ply stiffness from measured laminate data. The constraining effects of adjacent plies occurring in laminates are shown in data from Bailey and others [13,20,21,26,27], which can elevate the in-situ stiffness from the lamina stiffness. In-situ transverse stiffness will, therefore, be used for fatigue analysis.

The ply level shear stiffness, G12, was measured from the $(\pm 45°)_{3S}$ tensile test at 0.71 Msi. Shear stiffness calculated by inverse rule-of-mixtures, Chamis' improved mechanics of materials, alternate improved mechanics, and Halpin-Tsai solutions presented in Equation 2 through 6 for 56 % fiber volume were, 0.4, 0.53, 0.63, and 0.77 Msi.

Ply level strength predictions using the rule-of-mixtures and assuming off-axis plies retain no stiffness are not in great error for cross-ply laminates but is substantially in error when applied to quasi-isotropic laminates. Laminate strength prediction for a 56% fiber volume cross-ply with total failure in the transverse plies, is based upon only the 0° ply strength, $a_{0deg}*X_{T0deg}$. This is equal to

Equation 18

$$X_{TLam} = a_{0\deg} \cdot (Vf \cdot E_f + Vm \cdot E_m) \cdot e_{ult} = 0.5(0.56 \cdot 10.5 + 0.44 \cdot 0.5) \cdot 0.02 = 61 Ksi$$

Laminate strength, X_{TLam}, is equal to the stiffness ROM times the nominal strain to failure of 2%, and a_{0deg} is the percentage of 0° plies in the cross-ply laminate. This is 2% low from the CP1 axial laminate's ultimate strength of 62.4 Ksi. This ROM is not appropriate for quasi-isotropic laminates because the angle plies offer substantial stiffness and strength at failure. For example,

the laminate designated QI1 in Table 2 has an estimated laminate failure stress of $a_{0deg}*X_{T0deg}$ equal to

Equation 19

$$X_{TLam} = a_{0\deg} \cdot (Vf \cdot E_f + Vm \cdot E_m) \cdot e_{ult} = 0.202(0.56 \cdot 10.5 + 0.44 \cdot 0.5) \cdot 0.0203 = 24.6Ksi$$

verses the failure stress of 34.8 Ksi shown in Table 4 where X_{TLam} is the stiffness ROM times the nominal strain to failure, 2.03%, and a_{0deg} is the percentage of 0° plies in the quasi-isotropic laminate. This prediction is 29.5% lower than the actual measured laminate strength. The ±45° plies offer substantial stiffness at failure and must be taken into accounted to yield realistic strength and stiffness predictions. A much more accurate analysis of ply level properties can be obtained as described below. Represent the transverse stiffness, E_2, by using the off-axis stiffness reduction of the cross-ply laminate, which has the same ratio of 0° to 90° ply thickness. This utilizes the elastic-plastic assumption shown in Figure 35 for the transverse plies to the applied load. Secondly, represent the G12 shear modulus with an elastic-semi-plastic assumption shown in Figure 38 for the angle-plies, ±45°, which is obtained from the quasi-static ±45° tensile test shown in Figure 34. With these assumptions more accurate ply level properties may be extracted and are shown in Table 5 and Table 6. These ultimate ply level strength values from Table 6 divided by their fiber volume are shown in Figure 42 [37]. The CRTM pultruded vinyl ester E-glass laminates fall between polyester and epoxy laminates found in literature.

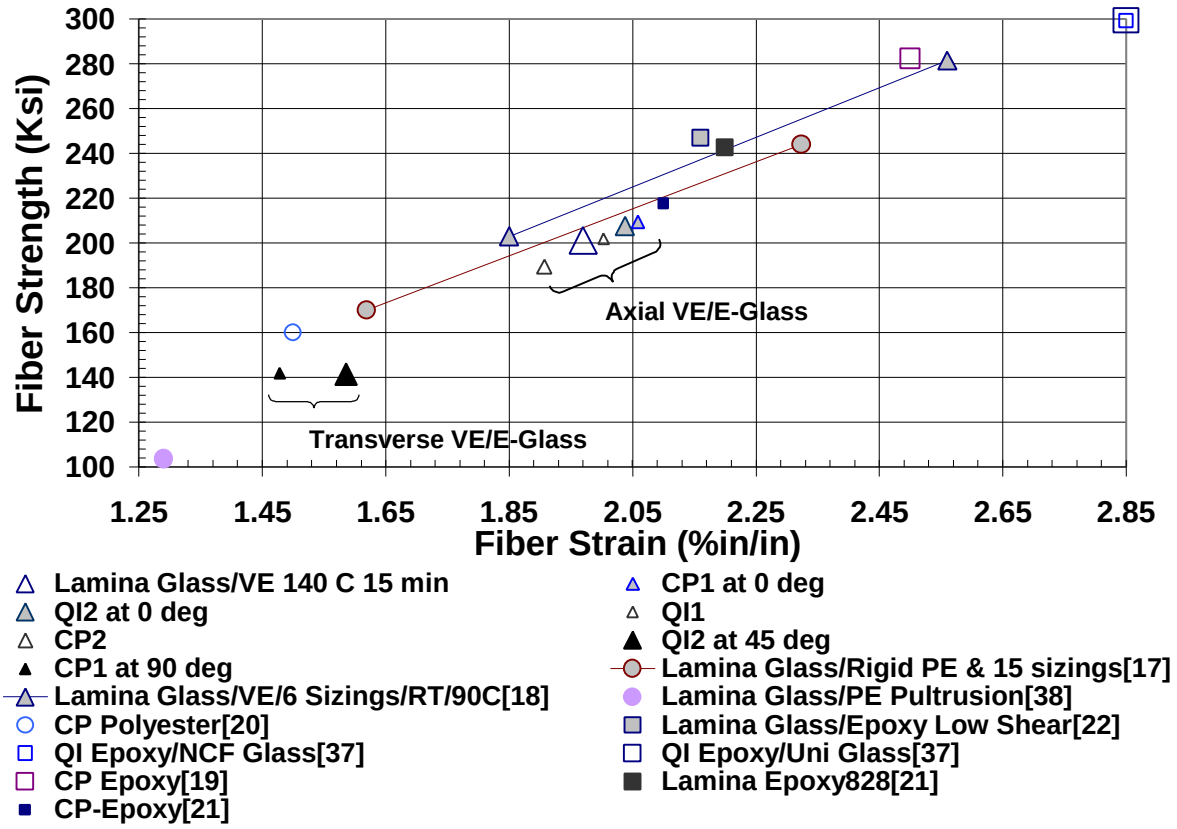

Figure 42: In-Situ Fiber Ultimate Tensile Strength/Strain Comparison with Literature.

The ply level strength, X_{Tf}, shown in Figure 28, extracted from the measured strength and stiffness data of the CRTM pultruded vinyl ester/E-glass non-woven stitched composite laminates, had much greater reductions when loaded in the transverse to pultrusion direction than the stiffness reduction noted above. For cross-ply laminate, CP1, from applied loading 0° and 90° to the pultrusion axis, the strength was reduced by 44% in the 90° loading test. For quasi-isotropic laminate, QI2, strength was reduced by 18% when loading at 45° to the pultrusion axis, and reduced by 32% when loading at 90° to the pultrusion axis. For these CRTM pultruded laminates fiber undulation is much greater in the direction transverse to the pultrusion axis. The tricot stitch of the non-woven fabric gathers the axial fiber into bundles with gaps of ¼ to ½ the width of the fiber bundle; when layers of fabric are stacked and compressed into the pultrusion die, the transverse plies are forced into these gaps. The stiffness and the strength suffer in the off-axis to pultrusion directions due to this fiber undulation.

From the literature review for cross-ply and quasi-isotropic laminates, it has been shown that the strain at which transverse and shear failure occurs as off-axis ply failure is dependent upon ply thickness, ply stacking sequence, fiber volume, strength and stiffness of the matrix, fiber, and interface, and residual stress state. Keis transverse strength is predicted with a strain concentration of 1.87 for 60 % fiber volume and as high as 9.2 strain concentration for fibers that are in contact with each other. Using 1.9% matrix failure strain and Keis' strain concentration factor predicts anywhere from 0.20% to 1.0% transverse failure strain. Keis doesn't consider thermal stresses, which would lower the strain to failure. When comparing actual composite transverse failure strain with the Keis' predictions as off-axis ply failure of the laminates of 0.19 to 0.37% for all laminates, it's seen that the upper bound of 1.0% strain is excessively high. The addition of residual laminate thermal strain and random variation of fiber packing, which would lower the transverse failure strain, can explain this.

Conclusions: Quasi-Static Evaluation

Several conclusions can be drawn from the quasi-static evaluation of CRTM pultruded vinyl ester/E-glass non-woven tricot stitched composite laminates including the physical description of as-processed laminates, the laminate strength and stiffness, and the ply level strength and stiffness extracted from the measured laminate properties. Physical description of as processed pultruded composite includes fiber undulation, resin rich regions, microcracking, delamination, and voids found in the fiber bundle. Fiber undulation of the plies aligned transverse to the pultrusion axis is significantly higher than the fiber undulation of the plies aligned along the pultrusion axis. The non-woven tricot stitched fabric gathers the axial fiber bundle aligned along the pultrusion axis leaving a gap between adjacent axial fiber bundles of ¼ to ½ the width of the axial fiber bundle. The fiber undulation occurs when the axial fiber bundles of adjacent plies in the laminate become nested into these gaps which forces the transverse and angle plies into an undulating pattern. This undulation can be exaggerated as shown in Figure 9, where two adjacent plies have their axial fiber bundles aligned of which a third ply's axial fiber bundle is nested, which creates an even greater off-axis fiber undulation. Microcracking occurs both axial and transverse to the pultrusion axis in the as-processed composites always parallel with the fiber and within a resin rich region. These resin rich regions occur when the axial fiber bundles of two adjacent plies are aligned which creates a large resin region between the fiber bundles as seen in Figure 20 and Figure 14. Delaminations are seen in Figure 20 stemming from the microcrack and running along the interface between 0° and 90° plies through a stitch. Microcracking and delamination in the as-process state is a result of the high thermal and

chemical shrinkage of the vinyl ester matrix which has 6% shrinkage of a neat resin specimen. Voids can be seen in Figure 12 within the fiber bundle, which could be a result of high fiber volume and inadequate injection pressures during the CRTM pultrusion process.

For the quasi-static evaluation of CRTM pultruded unidirectional, cross-ply, and quasi-isotropic laminates, ultimate failure strain, ε_{ult}, and transverse failure strain of the off-axis plies, ε_{90f} are of most interest for comparison purposes. Ultimate failure strain ranged from 1.29% to 2.08%. The ultimate failure strain of laminates loaded along the pultrusion axis is 1.91% to 2.08%, and ultimate failure strain of laminates loaded transverse to the pultrusion axis is 1.29% to 1.59%. Epoxy E-glass laminates have been reported in literature to have strains from 2.1 to 2.85%, and polyester E-glass laminates range from 1.25% to 2.3% as shown in Figure 42. These CRTM pultruded laminates fall at the low end of epoxy laminates and at the upper end of the polyester laminates.

The transverse failure strain of the off-axis plies to the applied load ranges from 0.19% to 0.37%. Bailey has reported transverse failure strains for polyester cross-ply laminates ranging from 0.13% to 0.60% and epoxy cross-ply laminates, which range from 0.55% to 0.60% for cure temperatures ranging from 130° C down to room temperature. Bailey also reported that the thickness of the transverse plies to the applied load affects the transverse failure strain. With very thin transverse plies, the transverse failure strain has been shown to increase above the ultimate failure strain for carbon/polymer laminates. Cross-ply laminate designated CP1 in Table 2 has thinner transverse plies to pultrusion axis than does CP2 cross-ply laminate. QI2 laminate has the same ratio of 0° and 90° plies as CP1, and QI1 laminate has the same ratio as CP2. QI2's transverse failure strain of the off-axis plies ranges from 0.32% to 0.37% verses CP2 and QI1 both at 0.22%. This follows Bailey's findings.

The failure mechanisms began with microcracking parallel to fiber in the plies off-axis to the applied load. These microcracks occur in both 90° and then in ±45° plies. Delamination occurred in the non-symmetric cross-ply laminate CP1 from the transverse microcracks at the 0°/90° interface. Delamination also occurred at the interface of 90°/±45° plies of the quasi-isotropic laminates initiating from the intersection of the microcracks in both 90° and ±45° plies and the edge of the specimen.

As the load is increased during quasi-static loading, microcracking accumulates in the plies off-axis to the applied load, and delamination may initiate from the microcracks and propagate between plies. The stiffness of the laminate and the off-axis plies are reduced due to the microcracking and delamination that occurs. The stiffness in the off-axis plies is reduced but does not reduce to zero. FEA or shear lag analysis shows that the region in the off-axis plies between microcracks does carry a reduced level of load but these techniques are rather complicated. A simple approach involving mechanics-of-materials involves the use of an elastic-plastic representation of the transverse ply response which is $E_{90°} = E_2$, as shown in Figure 28. With this elastic plastic assumption and the assumption that during the quasi-static testing, the axial stiffness, $E_{0°} = E_1$, is constant, the force balance and ROM formulation shown in Equation 14 can be solved to determine the ply level stiffness, E_1 and E_2, from which the strengths can be calculated. For quasi-isotropic laminates with 0°, 90°, and ±45° plies, an additional two stiffness values are added to the force balance Equation 16 which requires additional assumptions to reduce the number of unknowns to the number of equations. The assumptions are that $E_{0°} = E_1$, is constant, that the elastic-plastic assumption for transverse stiffness $E_{90°} = E_2$ from similar cross-ply is valid, and that the ±45° tensile stress/strain curve will be used to represent shear behavior. With these assumptions, the ply level stiffness, E_1 and E_2 can be determined. Equation 15 and

Equation 16 does not include the Possion effect, so after these equations were solved, Classical Laminate Theory (CLT) was used with the E_1 and G_{12} found from Equation 15 or Equation 16 to determine E_2 which implies that the elastic-plastic assumption is slightly relaxed.

Chapter 5: Literature Review for Fatigue of E-Glass Composite Laminates

Literature Review: Material Effects on Fatigue of Polymer/Glass Composites

A brief literature review will be presented on the fatigue of E-glass composite materials. This is introduced to show that many factors affect the fatigue performance of composite materials, test parameters as well as material properties. While the current research performed only one frequency, 10 Hz, and one R-ratio of maximum to minimum applied load, 0.1, and at room temperature conditions, one should be aware that the different material properties, test parameters, and environmental conditions could produce drastically different fatigue results. Fiber strength, modulus and configuration, matrix normal and shear strengths and moduli, interfacial bond strength, and residual curing stresses are material properties, which can affect fatigue performance. Fatigue frequency, or static fatigue, mean stress, and R-ratio are test parameters, which can affect fatigue performance. Test temperature, fluid immersion, and ultraviolet exposures are environmental conditions, which can affect fatigue performance.

Fiber properties play the most important role in fatigue performance [03]. Higher modulus fiber composites have higher fatigue resistance. High modulus graphite has nearly a flat maximum fatigue stress to fatigue cycles (S-N) curve resulting in sudden death behavior. E-glass fiber composites have a more gradual fatigue strength reduction of approximately 10% per decade of life, log(N) [03]. Mandell has shown that fatigue cycling below one million cycles, for glass composites of epoxy unidirectional and quasi-isotropic laminates ($0.16<V_f<0.5$), epoxy sheet molding compound (SMC), injection molded polycarbonate and nylon short fiber filled, polyester unidirectional and chopped strand mat, have slopes of approximately 0.1 on S-log N chart. [03] Woven composite laminates have been shown to have much lower S-N curves than cross-ply laminates with similar composition [03] and page 259 of [38] .as shown in Figure 43 and Figure 44 The out-of-plane fiber undulation increases the local stress state and decreases the fatigue resistance. Figure 43 shows the effects of fiber undulation on the S-N curves of a woven style 181 E-glass laminate compared to unidirectional lamina, and Figure 44 compares woven style 181 E-glass laminate with cross-ply. This fiber undulation plays an important role in the pultruded vinyl ester/E-glass non-woven tricot stitched laminates tested in this research.

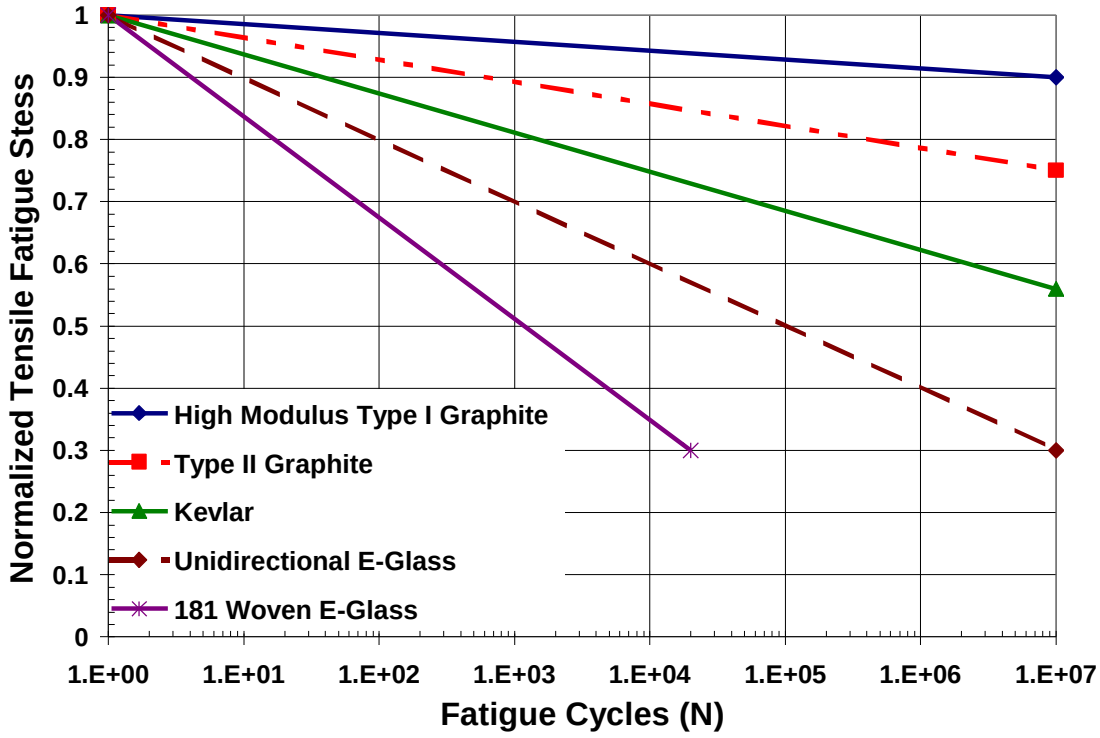

Figure 43: Unidirectional 181 Woven Tensile Fatigue Comparison [03]

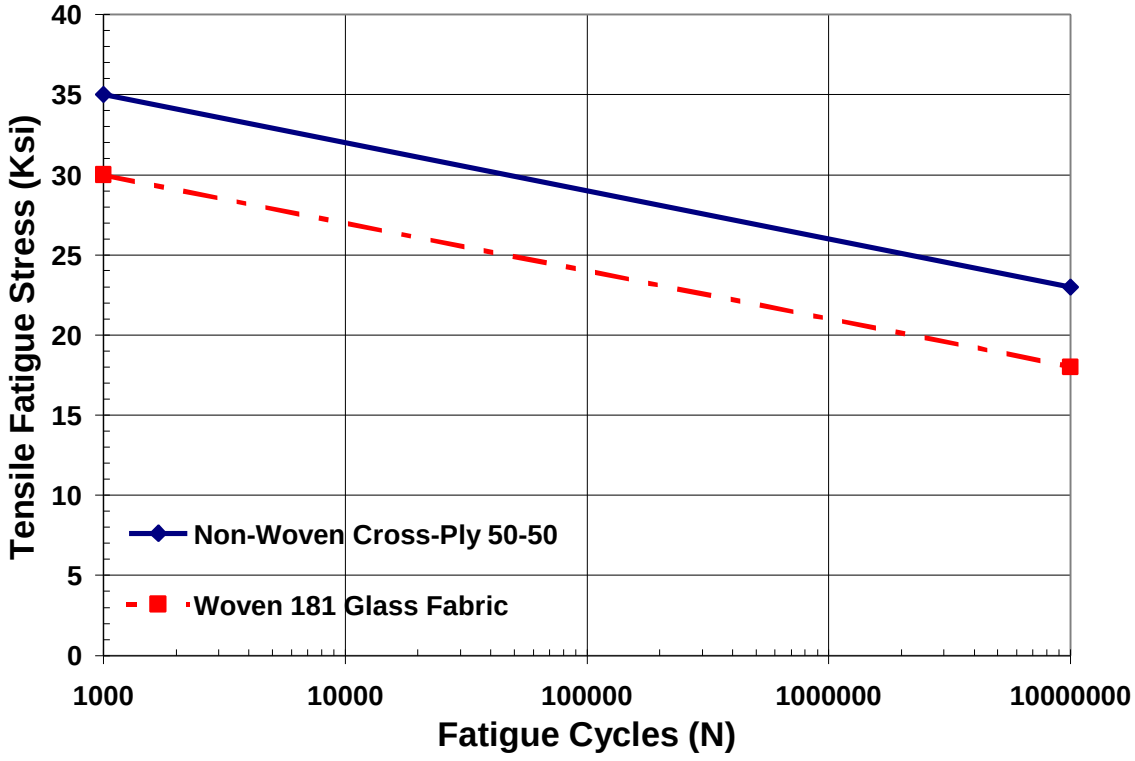

Figure 44: Non-Woven Cross-Ply and Woven 181 E-Glass Tensile Fatigue Comparison

Fiber orientation, also, has been shown to greatly affect the S-N curve. Rotem and Hashin have shown that angled-ply, epoxy/E-glass laminates greater than ±45° have nearly flat S-N curves while laminates below ±45°, have increasing slope with decreasing ply angle. [39] These flat S-N curves for laminates greater than ±45° are a result of the brittle-type nature of tensile matrix properties where the tensile and shear matrix properties are the main contributor in off-axis laminate strength. Matrix affects not only transverse and shear properties but also affects axial loaded unidirectional fatigue properties shown in Table 7; where the effects of low strength/stiffness resin verse higher strength/stiffness resin are show for a semi log S-N curve for fiber bundle specimens and unidirectional specimens [40]. The S/Sult intercept is higher and the slope B is steeper for the lower strength, more ductile matrix. For unidirectional laminates, the effect of brittle verses ductile matrix is reflected in the failure mode. If the matrix has lower ductility than the fiber, the matrix cracks causing bridging by the fiber, and eventually fiber fracture or delamination along the fiber/matrix interface caused splitting. If the matrix has higher ductility than the fiber, the fiber fractures multiple times along it's length shedding the over-load through shear of the matrix to adjacent fibers. For the CRTM pultruded laminates evaluated in this research, the ultimate failure strain of the resin is approximately 1.9%; therefore, the resin is brittle in nature rather than what is shown in Table 7 and Figure 45.

Table 7: Resin Effects on Strength, Stiffness & S-N Behavior

Resin	Mod-ulus Msi	Ultima te Stress psi	Strain at Ul-timate Stress %in/in	Failure Stress psi	Strain at Failure Stress% in/in	Compos-ite Type	S/Sult A	LogN B
815	0.3	6598	4	5250	14	Bundle	1	0.148
						Lamina	1.374	0.157
828	0.5	12382	5	12024	9	Bundle	0.847	0.097
						Lamina	1.093	0.111

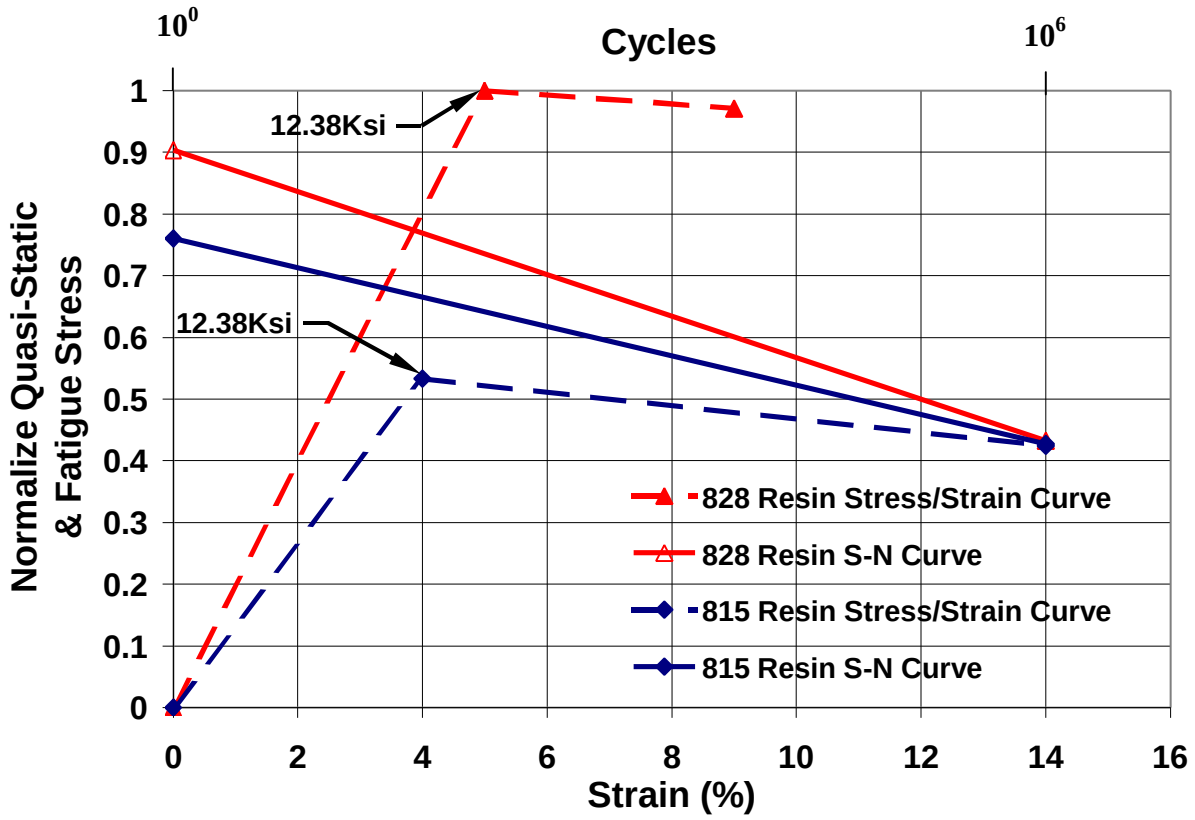

Figure 45: Matrix Stress/Strain Curves and Associated Unidirectional Epoxy/E-Glass S-N Curve [40]

Failure Mechanisms of Polymer/Fiber Composites

Kim and Ebert [41] have discussed three stages in the fatigue failure of Derakane 470-45 vinyl ester/E-glass unidirectional composites, cured at 185°F. Within the first few cycles, a reduction in stiffness was observed which when analyzed was associated with propagation of flaws on the surface of the fibers. During Stage 1, these fiber surface flaws become larger but tend to stabilized becoming more blunt. Stage 2 includes interfacial failures coalesce into matrix transverse and shear cracks which propagate around the fibers and coalesce in a plane parallel to the loading direction. During Stage 2, the stiffness remains nearly constant; yet, the hysteresis loop energy increases. Stage 3 includes sudden complete fiber failure on this parallel plane created from coalesce of matrix cracks; this results in through delamination, the sudden drop of stiffness, and increase in hysteresis loop energy. [41]

Fatigue of cross-ply and quasi-isotropic laminates includes the additional failure mechanisms of off-axis plies. For cross-ply and quasi-isotropic laminates, the matrix properties affect the knee in the stress/strain curve, which reflects the initiation of matrix cracking in the transverse and angle or off-axis plies. In fatigue, this transverse microcracking occurs rapidly at fatigue loads near this knee point, often occurring in the first few fatigue cycles. Reifsnider [38] has defined 3 regions of damage development in cross-ply and quasi-isotropic laminates. In Region I matrix microcracking occurs parallel to the transverse fiber through the thickness of off-axis, transverse and angle, plies. The microcracking develops quickly if the fatigue load is near the stress/strain knee but stabilizes quickly into a uniform spacing designated the

characteristic damage state (CDS). This damage state developed in fatigue is often similar to damage developed in quasi-static testing. The CDS is a function of the material properties, ply thickness, and stacking sequence. The CDS has been found to be independent of load history, environment and, residual stresses in many cases page 270 of [38]. The rate of microcracking over the remainder of life is very gradual with an increase often occurring near the end of life. In Region II coupling and growth of matrix microcracks occurs that ultimately lead to debonding at fiber-matrix interfaces and delaminations at the interface between plies.

The susceptibility of ply level delamination is dependent upon the ply stacking sequence, fiber orientation, and ply properties. Agarwal and Dally found that delaminations do not propagate for nearly 95% of the fatigue life at a given stress level [42]. The last 5% of fatigue life, delaminations propagate rapidly across the 0°/90° interfaces prior to fiber failure in the 0° plies [38]. Edge delamination may occur if the laminate stacking sequence yields high interlaminar stresses. Delamination leads to decreased load sharing of the off-axis plies, which increase the stress in the 0° plies. The principal failure mechanism in Region III is fiber failure in the 0° plies leading to fiber/matrix interface delamination denoted as longitudinal splitting. These fiber fractures often initiate near microcracks in adjacent off-axis plies. Fiber fracture occurs in both region II and III but at a much higher rate in region III [38].

Frequency, R-ratio and Waveform Effects on S-N Performance of E-glass Laminates

Mandell and Meier [43] have compared static fatigue to various square wave cyclic forms. A S-logN fatigue curve fit is compared below to static fatigue which shows 3-4 times increase in slope B of the fatigue cycled verses static fatigue. Time, t, was used in Equation 20 since the authors consider creep also; "t" may represent "N" cycles when in cyclic fatigue and time in second when in static fatigue.

Equation 20

$$S = A - B \cdot Log(t)$$

Also, R-ratio was studied with square wave and constant maximum fatigue stress that as R approached 1, the cyclic fatigue failure time approached the static fatigue time at that maximum stress. Considering column B in Table 8, the slope, B, of the S-N curve decreases with increase frequency; yet, the initial strength or intercept, A, also decreased with increased fatigue frequency as seen in Figure 46. Comparing different wave forms showed that the wave form with the least time at ultimate tensile stress yielded the highest initial strength intercept A, but conversely, exhibited the steepest slope B; thus having the greatest reduction in strength per decade of cycles as seen in Figure 47.

Table 8: Mandell Frequency and Wave Form Comparison

Description of Load	Frequency (Hz)	Material Batch	A Y-Intercept	B Slope
Static Fatigue	0	1	369	16.5
Spiked Wave	0.1	1	508	58.8
Square Wave	0.1	1	446	49.9
Spiked Unloaded Wave	0.1	1	428	42.6
Static Fatigue	0	2	424	23.4
Square Wave	1.0	2	405	45
Square Wave	0.1	2	378	40.7
Square Wave	0.01	2	355	37

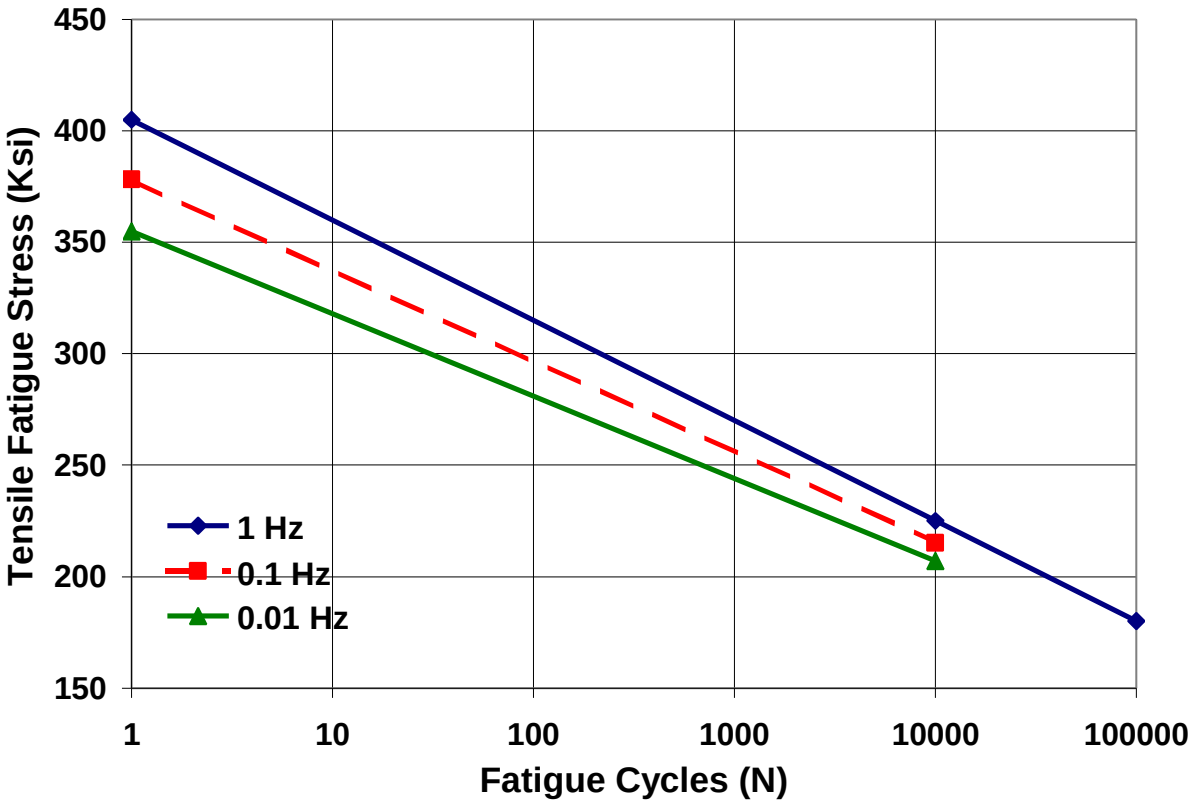

Figure 46: Frequency Effects on Cross-Ply Epoxy/E-Glass Composite

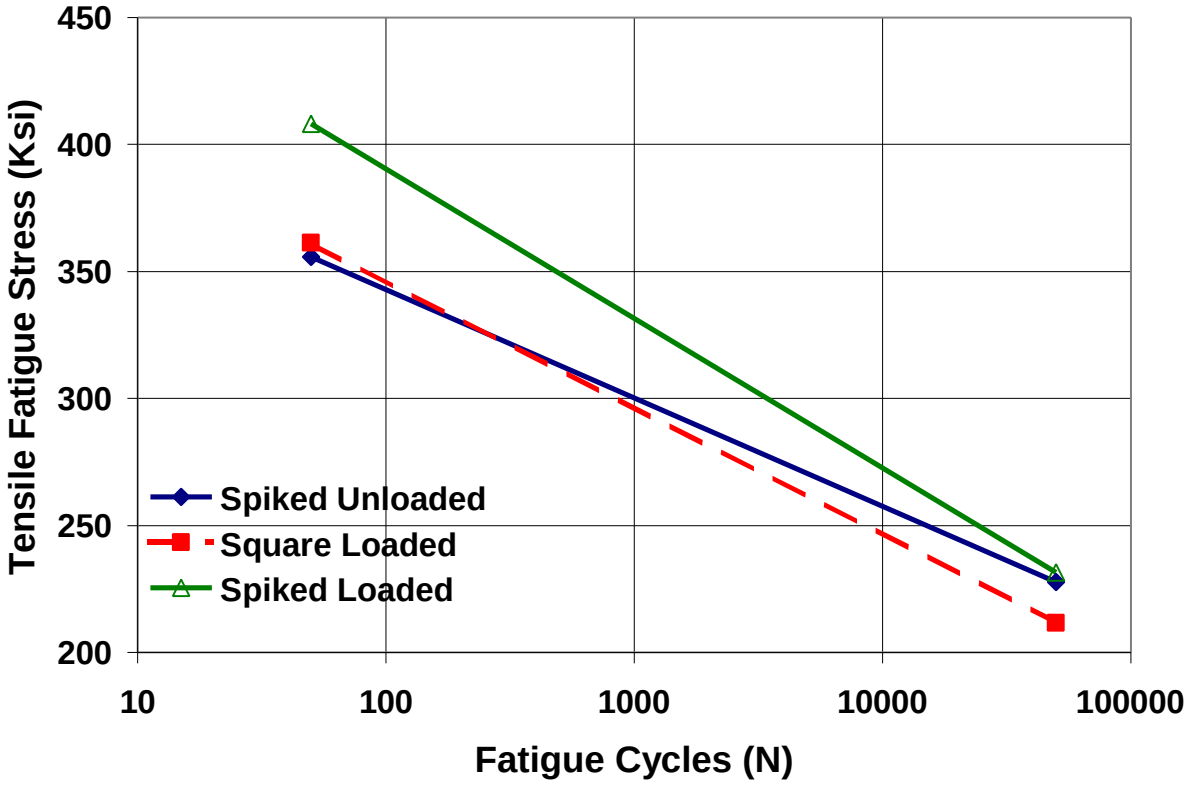

Figure 47: Waveform Effects on Cross-Ply Epoxy/E-Glass Composite

Fatigue Residual Strength

Residual strength of laminated composites is of great importance in the prediction of useful life of laminated composite products. When the residual strength is equal to the applied stress, failure results. Shokrieh and Lessard [44] have reviewed many residual strength models found in literature and normalized all to allow comparison. They attribute the earliest wear out model to Halpin, which was a power-law growth equation for residual strength.

Equation 21

$$\frac{dR(n)}{dn} = -A(s)/m[R(n)]^{m-1}$$

After integration from 0 to n cycles with constant applied stress, σ, linearizated by considering one step to failure, and normalizing for comparison; Halpin's form is

Equation 22

$$\frac{R^m(n) - s^m}{R^m(0) - s^m} = 1 - \frac{n}{N_f}.$$

Reifsnider proposed the following form with J a residual strength curve shape parameter found experimentally as described in detail later

Equation 23

$$\frac{R(n)-s}{R(0)-s}=1-\left[\frac{n}{N_f}\right]^J.$$

Harris is slightly different with α and β are curve fit parameters found experimentally

Equation 24

$$\left(\frac{R(n)-s}{R(0)-s}\right)^a=1-\left[\frac{\log(n)-\log(0.5)}{\log(N_f)-\log(0.5)}\right]^b.$$

Figure 48 shows a comparison of the residual strength curves for E-glass composites from Adams and Harris [45] with this current research.

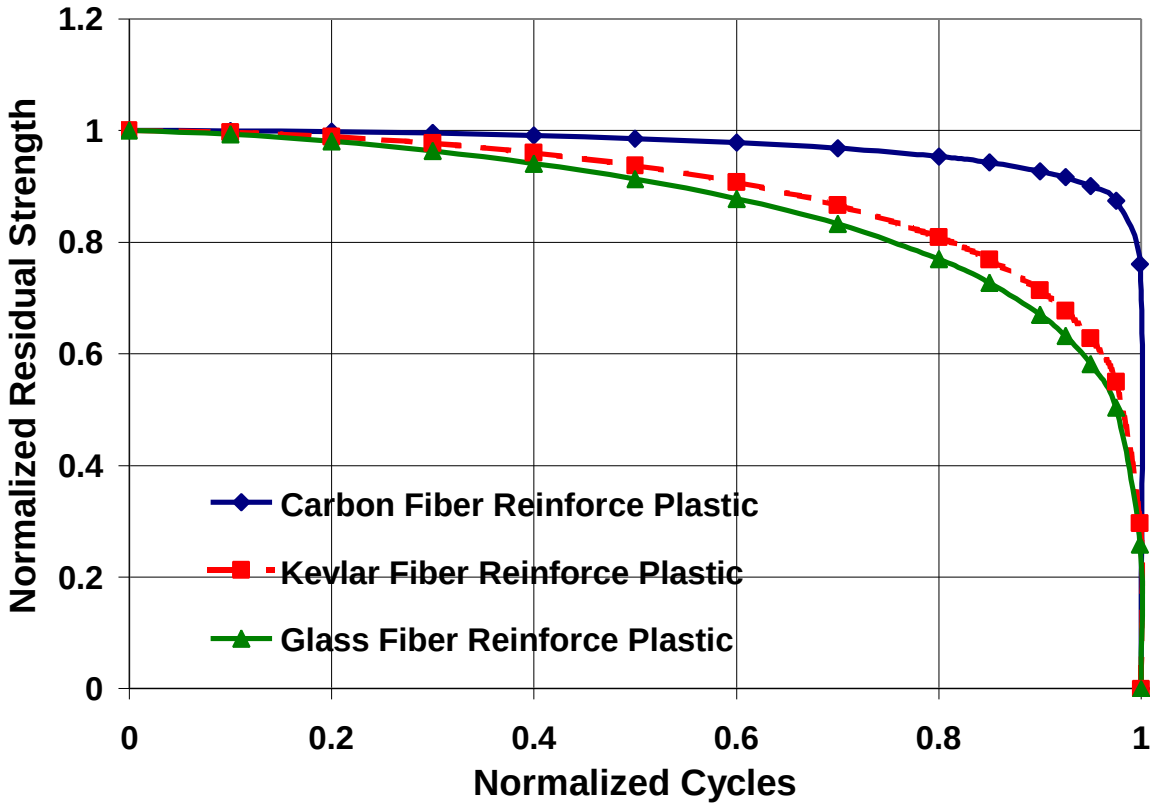

Figure 48: Normalized Residual Strength Comparison of Carbon, Kevlar, and Glass Fibers

Residual Strength and Life Prediction Methodology

Reifsnider's residual strength and life prediction methodology [04] [46] was used in this research to analyze residual strength and life of the pultruded vinyl ester/E-glass non-woven tricot stitch non-crimped fabric composites. In the form given below, this predicted normalized residual strength (Fr) of the critical element, the 0° lamina to the load direction, is based upon the increase in normalized applied stress, Fa(0°), over time measured in cycles [04]. This increase in Fa over accumulated cycles is calculated continuously in Equation 25 and iteratively in Equation

26. The calculated stiffness reduction of the sub-critical elements which are stiffness, E_2 and G_{12} of the off-axis lamina, are applied to a Classical Laminate Theory (CLT) model of the laminate to obtain an increase in normalized applied stress, Fa(0°), of the critical element. In equation form, the residual strength is a function of elapsed fatigue cycles, fatigue life, applied load or applied strain, and the shape of the residual strength curve "J" in continuous form as shown by

Equation 25

$$Fr(n) = Fr(0) - \int_0^{\frac{n}{N}} \left(1 - Fa(n)\right) \cdot J \cdot \left(\frac{n}{N}\right)^{J-1} \cdot d\left(\frac{n}{N}\right)$$

n = elapsed number of fatigue cycles
N = life in cycles at the applied stress or strain obtained from inversion of the S-N curve
Fa = normalized applied stress to initial strength of the critical element
Fr = normalized residual strength of the critical element

J = curve fit parameter, shape of the residual strength curve of the critical element

In a form ready for iteration, this life prediction scheme becomes

Equation 26

$$Fr_1 = 1 - (1 - Fa_1) \cdot \left(\frac{\Delta n}{N_1}\right)^J$$

iteration

$$no_i = \left(\frac{1 - Fr_{i-1}}{1 - Fa_i}\right)^{1/J} \cdot N_i$$

$$Fr_i = Fr_{i-1} - (1 - Fa_i) \cdot \left[\left(\frac{no_i + \Delta n_i}{N_i}\right)^J - \left(\frac{no_i}{N_i}\right)^J\right]$$

Δn_i = time increment in number of cycles for the i^{th} iterative step

no_i = "pseudo cycles" representing the elapsed cycles as if the fatigue occurred at the current stress state (Fa) for it's entire life until it reaches the current remaining strength (Fr_i) value.

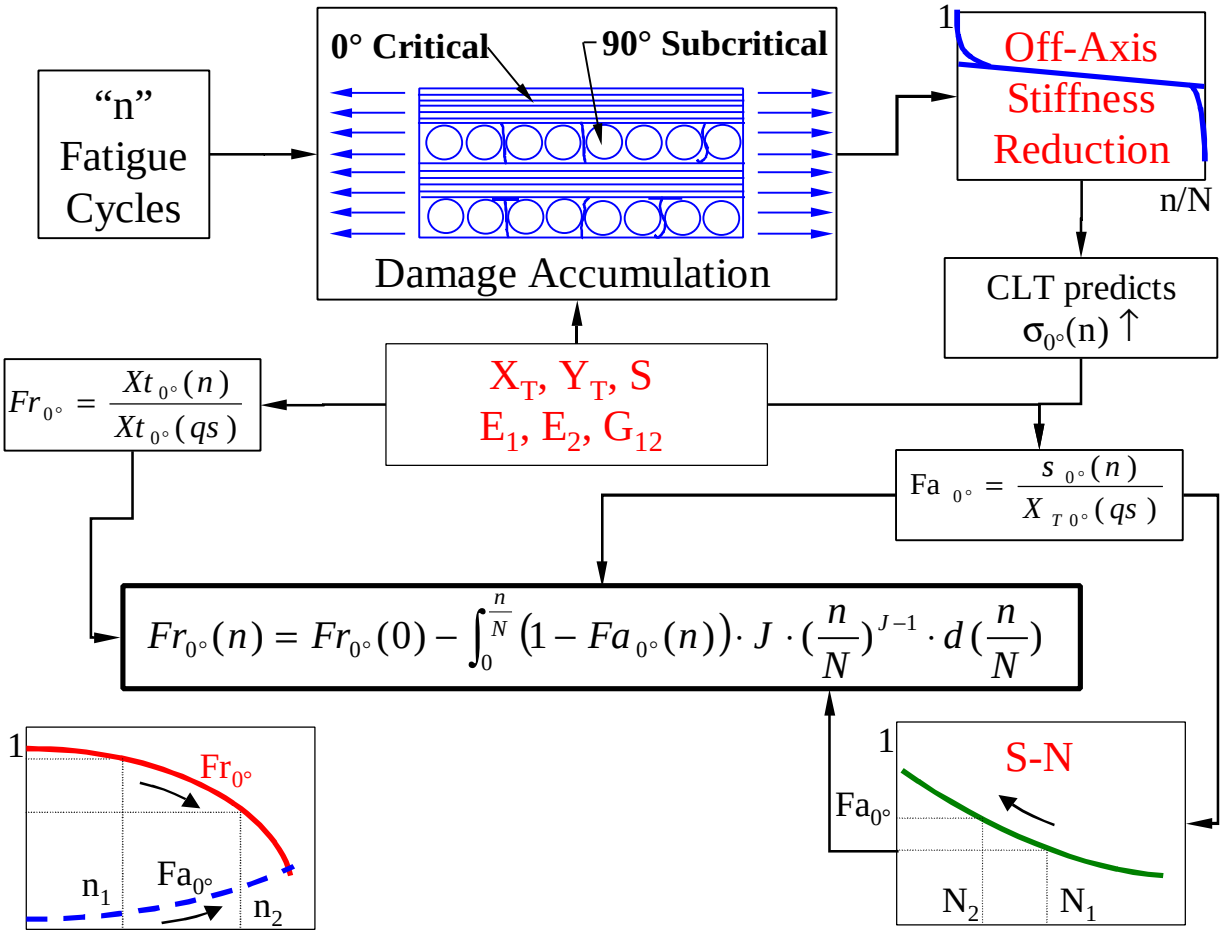

Figure 49: Cyclic Fatigue, Damage Accumulation, Subcritical Element Stiffness Reduction, Critical Element Stress Increase, Residual Strength Decrease, and Life Prediction

Prior to the development of residual strength theory, Miner's Rule, as seen in Equation 27, had been successfully used for prediction metal fatigue life. Metals were relatively uninfluenced by or independent of the sequence of the range of applied loading.

Equation 27

$$N_f = \sum_{i=1}^{l} \frac{n_i}{N_{fi}}$$

This was acceptable for metals, which are relatively homogeneous when compared to laminated composites. Fatigue of laminated composites has been found to depend greatly upon the sequence of the applied loading [47] Low to high loading has been found to be less damaging for laminated composites when compared with high to low loading. This difference would not be distinguished using Miner's Rule which states that the fatigue life is the sum of the ratios of number of cycles spent at a stress level divided by the fatigue life at that stress ratio. This in effect assumes that remaining strength curve shape factor is infinite when using Miner's Rule.

As discussed in the quasi-static section, there has been little evaluation of pultruded laminated composites found in literature for quasi-static as well as fatigue performance. The

literature concerning fatigue performance reviewed in this research was based upon aerospace grade composites, which are very high quality laminates fabricated from tough, low shrinkage, epoxy with low void content, no visible damage in the as-processed condition, and very little fiber distortion due to a careful, tedious fabrication process. On the other hand the CRTM pultruded laminated composites have been shown to have substantial fiber undulation, voids, as-processed microcracking and delamination, and uses a much more brittle matrix than found in fatigue literature. Each of these characteristics tends to reduce the stiffness, strength, and fatigue performance. How do these characteristics affect the fatigue performance of these CRTM pultruded vinyl ester/E-glass non-woven tricot stitched non-crimped fabric composite laminates?

Chapter 6: Fatigue Properties & Analysis of CRTM Pultruded Vinyl Ester/E-Glass Composite Laminates

Research Goals and Significance: Fatigue Evaluation of Pultruded Composites

The primary goal of the research is to obtain and analyze the fatigue response of cross-ply, angle-ply, and quasi-isotropic vinyl ester/E-glass non-woven tricot stitched non-crimped fabric (NCF) composite laminates fabricated from the Continuous Resin Transfer Molding (CRTM) pultrusion process. Laminate residual strength, Fr-n, laminate stiffness reduction, Elam(n), and laminate applied fatigue stress to fatigue failure cycles, S(Lam)-N, are the fatigue parameters which were obtained. Stiffness reduction is crucial to the performance of composite structures in the civil infrastructure where most designs are deflection controlled. Accurate predictions of residual strength, stiffness, and life will assist in the implementation and monitoring of pultruded composite laminates in infrastructure applications. A secondary goal is to characterize the effects of the non-woven tricot stitched non-crimp fabric, the vinyl ester matrix, and the pultrusion process on these fatigue properties.

Description of Materials for Fatigue Evaluation

Matrix, Fiber, & Stitch

The materials investigated were pultruded laminates fabricated by Hexcel, Kent Washington, using Dow Chemical's Derakane 441-400 vinyl-ester modified epoxy with PPG Hybon 2002 E-glass. Both resin and fiber components were selected for cost and compatibility with the pultrusion process. To aid in the continuous resin transfer molding (CRTM) process, resin viscosity was reduced by the addition of styrene at 28% by resin volume. The vinyl ester cure process causes high shrinkage when compared with epoxies; a 6% shrinkage in a pure resin specimen was measured when cured with the pultrusion cure cycle. For handling purposes, the unidirectional glass was pre-stitched, 0° stitched to 90° and +45° stitched to -45° ply. The 90° transverse plies were actually stitched with fiber bundles at 86° and 94° by non-woven, non-crimped fabric (NCF) stitch fabrication process. Polyester at 70 denier in a tricot stitch was arranged parallel to the 0° for 0/90°, and a chain stitch was used for the ±45° with the stitch direction at 45° to the ±45° fiber. The stitch was arranged at 7 stitches per inch transverse to the stitch direction and a penetration along the length of stitching direction of approximately 1/10 inch. The stitch by weight composed 1 % of the glass fiber weight. The tricot stitch, appearing as a zigzag stitch loops around the 0° and 90° fiber bundles and passes under a carrier thread then looping back over the 0° and 90° fiber bundles farther down the length of the 0° fiber bundle. This tricot stitch gathered each axial 0° fiber bundle into a regular pattern of fiber bundle with a gap between fiber bundles of approximately 25-33% of the fiber bundle width shown in Figure 6a and Figure 9. The 90° fiber bundles aligned transversely to the pultrusion axis were rounded by the tricot stitch looping around the carrier stitch. A slight gap between bundles is shown in Figure 6a and Figure 14. The chain stitch used for the ±45° plies is shown in Figure 6b.

Lamina & Laminates

Cross-ply $(0/90)_{5T}$ and $(0/90)_{3S}$, and quasi-isotropic laminates $(0/90/\pm45/0/90)_{2T}$, $(90/0/(\pm45)_2/0/90)_{2T}$ as shown in Table 2 were tested. The $(0/90)_{5T}$ cross-ply laminate was

balance but non-symmetric and $(0/90)_{3S}$ was symmetric but unbalanced. Balanced is defined to have equal areal weighting of the 0° to 90°. The $(0/90)_{3S}$ cross-ply laminate had a 1.5 to 1 ratio of 90° to 0° ply thickness or areal weight. The $(0/90/\pm45/0/90)_{2T}$ was non-symmetric and balanced. The quasi-isotropic laminate $(90/0/(\pm45)_2/0/90)_{2T}$ was nearly symmetric with the ±45 plies being non-symmetric and 0/90 plies symmetric, but was unbalanced similar to $(0/90)_{3S}$. Thickness ratios are based on areal weights shown in Table 2. The angle-ply laminate, $(\pm45)_{3S}$, was cut from the cross-ply $(0/90)_{3S}$; thus, the laminate was unbalanced since the +45° was 9.6 oz/yd^2 and the -45° was 15.1oz/yd^2 fabric. The ±45 plies plies in the quasi-isotropic laminates above are balanced as shown in Table 2, but a purely ±45 laminate cannot be pultruded since there is no axial fiber to pull through the die.

Physical Description of As-Pultruded Laminates

A general discussion of the physical description of all the laminates will first be discussed followed by a description of each laminate associate with microscopic photographs shown in Figure 9 through 25. These CRTM pultruded glass/vinyl ester composites had a variety of as-pultruded imperfections including warp of the specimens, local fiber volume variations, pure resin rich region, microcracking, delaminations, voids, and fiber undulation. The unidirectional lamina possessed local fiber volume variations noticeable as light and dark streaks. The six-inch wide unidirectional E-glass pultrusion possessed high curvature in the transverse direction. The chord height of this curvature was 0.017 inch over the six-inch width; this curvature when straightened in the grips of the Instron strained the specimens to a maximum of 37% of its ultimate transverse failure strain. Matrix shrinkage, seen as surface sink marks in low fiber areas gave the unidirectional and laminate specimens a rough textured appearance. Matrix shrinkage interior to the laminates in low fiber volume areas often exceeded the ultimate axial tensile strain; thus to relieve the strain, debonding and microcracking resulted parallel to the fiber. A statistical analysis of microcracking and delamination densities was not conducted at this point; rather a qualitative analysis was performed. Microcracking was seen in both the axial and transverse views always occurring in a resin rich region between fiber bundles. In the axial view aligned to the pultrusion axis, microcracking occurred more often when the 0° fiber bundles were in the aligned configuration as shown in Figure 7 where a larger resin rich region existed between the 0° fiber bundles than in the nested configuration as shown in Figure 8.

Fiber undulation was apparent in all laminates tested. The tricot stitch from the non-woven fabric forced the fiber into a non-uniform fiber pattern in both the axial and transverse directions to the pultrusion axis. The axial 0° fiber bundles aligned with the pultrusion axis were gathered by the tricot stitch into a bundle, which created gaps between axial fiber bundles of width approximately 25-33% of the axial fiber bundle width. The off-axis plies to the pultrusion axis were forced into an undulating pattern in one of two geometries. The 0° fiber bundles of one ply could either be nested or aligned with the 0° fiber bundles of adjacent plies. When the 0° fiber bundles of one ply were aligned to the 0° fiber bundles of an adjacent ply as seen in Figure 7, a pure resin pocket filled the gap between the 0° fiber bundles. Because the off-axis plies have no applied tensile forces as do the axial plies to the pultrusion axis during the pultrusion process, the off-axis plies may bulge in this resin rich pocket. This produce slight undulation of the off-axis plies, but a matrix crack often occurred spaced in the gap between the 0° fiber bundles, which implied excessive processing shrinkage. The nested configuration of adjacent 0° fiber bundles as

shown in Figure 8 resulted in the greatest fiber undulation of the transverse plies to the pultrusion axis. Axial fiber undulation, in the direction of pultrusion, also occurred but was much less than that of the transverse plies since the tricot stitch of the fabric created only a slight gap in the transverse. The laminates with the thicker transverse plies appeared to possess greater fiber undulation in the axial fiber, which is reasonable since there is greater undulation possible with thicker than thinner transverse and angle plies. Quasi-isotropic plies tend to have less fiber undulation than the cross-ply laminates since there is fewer 0° plies and additional angle plies to diffuse the undulation created by the 0° fiber bundle and gap pattern. In many of these photographs the full stacking sequence cannot be seen; this is due to the cut cross-section falling on the gap between plies as shown as section AA in both Figure 7 and Figure 8.

Description of Testing for Fatigue Evaluation

The typical S(Lam)-N, laminate strength-fatigue cycles, normalized residual strength-fatigue cycles curves, Fr-n, and normalized residual stiffness, Elam(n)/Elam(qs)-n/N, were obtained during load control fatigue cycling at 10 hertz and R ratio of 0.1 tension-tension on a MTS hydraulically controlled load frame with TestLink controlling software. The S-N curves are renamed Fa(Lam)-N when applied stress is normalized to quasi-static strength. Length and width of specimens were 8 by 1 inches cut, ground and polished. Gripping length was 2 inches with 1000 series aluminum 0.020 inch thick shim stock used for gripping in fatigue. No damage was apparent to the composite due to gripping. Strain gage and extensometers used to measure strain/elongation for quasi-static testing and a single extensometer to measure elongation for fatigue testing. ASTM Standards D3039-95a, and D3518-94 were followed for tension and shear tests respectively.

Results and Discussion: Fatigue Analysis of Pultruded Vinyl Ester/E-Glass Laminates

The fatigue analysis of the CRTM pultruded laminates began with an S-N curve evaluation. From the extensometer data along with the load cycle history, the laminate stiffness reduction was evaluated. With simplifying assumptions, the off-axis stiffness and the critical element S-N curve were extracted from the laminate stiffness reduction and laminate S-N curve. For the residual strength analysis, specimens were fatigued at different stress levels to various percentages of their predicted life. These specimens were then quasi-statically tested to failure to determine their residual strength. Residual strength analysis was conducted to determine the effects of variations in stiffness reduction, S-N curve, and remaining strength curve shape in prediction of residual strength and life. Simplifying assumptions will first be discussed which allow the implementation of Reifsnider's residual strength and life theory. Stiffness reduction, S-N curve, and Remaining strength discussion and analysis will follow.

This residual strength analysis can be applied in many forms. For this analysis of the CRTM pultruded vinyl ester/E-glass non-woven composite laminates, the following assumptions and approach were used.

1. Laminate stiffness reduction is assumed to occur only in the off-axis plies. The off-axis stiffness, E_2 and G_{12}, are determined from the measured laminate stiffness reduction curves. This is accomplished using simple rule-of-mixtures mechanics-of-materials approach. Assuming that stiffness of the 0° plies to the load direction is constant and that transverse plies reduce in an elastic-plastic manner, the off-axis

stiffness reduction may be approximated for cross-ply laminates. An added assumption for quasi-isotropic laminates is required; assuming that G_{12} can be represented by the quasi-static stress/strain curve in fatigue, off-axis stiffness may be estimated. The assumption that stiffness reduction does not occur in the 0° plies is perhaps the least accurate assumption, since there is fiber undulation in the 0° direction, which would allow stiffness reduction of the critical element, the 0° plies.

2. In estimating the S-N curve of the critical element from the measure laminate S-N curve, it is assumed, that in load control, the average normalized applied stress to the critical element, Fa(0°), can represent the actual situation where gradual increase in applied stress occurs due to the stiffness reduction of the off-axis plies.
3. It is assumed that the residual strength shape factor "J" obtained from laminate remaining strength testing is the same for the critical element of the laminate, the 0° plies. This is a good assumption, since the ultimate strength of the laminate is controlled by the strength of the critical element, the 0° plies. This also has the added benefit that this method includes any processing defects and laminate effects, which lower the residual strength such as fiber undulation.
4. The "J" value for the critical element was determined from curve fits of Equation 26 to residual strength laminate data. This reveals the final assumption that the Fa(0°) of the critical element and the N fatigue life at that Fa(0°) is constant thus assuming that the average value of Fa(0°) can be used to represent the normalized applied stress on the critical element over its entire life.

Consider the failure mechanisms of a cross-ply or quasi-isotropic laminate. In fatigue, laminate stiffness reduction is seen immediately at high stress levels, where the transverse and angled plies to the principal load direction begin microcracking. At low stress levels, the microcracking is slower to occur, initiating from flaw sites such as voids or higher stress areas such as low fiber content areas, which are thermally stressed upon cure cool-down. This microcracking continues over much of the life until fully saturated. If the laminate stacking sequence is non-symmetric or is loaded in beading or shear, delamination may result from these microcracks. If the laminate stacking sequence is symmetric, then delamination occurs from the interaction between microcracks of adjacent transverse and/or angled plies.

Consider residual strength Equation 26, as fatigue cycles (n) increases a time step Δn, the stiffness of the off-axis plies decrease; thus, the stress applied to the critical element, the 0° plies, is increased. Using Classical Laminate Theory, CLT, the increase in stress on the critical element is calculated by reducing the off-axis stiffness, E_2 and G_{12} of the off-axis plies, due to this time step increment. Thus, the normalized applied stress, Fa(0°), increases on the critical element. The S-N(0°) curve of the critical element is used to calculate a new lower value of, N, life expectancy from the increased normalized applied stress, Fa(0°). This lower value of N since in the denominator and the increase in Fa(0°) seen in Equation 26 decreases the residual strength of the critical element.

Through iteration of Equation 26, a lower residual strength value is calculated. Iteration continues with increasing cycles Δn, decreasing the off-axis stiffness E_2 and G_{12} in cyclic time; thus decreasing N as Fa increases, until the normalized applied stress Fa(0°), calculated in CLT, has increased to meet the decreasing normalized residual strength, Fr, at which failure is predicted.

Stiffness Reduction Evaluation

Extraction of Off-Axis Stiffness Reduction

The stiffness reduction curves of each laminate were obtained from the fatigue data and were converted to off-axis-lamina stiffness reduction curves. It was assumed that the stiffness reduction was due solely to the off axis lamina; the 0° lamina were assumed to have no stiffness degradation. For example, the cross-ply (CP) laminate's stiffness reduction can be written as shown below. Solve for $E_{90deg}(n)$ to obtain the stiffness reduction of the off-axis lamina, 90° in this case, with the assumption that the stiffness in the fiber direction $E_{0deg}(n)= E_{0deg}$(quasi-static). The present analysis assumed that the stiffness of E_2 and G_{12} were equally reduced and that E_1 had no stiffness reduction. This Rule-of-Mixtures for cross-ply and quasi-isotropic approximation doesn't account for Poisson's interaction.

Equation 28

$$\frac{E_{Laminate}(n)}{E_{Laminate}(qs)} = \frac{E_{0\deg}(n=qs)\cdot Af_{0\deg} + E_{90\deg}(n)\cdot Af_{90\deg}}{E_{0\deg}(qs)\cdot Af_{0\deg} + E_{90\deg}(qs)\cdot Af_{90\deg}}$$

$$\frac{E_{Laminate}(n)}{E_{Laminate}(qs)} = \frac{E_{0\deg}(n=qs)\cdot Af_{0\deg} + E_{90\deg}(n)\cdot Af_{90\deg} + E_{45\deg}(n)\cdot Af_{45\deg}}{E_{0\deg}(qs)\cdot Af_{0\deg} + E_{90\deg}(qs)\cdot Af_{90\deg} + E_{45\deg}(qs)\cdot Af_{45\deg}}$$

The off-axis stiffness reduction curves, shown in the figures were represented by linear fit as shown in Table 9. The drastic reduction in the first 5% of life and the associated drop or rise in stiffness beginning at 95% of life was not modeled with this linear curve fit. This linear representation is shown to work well for residual strength analysis at mid to high Fa ranges, but at low Fa loads, the linear approximation, substantially, over predicts failure. The laminate stiffness reduction for Angle-ply $(\pm 45°)_{3S}$ is shown in Figure 50. Laminate and off-axis stiffness reduction for cross-ply laminate, designated CP1 in Table 2, is shown in Figure 51 through Figure 54. Laminate and off-axis stiffness reduction for cross-ply and quasi-isotropic laminates, designated CP2, QI1, QI2, and QI2 at 45° in Table 2, is shown in Figure 55 through Figure 66. The extracted off-axis stiffness per Equation 28 is shown in Figure 53, 54, 57, 60, and 63. The modulus was normalized to the quasi-static modulus, in all cases, except where noted for comparison purposes. Figure 57 and Figure 58 show the difference between normalization with quasi-static modulus and with fatigue modulus at first cycle. Modulus was measured by stress(max-min)/strain(max-min) from the R=0.1 ratio.

Approximation of Fatigue Stiffness Reduction from Quasi-Static Data

In the preliminary design stages of product development, fatigue stiffness reduction data may not be known. The fatigue stiffness reduction, in this case, could be approximated from the stiffness reduction of the quasi-static laminate response. The initial fatigue stiffness can be approximated by determining the secant stiffness at the fatigue stress on the quasi-static stress/strain curve shown in Figure 28. The fatigue stiffness at failure, n/N=1, can be approximated by determining the secant stiffness at quasi-static failure. The off-axis stiffness reduction can be calculated from this quasi-static approximation using Equation 28. Figure 54, 58, 61, and 64 show the approximation of fatigue stiffness reduction from these quasi-static assumptions.

Results: Fatigue Modulus Reduction

Table 9: Normalized Tensile Fatigue Modulus Reduction: Laminate and Off-Axis

LAMINATE	ELam(n)/ELam(qs)	Eoff-axis(n)/Eoff-axis(qs) =	Eoff-axis(n/N=1) /Eoff-axis(qs)	Fa(Lam) Range
CP1	-0.0556n/N + 0.8832	-0.2307n/N + 0.6053	0.37	14-44
CP1	-0.0688n/N + 0.9272	-0.2463n/N + 0.7364	0.49	17-24
CP1	-0.0996n/N + 0.8797	-0.3565n/N + 0.5663	0.21	30-44
CP2	-0.0998n/N + 0.8954	-0.2805n/N + 0.7055	0.43	18-33
CP2	-0.1294n/N + 0.9780	-0.3640n/N + 0.9380	0.57	18
CP2	-0.0701n/N + 0.8127	-0.1970n/N + 0.4730	0.28	33
QI1	-0.1034n/N + 0.8904	-0.3170n/N + 0.6427	0.33	20-41
QI2	-0.0696n/N + 0.8526	-0.1483n/N + 0.6564	0.56	22-50
QI2	-0.0658n/N + 0.8715	-0.1483n/N + 0.7107	0.56	22-25
QI2	-0.0733n/N + 0.8337	-0.1483n/N + 0.6021	0.45	30-50
QI2at45°	-0.2720n/N + 0.8804	-0.4598n/N + 0.8228	0.28	26-49
QI2at45°	-0.2444n/N + 0.9443	-0.4870n/N + 0.9315	0.28	26-32
QI2at45°	-0.2444n/N + 0.8166	-0.4325n/N + 0.7141	0.28	35-49
AP	-0.3005n/N + 0.9872	-0.3005n/N + 0.9872	0.68	44-63

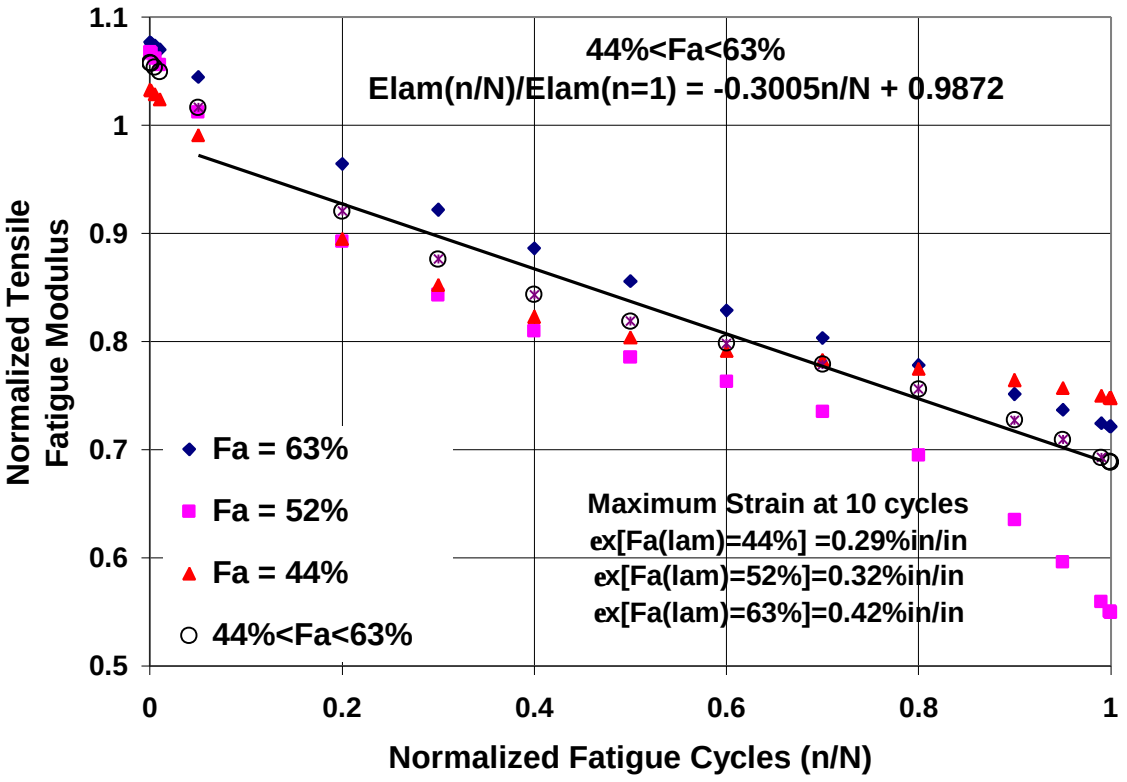

Figure 50: Tensile Fatigue Laminate Modulus Reduction for <u>Angle Ply ±45°</u>. Normalized to Quasi-Static Modulus from S-N Specimens Measured with Extenso- meter. Modulus is Measured by stress(max-min)/strain(max-min) from the R=0.1.

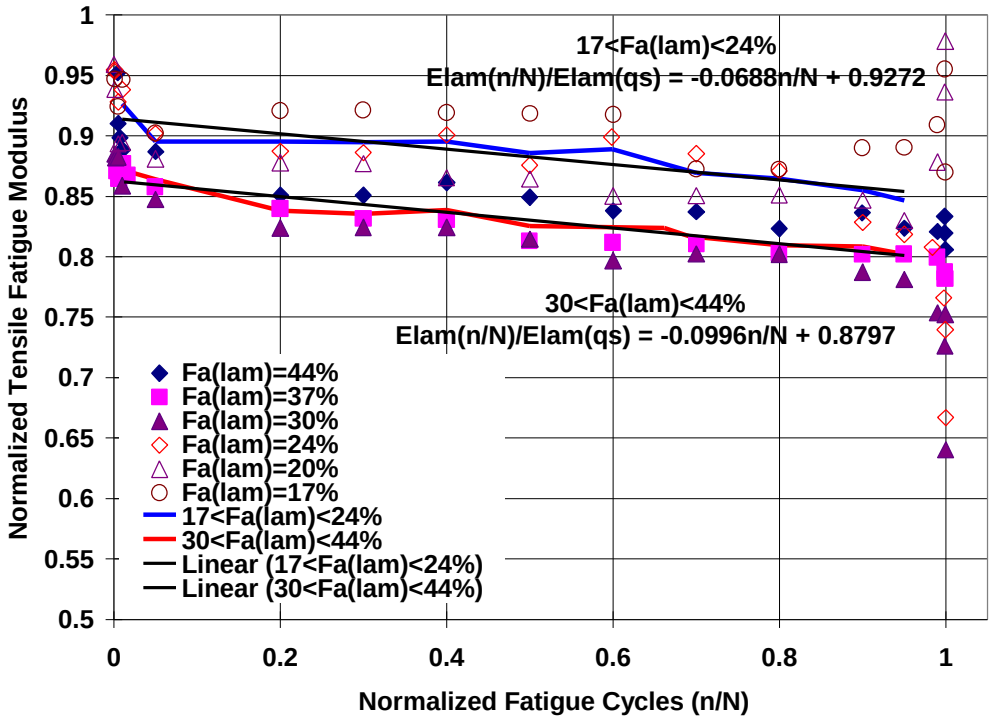

Figure 51: Normalized <u>Laminate</u> Tensile Fatigue Modulus for <u>Cross-Ply CP1, (0,90)5t</u>. Each Curve is Average of 3 Specimens.

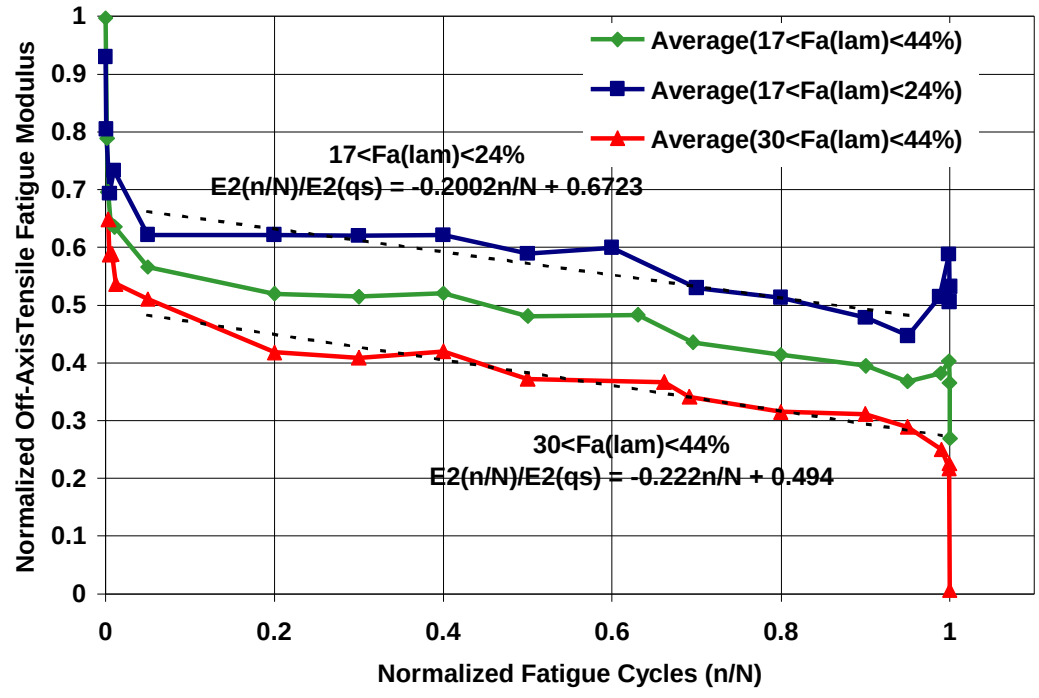

Figure 52: Normalized <u>Average Laminate</u> Tensile Fatigue Modulus Reduction for <u>Cross-Ply CP1 with Different Normalized Applied Fatigue Stress Ratios, Fa</u>.

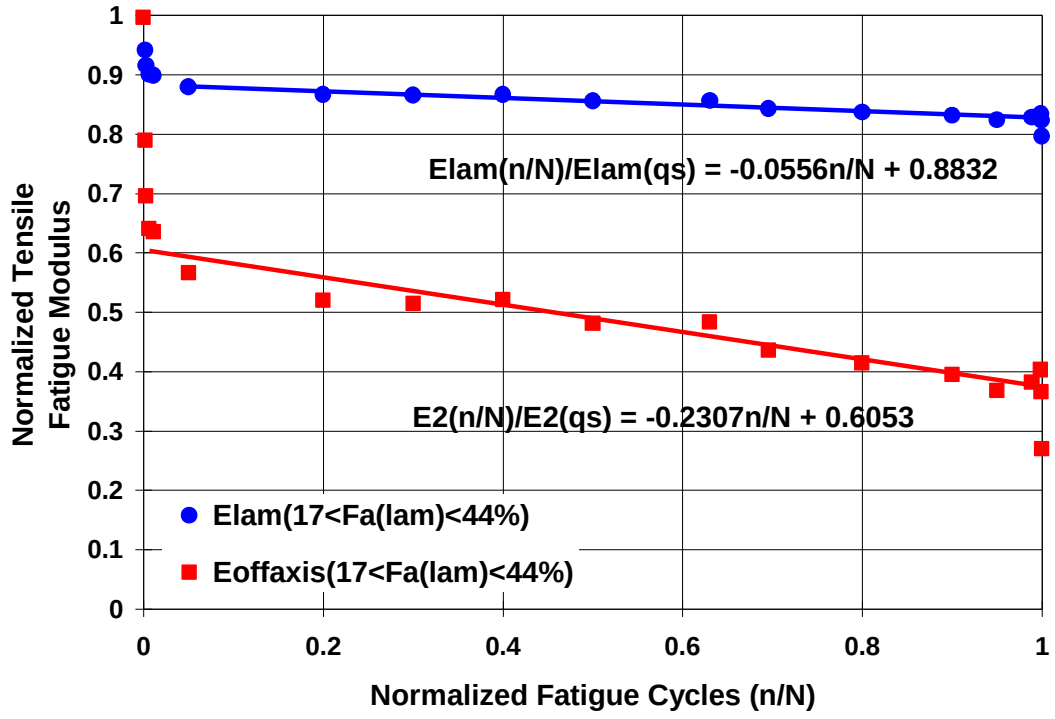

Figure 53: Normalized Tensile Fatigue Laminate and Off-Axis Stiffness Reduction for CP1 Laminate with Average of All Normalized Applied Fatigue Stress, Fa.

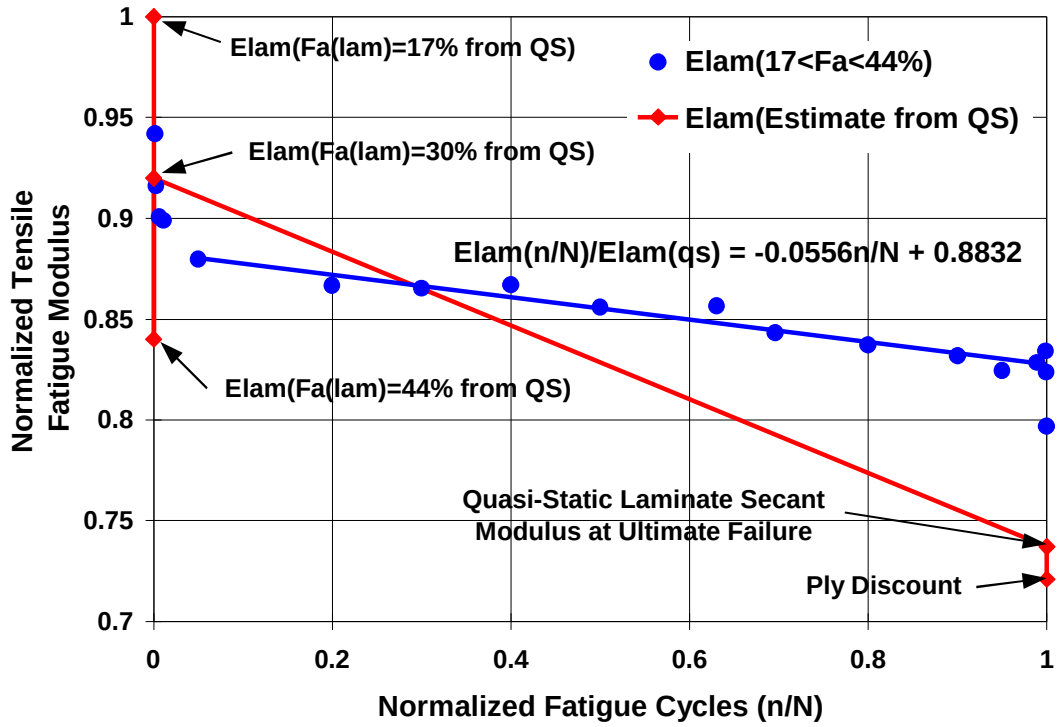

Figure 54: Normalized Tensile Fatigue Laminate Modulus Approximated from Quasi-Static Data for CP1 Laminate.

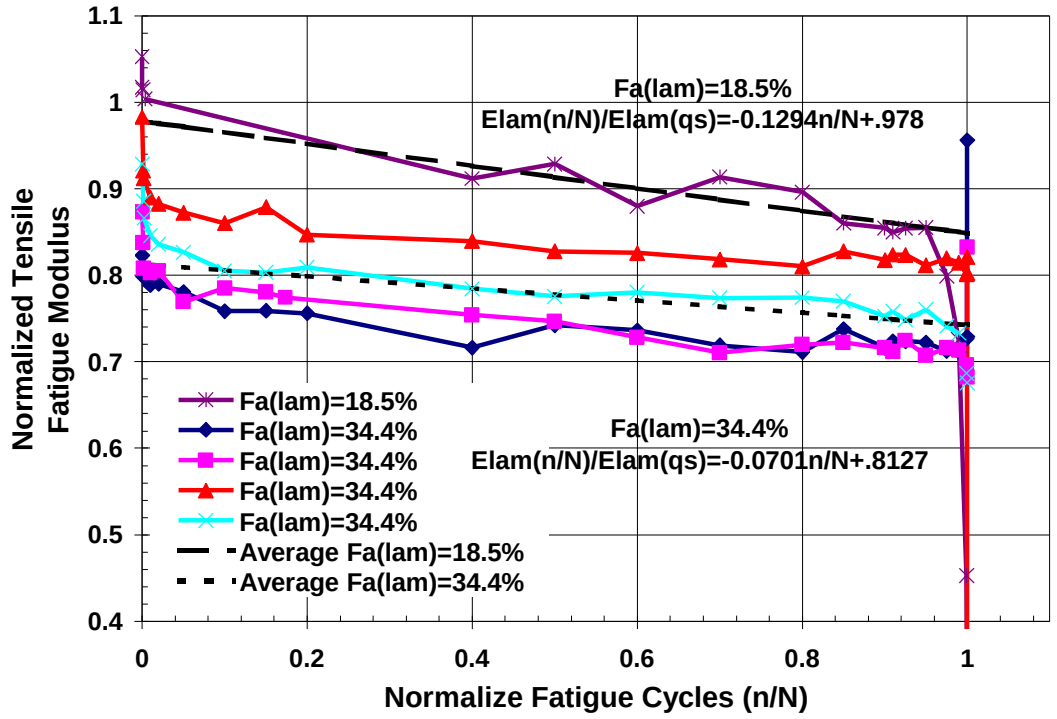

Figure 55: Normalized <u>Laminate</u> Tensile Fatigue Modulus for <u>Cross-Ply CP2, (90,0)3s,</u> Laminate.

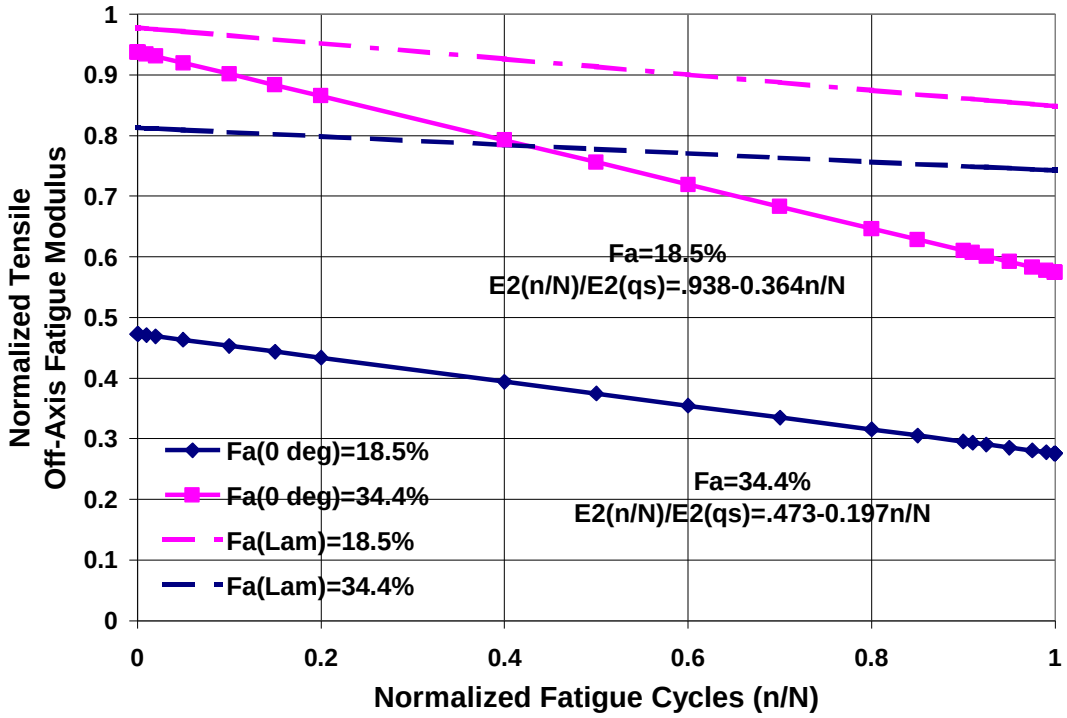

Figure 56: Normalized Tensile Fatigue <u>Off-Axis</u> Stiffness Reduction for <u>CP2</u> Laminate.

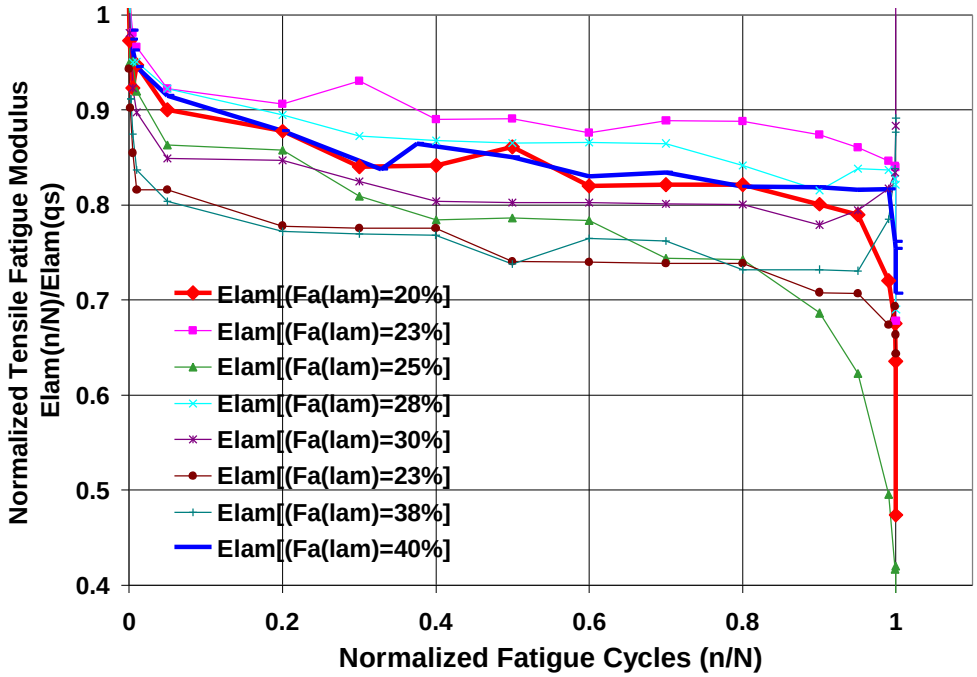

Figure 57: Normalized Tensile Fatigue Laminate Modulus for QI1, $(90,0,2(\pm 45),0,90)_{2T}$, Laminate Normalized to Quasi-Static Modulus from S-N Specimens Measured with Extensometer. Modulus is Measured by stress(max-min)/strain(max-min) from the R=0.1 ratio.

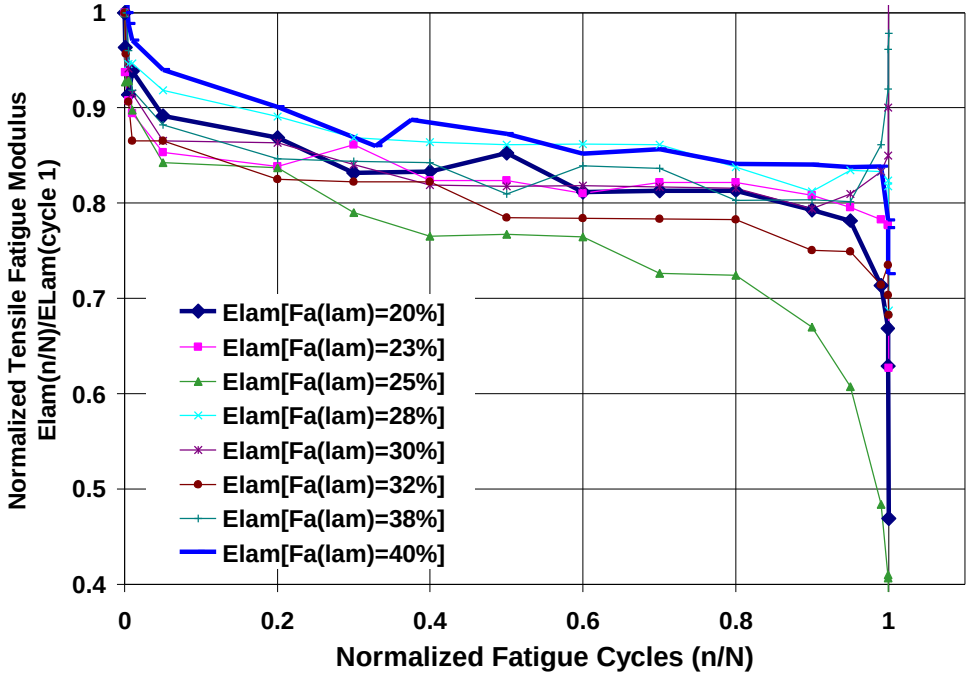

Figure 58: Normalized Tensile Fatigue Laminate Modulus for QI1 Normalized to 1st Cycle Fatigue Modulus

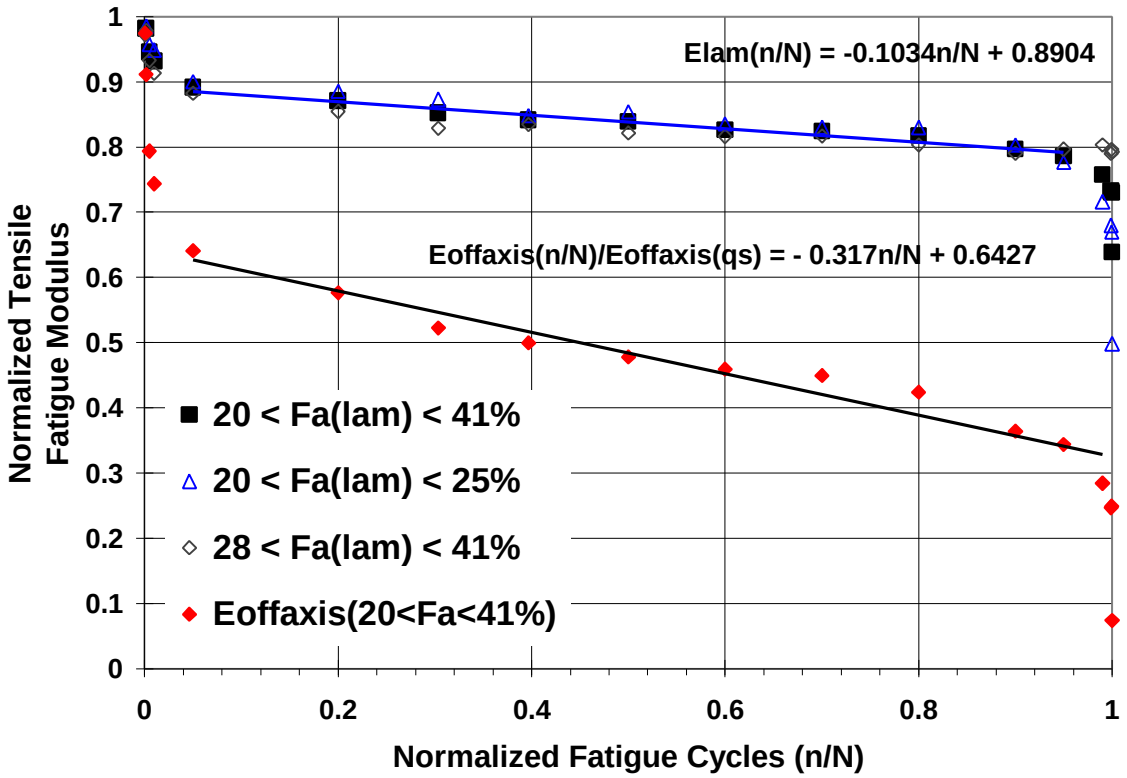

Figure 59: Normalized Tensile Fatigue Off-Axis Modulus Reduction for QI1.

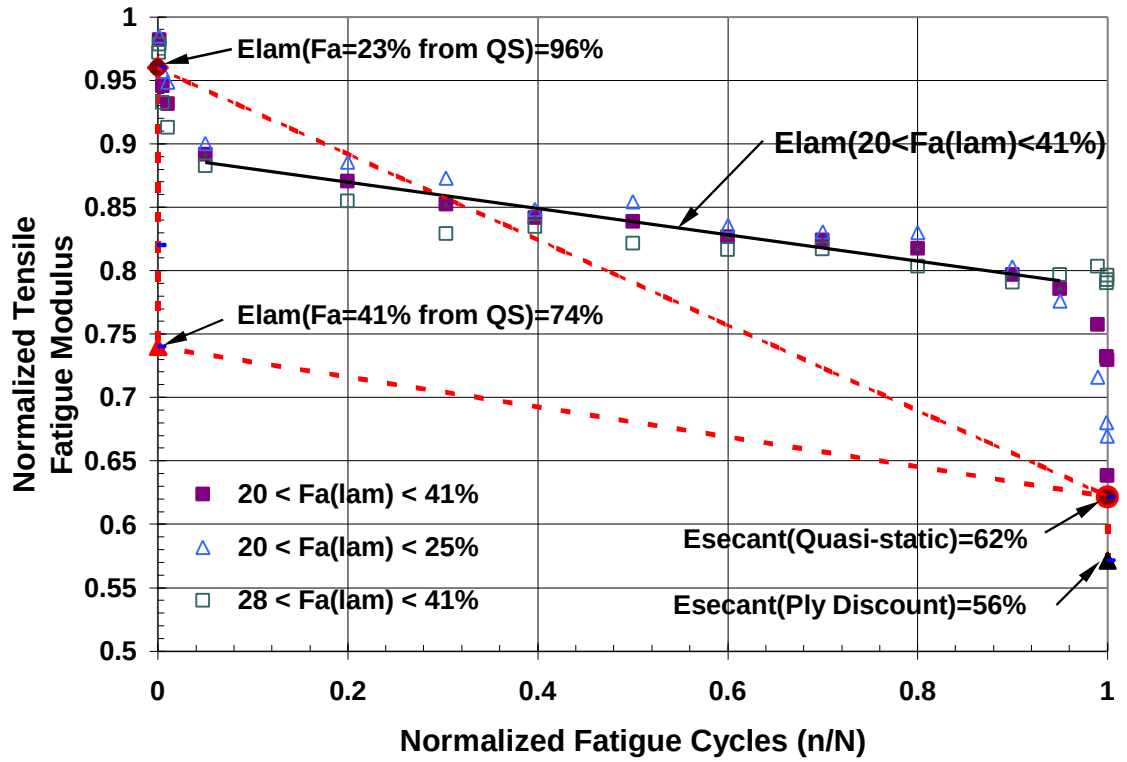

Figure 60: Normalized Tensile Fatigue Laminate Modulus Reduction for QI1 Laminate with from Quasi-Static Estimate.

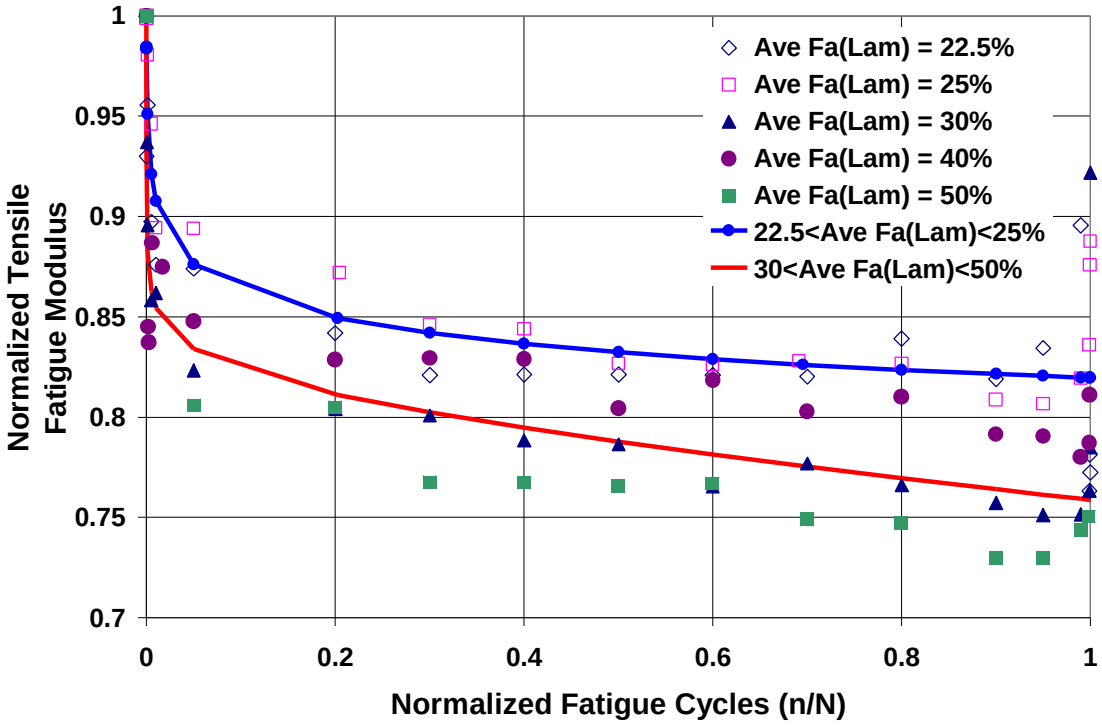

Figure 61: Average Normalized Tensile Fatigue Laminate Modulus at Each Applied Load Level, Fa, for QI2, $(0,90,\pm45,0,90)2_T$, Laminate.

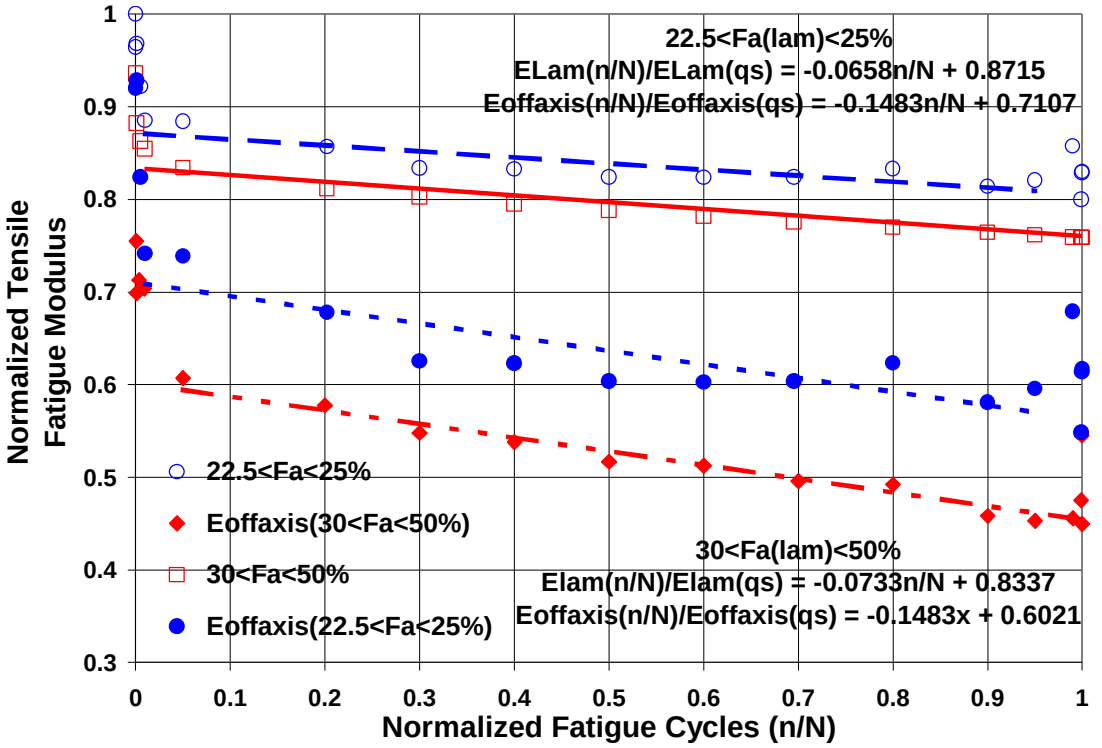

Figure 62: Normalized Tensile Fatigue Off-Axis Modulus Reduction for QI2 Laminate

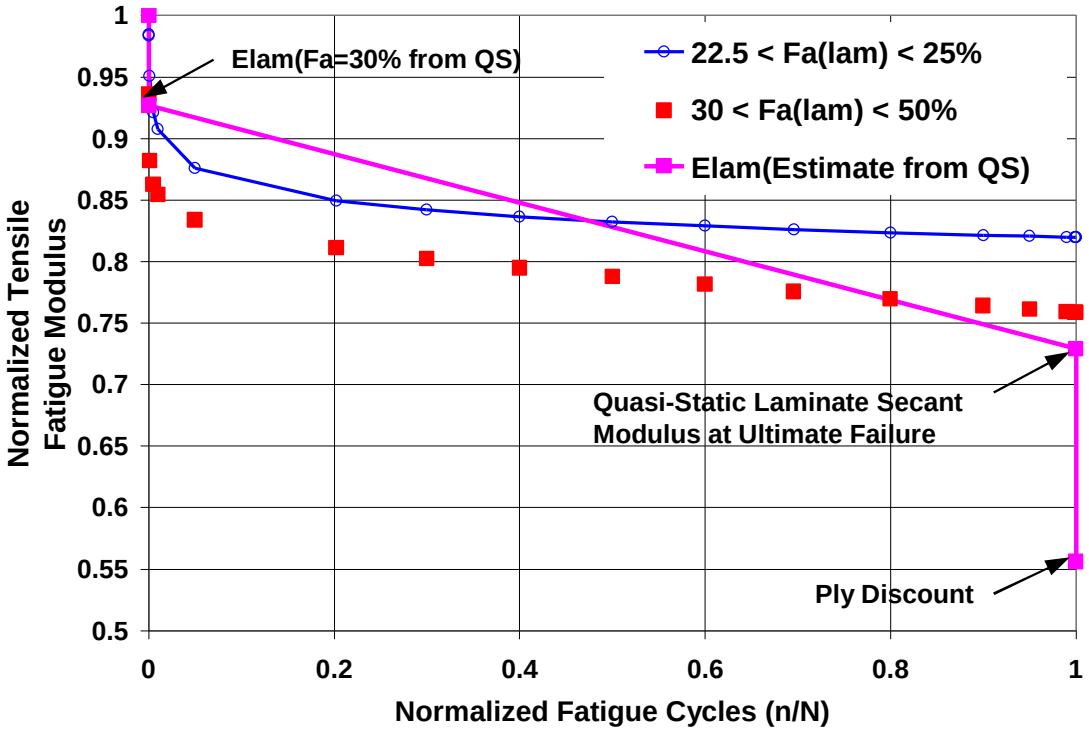

Figure 63: Normalized Tensile Fatigue Laminate Modulus Reduction for Quasi-Isotropic QI2 Estimated from QI2 Quasi-Static Data.

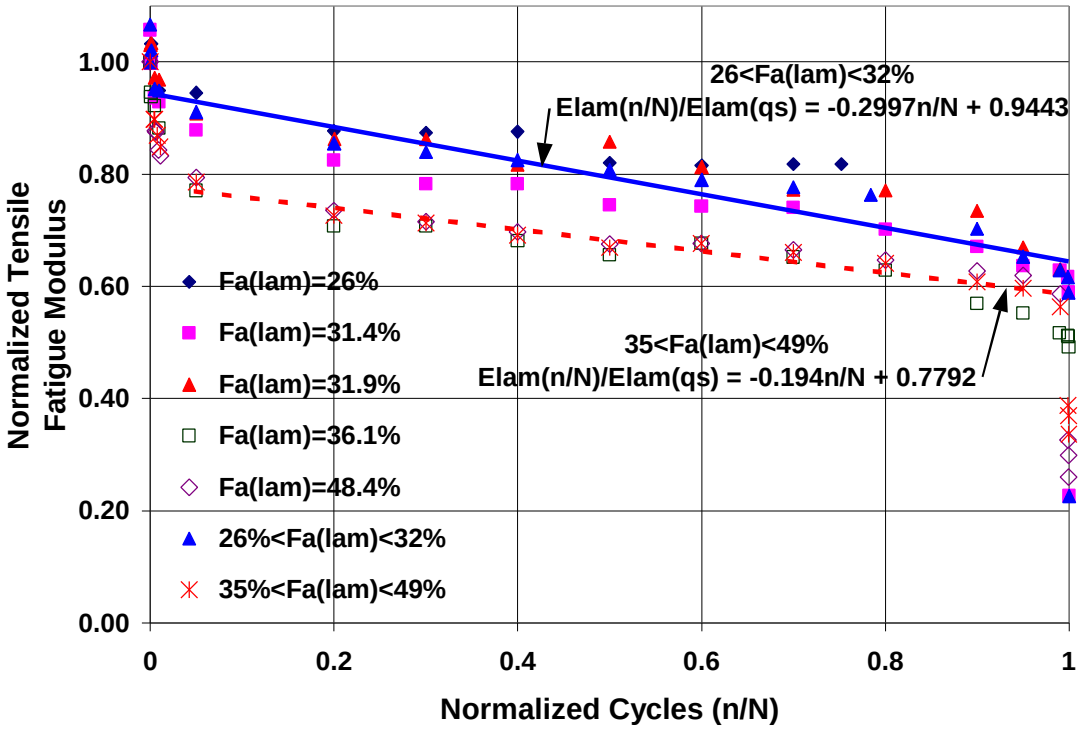

Figure 64: Normalized Tensile Fatigue Laminate Modulus for QI2 Laminate at 45°.

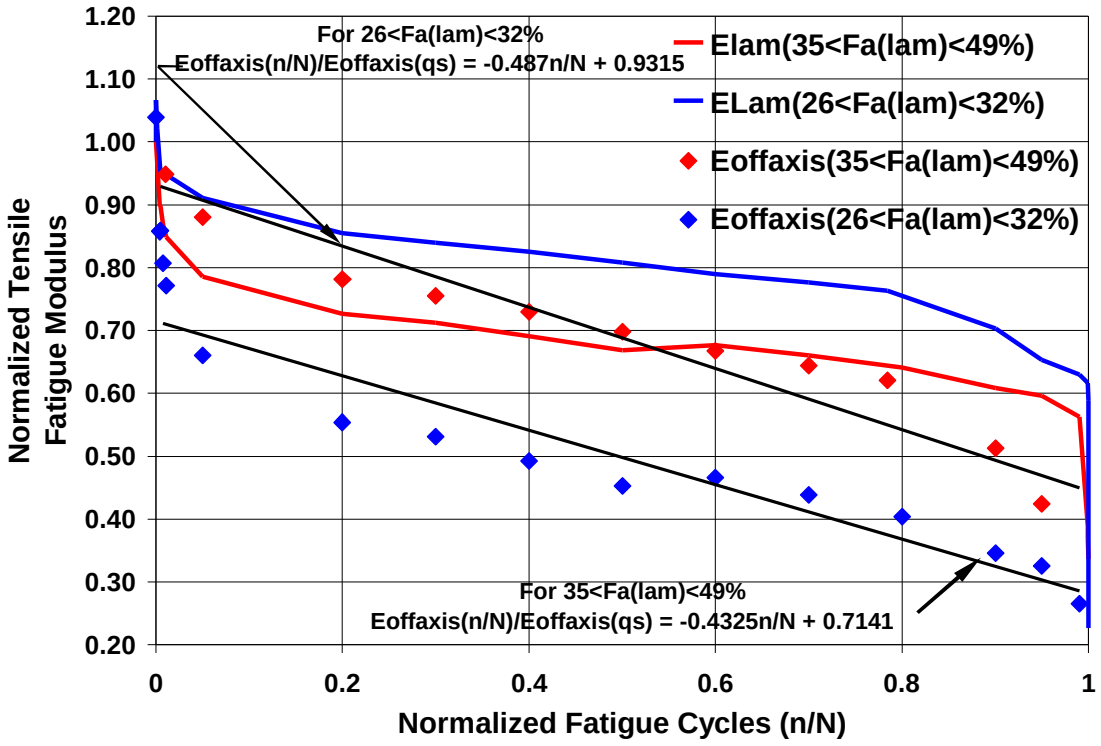

Figure 65: Normalized Tensile Fatigue Off-Axis Modulus Reduction for QI2 at 45 °.

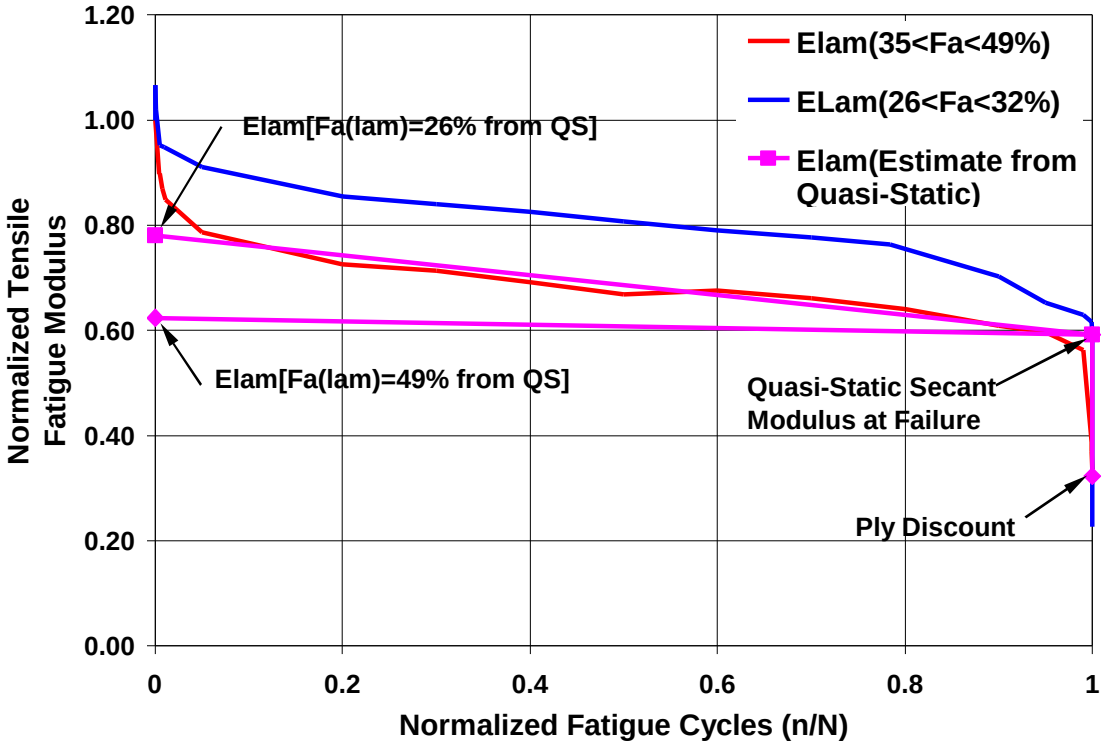

Figure 66: Normalized Tensile Fatigue Laminate Modulus Reduction of QI2 at 45 ° Estimated from Quasi-Static Data.

S-N Evaluation

Extraction of the Critical Element's S-N from Laminate S-N in Load Controlled

For residual strength analysis of the critical element, the 0° plies, the S-N curve of the critical element is needed. This fatigue testing was performed in load control; this means that the applied stress to the critical element, the 0° plies, continues to increase as the stiffness of the off-axis plies are reduced. If the control method were strain controlled, the critical element would see the same applied strain throughout the fatigue life and that would be the laminate strain. The measured laminate fatigue strength to fatigue failure cycles curve, S(lam)-N, of each laminate was converted to the S(0°)-N, for the critical element, the 0° plies aligned to the load. Using CLT and the off-axis stiffness reduction curves, the normalized applied stress, Fa_{0deg}, on the critical element was calculated over the entire life. This was accomplished in CLT by incrementally reducing the stiffness, E_2 and G_{12} equally, of the off-axis plies to the load direction and obtaining the increased stress on the 0° plies. The normalized applied load to the critical element, Fa_{0deg}, was then calculated by dividing this stress by the quasi-static strength of the 0° plies shown in Table 6. These Fa_{0deg} values were averaged over the entire life, meaning the entire stiffness reduction curve, to approximate the average Fa_{0deg} on the critical element. The S-N curve from cross-ply laminate designated CP2 in Table 2 was obtained from research performed in reference [48].

Results: S-N Analysis

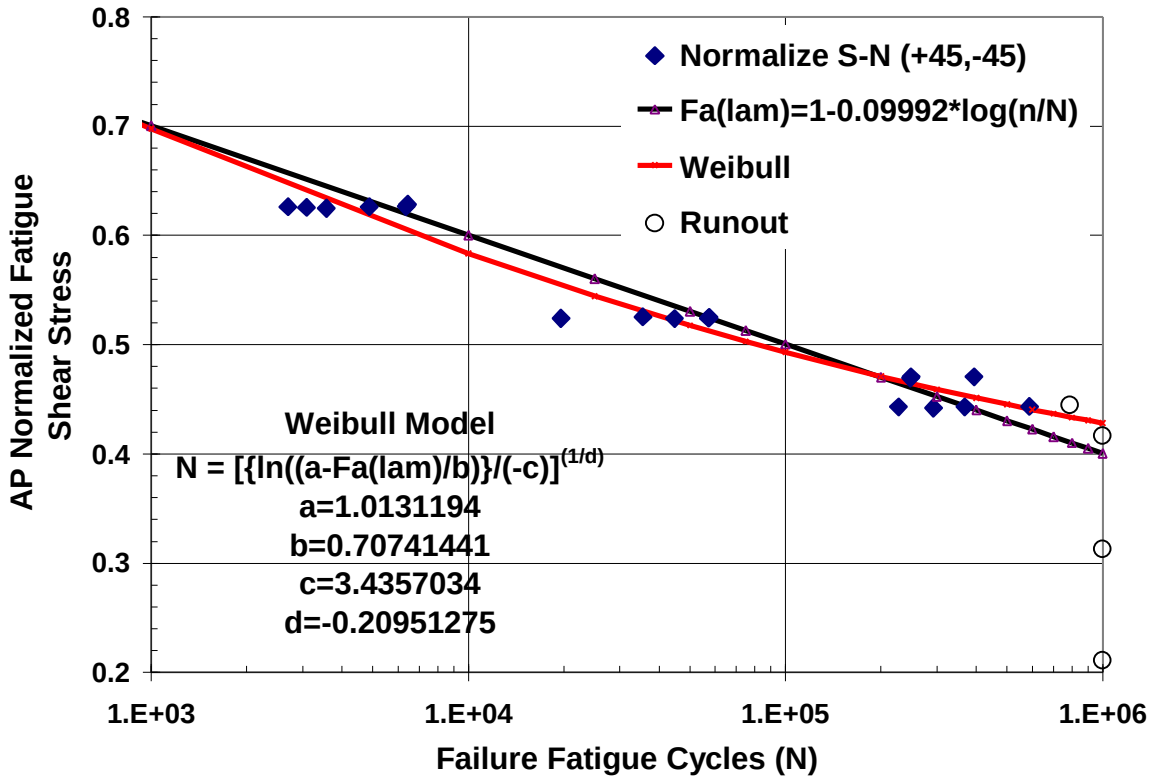

Figure 67: Normalized Fatigue Shear Stress vs. Failure Fatigue Cycles for <u>Angle-ply, AP, ±°45</u> Laminate: Measured Laminate

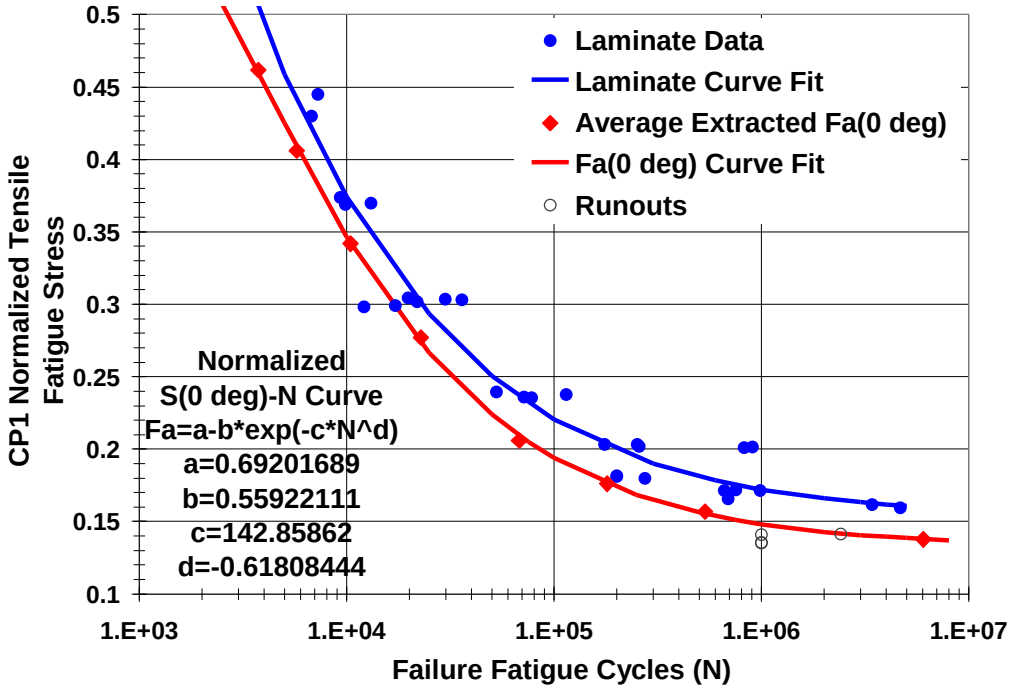

Figure 68: Normalized Axial Tensile Fatigue Stress vs. Failure Fatigue Cycles for <u>CP1</u> Laminate: Measured Laminate & Extracted Critical Element (0 °plies). Normalize Laminate Tensile Stress is Fa(Lam) = $s_{lam}(n)/X_T$; Normal 0 °Tensile Stress is Fa(0 °) = $s_{0°}(n)/X_{0°}$.

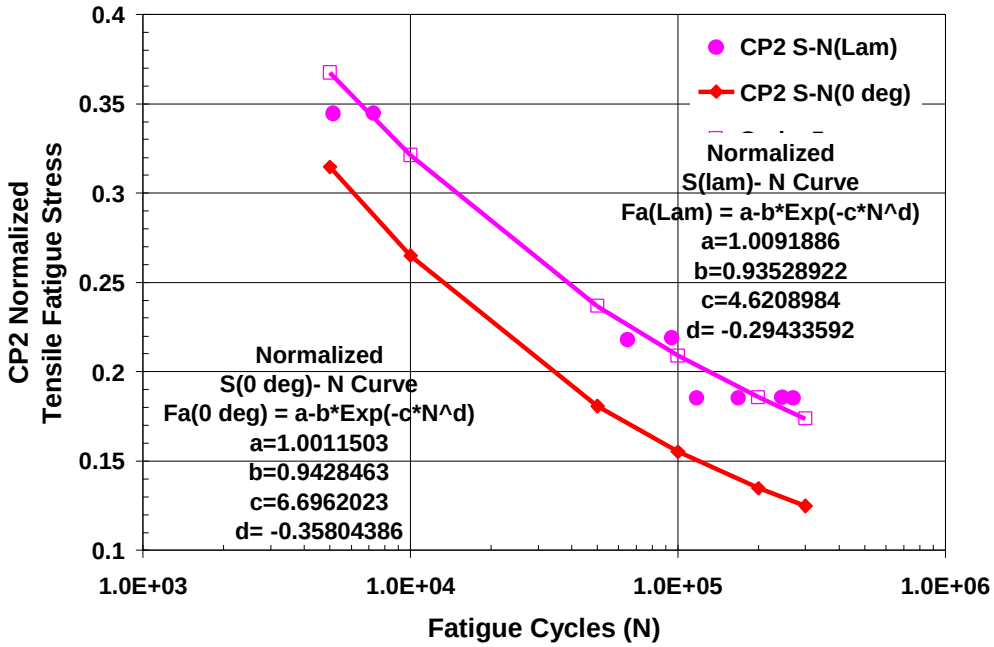

Figure 69: Normalized Axial Tensile Fatigue Stress vs. Failure Cycles for <u>CP2</u> Laminate: Measured Laminate & Extracted Critical Element (0 °plies).

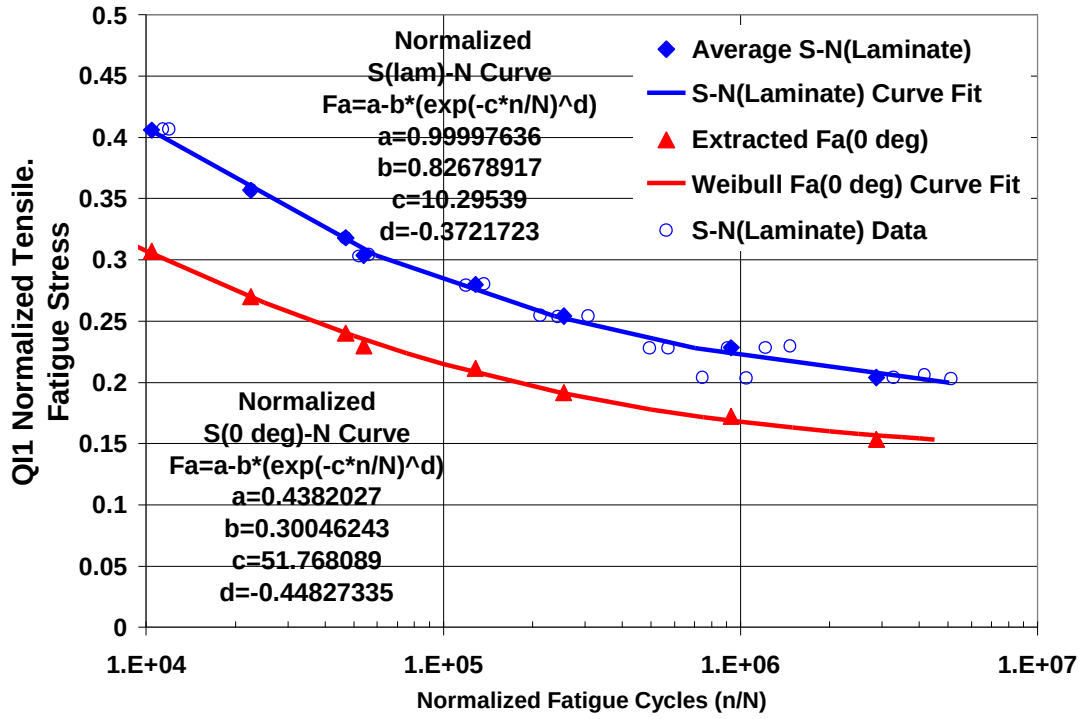

Figure 70: Normalized Axial Tensile Fatigue Stress vs. Failure Cycles for <u>QI1</u> Laminate: Measured Laminate & Extracted Critical Element (0 °plies)

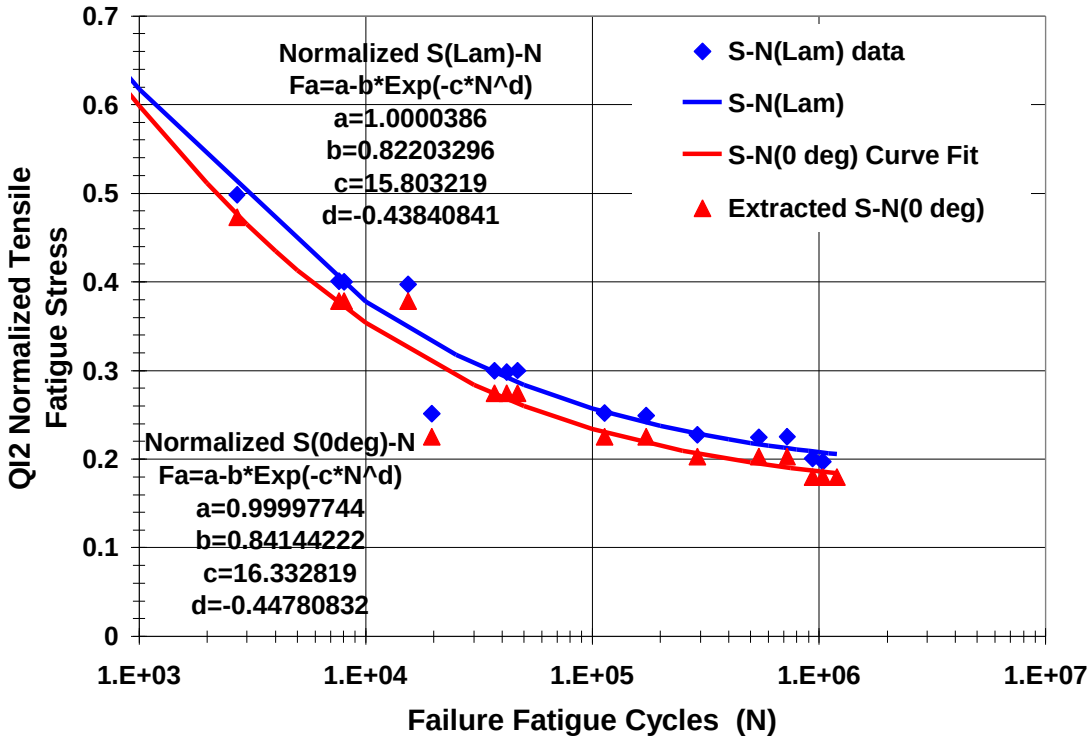

Figure 71: Normalized Axial Tensile Stress/ Fatigue Cycles Curve for <u>QI2</u> Laminate: Measured Laminate & Extracted Critical Element (0 °plies)

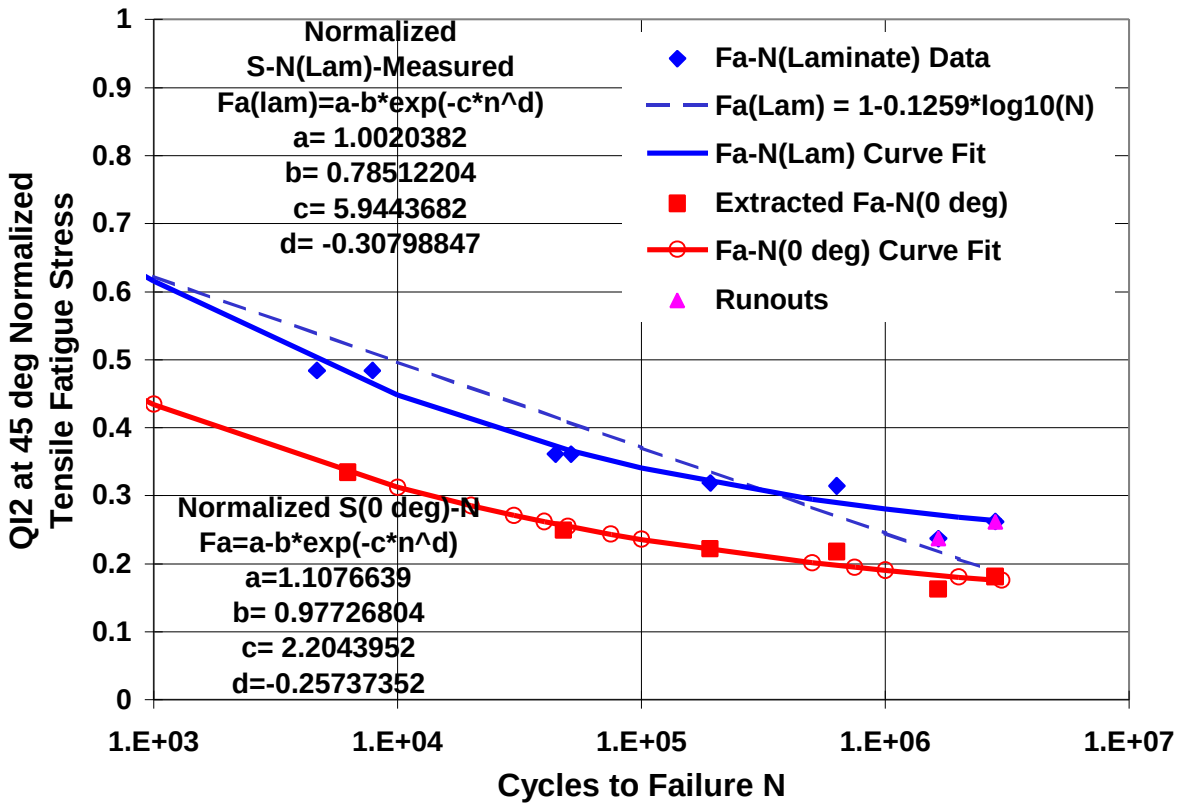

Figure 72: Normalized Tensile Fatigue Stress vs. Failure Cycles for QI2 at 45°: Measured Laminate & Extracted Critical Element (0°ply). Normalize Laminate Tensile Stress is Fa(Lam) = $s_{lam}(n)/X_T$; Normal 0°Tensile Stress is Fa(0°) = $s_{0°}(n)/X_{0°}$

Comparison of S-N Curves with Literature

The S-N curve of the critical element, the 0° plies, was found to be very dependent upon fiber geometry, and therefore dependent upon the process of manufacturing. In these tested laminates, the tricot stitch of the non-woven non-crimped fabric, NCF, gathered the axial fiber bundles and when in laminate form created a fiber undulation in both the axial and transverse direction to the pultrusion axis. This fiber undulation resulted in a lower S–N curve than curves found in literature for unidirectional and cross-ply laminates shown in Figure 73 and Figure 74. The literature cross-ply laminates were manufactured from pre-impregnated epoxy/E-glass tape, which has very little fiber undulation and usually are composed of thin plies, .005-.010 inch in thickness. The literature cross-ply laminate curves are noticeable higher than the 0° S-N curves that were extracted as described above from the cross-ply, and quasi-isotropic laminates S-N curves. These S(0°)-N extracted from the laminate S(lam)-N curves encompass the defects of the pultruded laminate, which included fiber waviness, stitch stress risers, and noticeable micro-cracking and slight delamination in the as-processed state. CP2 laminate having the thickest transverse fiber bundle with 60% of fibers in the 90° direction created a deeper cavity between fiber bundles. This allowed the 0° fiber bundles to dip farther, which created higher fiber undulation, and reduced the S(0°)-N curve.

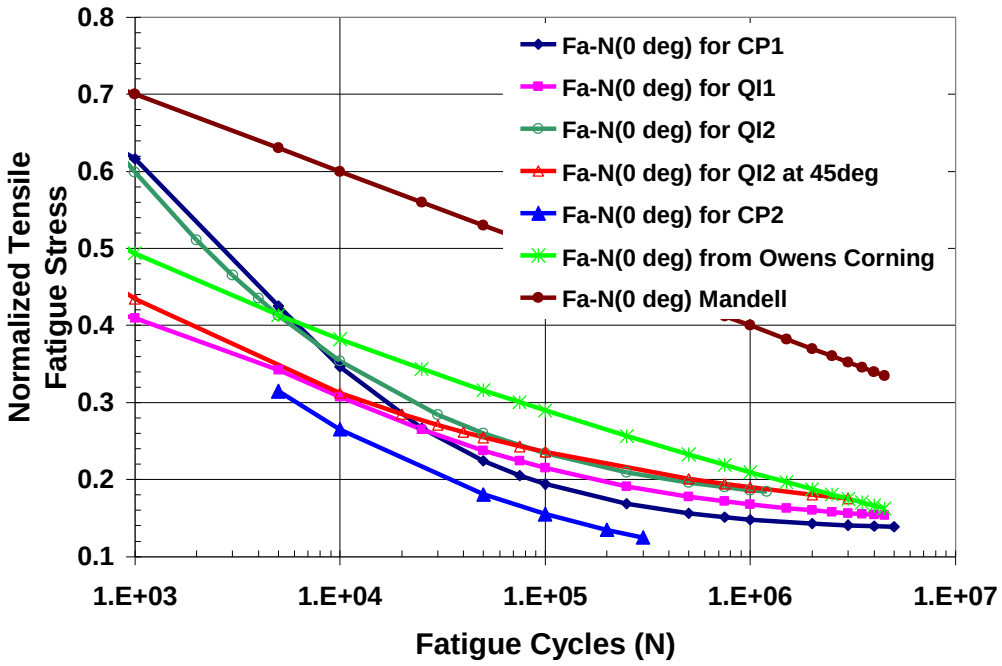

Figure 73: <u>Comparison of Normalized Unidirectional S-N Curves, Fa-N with Literature.</u> CP1, CP2, QI2, and QI2 at 45°are Current Research Pultruded Vinyl Ester/E-Glass Non-Crimped Fabric laminates. Mandell fabricated from Epoxy/E-Glass Tape.

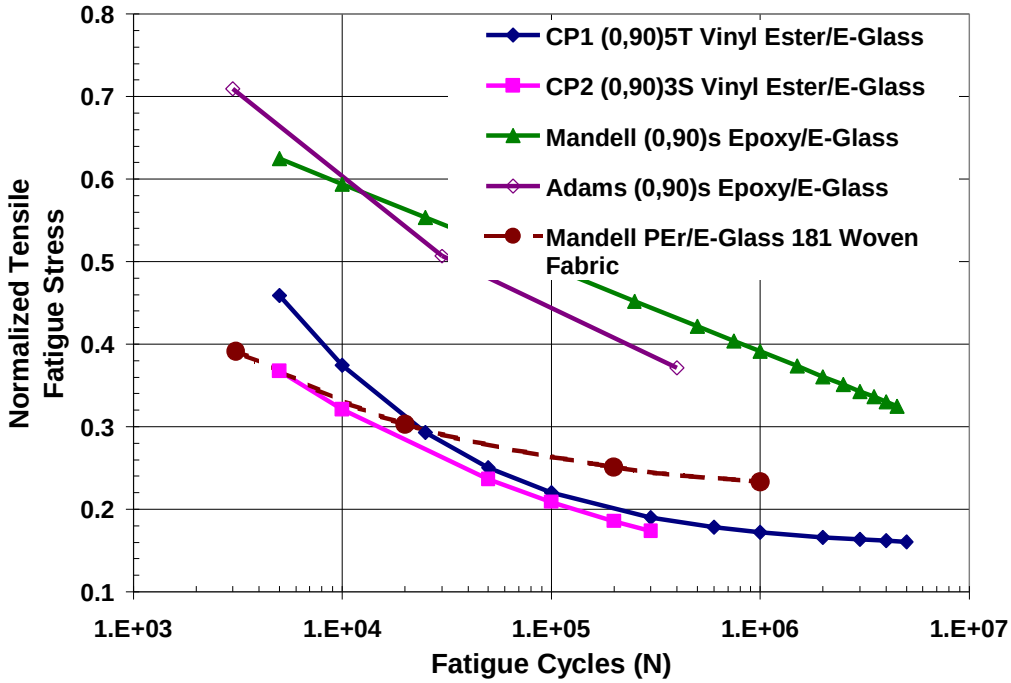

Figure 74: <u>Comparison of Laminate S-N Curves from Cross Ply and Woven Laminates</u>. CP1 and CP2 from Current Research Pultruded Vinyl Ester/E-Glass Non-Woven Tricot Stitched Non-Crimped Fabric. Mandell $(0,90)_S$ fabricated from Epoxy/E-Glass Tape. Adams $(0,90)_S$ fabricated from Epoxy/E-Glass Tape.

Residual Strength and Life Analysis

Assumptions for Residual Strength and Life Analysis

Residual strength testing involved fatigue cycling specimens to various percentages of life, n/N and at various load levels, Fa, as shown in Figure 75. In general, three specimens were fatigue to each of three various life percentages and this was repeated at three different load levels. Theses specimens were fatigued at these load levels and life percentages and then were quasi-statically failed to evaluate the residual strength. A curve fit of the residual strength equation, Equation 26, was applied to the residual strength data to determine the residual strength shape factor, "J". This shape factor was determined to be 0.95 for all tested vinyl ester/E-glass non-woven tricot stitched laminates fabricated from the Continuous Resin Transfer Molding (CRTM) pultrusion process. Figure 75 shows a typical curve fit for a cross-ply laminate designated CP1 from Table 2. For this analysis, the assumption was made that the remaining strength curve of the critical element had the same shape as the remaining strength of the laminate. This is logical since the remaining strength of the laminate is controlled by the strength of the critical element, which is the 0° lamina.

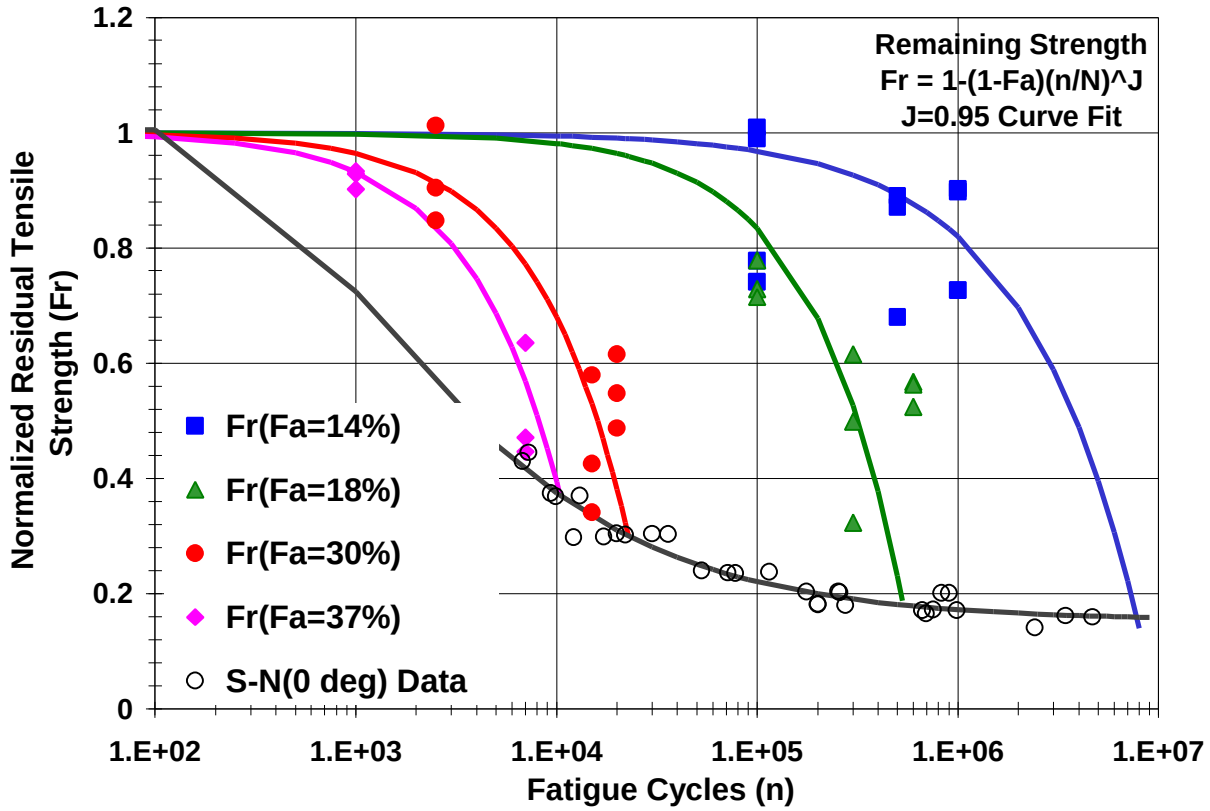

Figure 75: Normalized Residual Tensile Strength for CP1 Curve Fit for Remaining Strength Shape Factor J.

Correlation and Prediction

Correlation and predictions were performed on each laminate to determine the best method of prediction. Correlation involved using the stiffness reduction of the off-axis plies, the estimated S-N curve of the critical element, the 0° ply, the best fit "J" value of the strength

reduction curve fit, and the quasi-static strengths and stiffness all from the laminate to be analyzed. A prediction was different from the correlation in that the off-axis stiffness reduction, the critical element S-N curve, the curve fit "J", and the quasi-static strengths and stiffness of one laminate would be used to predict the residual strength of another laminate. One correlation "C1" and three predictions "P1"-"P3" were performed on these laminates as shown in Table 10. CP1, CP2, and AP are designations for laminate types defined in Table 2.

To explain the reasons for the different types of predictions, consider the following. From a product design engineer's viewpoint, there are different stages of product development. The first stage of product development is often trade studies where materials and process types are compared for cost and performance. Exact analysis is not required in this phase, but an approximate life prediction method would greatly enhance the ability to perform trade studies for cost-life evaluation. This could be performed with data from prior in-house testing or from data obtained from literature as shown in Table 10 labeled "P3". The subsequent stages of product development involve detailed design, prototype fabrication, testing, and evaluation. At this stage, quasi-static testing for strength and stiffness are nearly always available where "P1" and "P2" in Table 10 represent this option. Prediction "P1" represents the fatigue stiffness reduction from the quasi-static stress/strain curve. The initial stiffness would be the secant modulus at the applied fatigue load. The fatigue stiffness at fatigue failure would be represented by the secant stiffness at quasi-static ultimate failure. Prediction "P2" would represent the case where prior quasi-static and fatigue testing of similar cross-ply and angled-ply composites have been performed. Finally, prior to production, qualification tests are performed on the system, which includes vibration, environmental, mechanical, and field evaluations. If the product requires durability over an extended life, fatigue testing at component and/or specimen level is often required. At this point fatigue correlation testing would be performed.

Four basic data types are needed for life prediction. These are:

1. quasi-static ply level strength and stiffness,
2. fatigue stiffness reduction curves,
3. S-N curves for the critical element (0° plies), and
4. residual strength curve shape factor "J".

Each of these critically affects life prediction as will be shown. The residual strength curve shape was determined to fit J=0.95 for all pultruded vinyl ester/E-glass laminates tested. The S-N curves shown in Figure 73 and Figure 74 shows the variability of literature as well as each laminate tested. Table 5 and Table 6 show the ply level strength and stiffness variability between the current laminates tested. Figure 42 compares the variability of in-situ fiber strengths of literature and the current laminates tested. Table 9 shows the off-axis stiffness reductions for each laminate tested.

Table 10: Remaining Strength Analysis Matrix

Remaining Strength Analysis and Designation of X-Laminate	Quasi-Static Strength & Stiffness	Off-Axis Fatigue Stiffness Reduction	Normalized S-N Fa-N(0°) Critical Element	Remaining Strength Shape Factor J
Correlation C1	X-Laminate	X-Laminate	X-Laminate	X-Laminate
Prediction P1	X-Laminate	X-Laminate Quasi-Static Estimate	Y-Laminate	Y-Laminate
Prediction P2	X-Laminate	E_{2Red} from CP1 or CP2 G_{12Red} from AP(±45°)	Y-Laminate	Y-Laminate
Prediction P3	Y-Laminate	Y-Laminate	Y-Laminate	Y-Laminate

Residual Strength Compared with Literature

Figure 73 and Figure 74 compares residual strength curves found in literature to current research. Adams shows a much higher residual strength shape factor, J=7.5 for autoclaved preimpregnated epoxy/E-glass cross-ply laminates. Adams has shown that both Kevlar and HT-S carbon had even higher shape factors. [42] Many composites have been found to have a shape factor of J = 1.2 from research performed in house. To view the effects of higher shape factors, Figure 73 and Figure 74 show J= 0.95, 1.2, and 20 for normalized applied fatigue stress of 0.5. As J becomes larger, the residual strength approaches sudden death. When J = ∞, the residual strength approaches Miner's Law where residual strength is not considered and only the sum of the ratios of number of cycles at stress level to fatigue life at those stress levels determine fatigue life.

The following sections are broken down by laminate type. A brief discussion precedes the figures, which compares the correlation and predictions to measured residual strength.

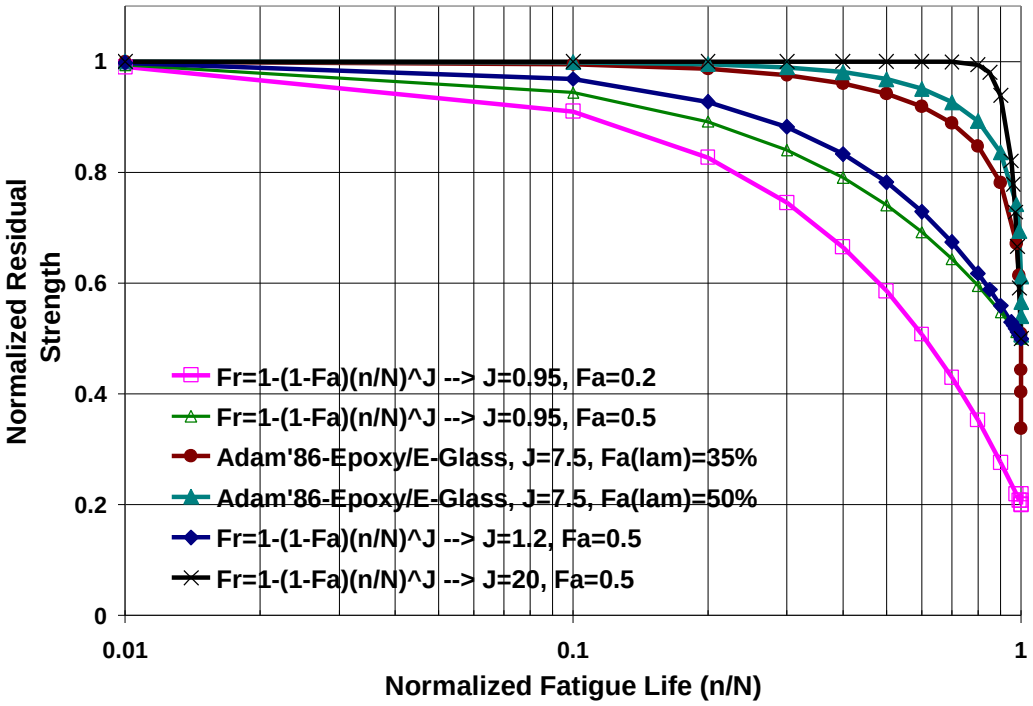

Figure 76: Comparison of Residual Strength Curves Epoxy/E-Glass from T. Adams with 35%<Fa<85% and Vinyl Ester/E-Glass from Current Research with 18%<Fa<40%, showing the lower Residual Strength of the Pultruded Vinyl Ester/E-Glass laminates in Log Time Scale, Log(n/N).

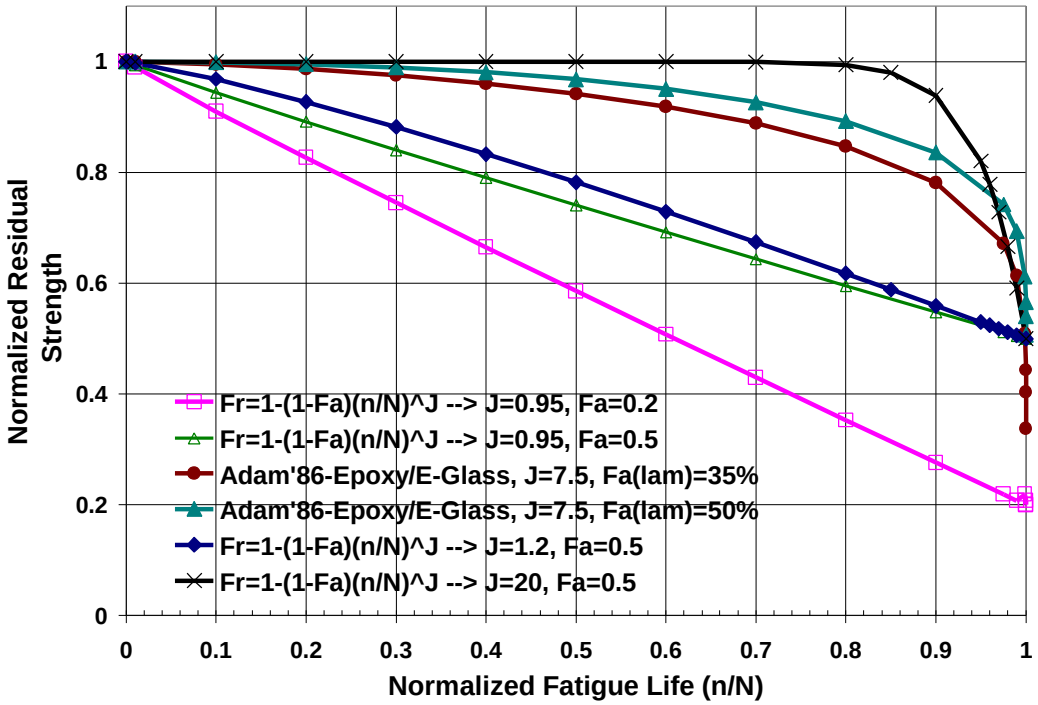

Figure 77: Repeat of Figure 74 in Linear Time Scale, n/N.

Residual Strength of Angle-ply Laminates

The residual strength of the ±45° laminates, shown in Figure 78, followed a very linear and slight reduction in residual strength until failure, which appears to take the form of sudden death failure that uniaxial and transverse lamina are typical. The extension beyond life of n/N =1 occurred because of the uncertainty of the life N at each load level.

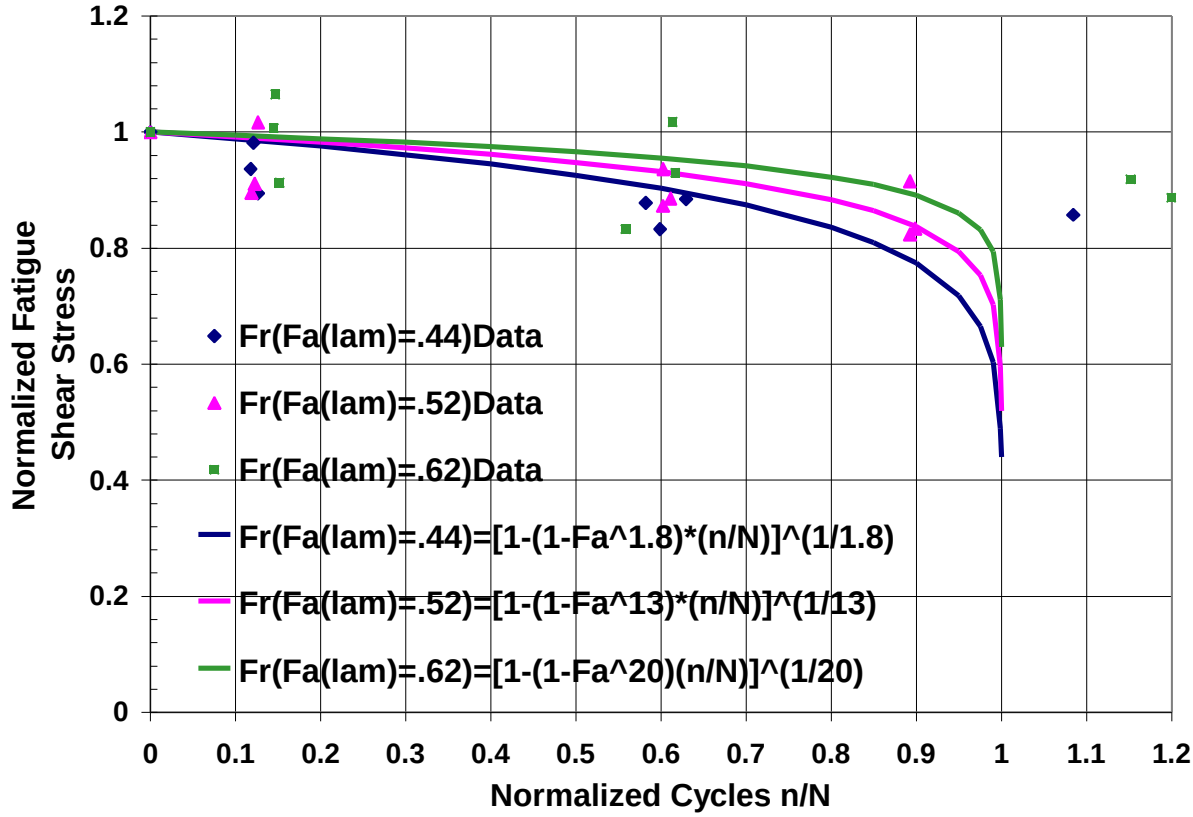

Figure 78: Residual Axial Strength for ±45°Tensile Specimens

CP1 Remaining Strength Analysis

Following the correlation in accuracy for residual strength of the cross-ply CP1 laminate, (0,90)5T, was the prediction using CP1's strength, X_i, and stiffness, E_i, the stiffness reduction curve and normalized S-N curve from QI1 laminate shown Figure 84. From Figure 73, the S-N curves for CP1 and QI1 are seen to be adjacent to each other. Table 9 shows that the fatigue stiffness reduction curves for CP1 and QI1 are similar. The quasi-static strength and stiffness are similar as seen in Table 5 and Table 6. The next best prediction is seen in Figure 81, prediction using CP1's strength, X_i, and stiffness, E_i, the stiffness reduction curve E2 from CP1 and G12 from angled ply laminate, AP, and the normalized S-N curve from QI1 laminate. When compared with the correlation, this shows the effects of different S-N curve. Figure 86 shows the predicted verses actual fatigue life for each correlation and prediction.

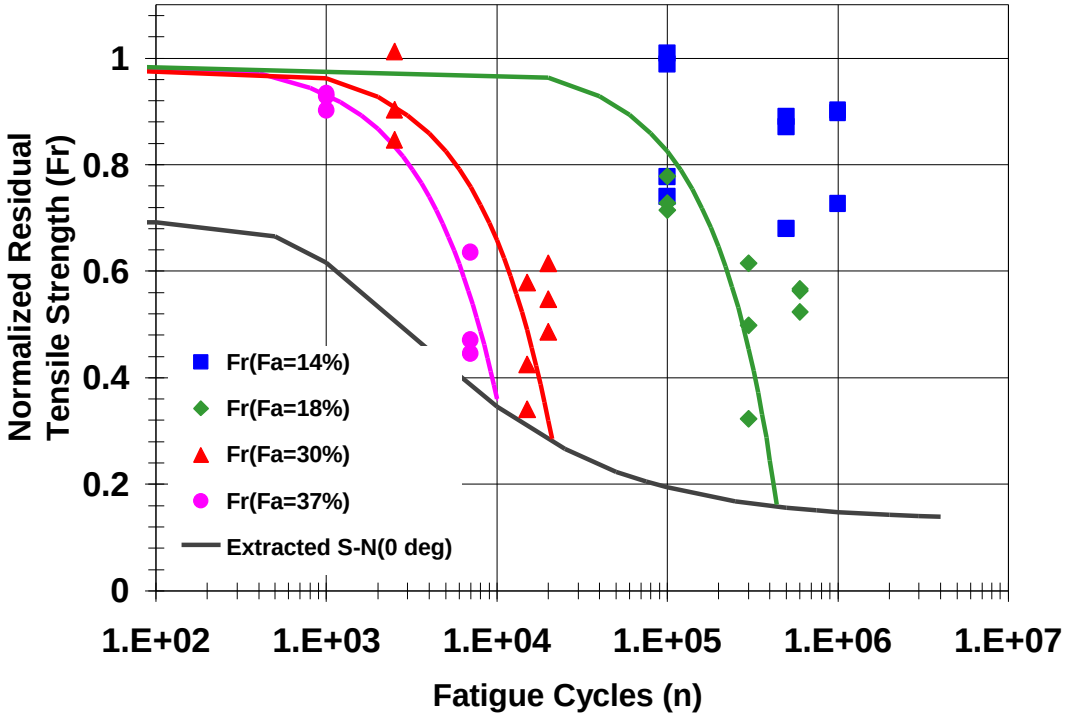

Figure 79: Normalized Residual Tensile Strength Correlation for CP1 with assumptions of off-axis stiffness reduction is equal for E2 and G12.

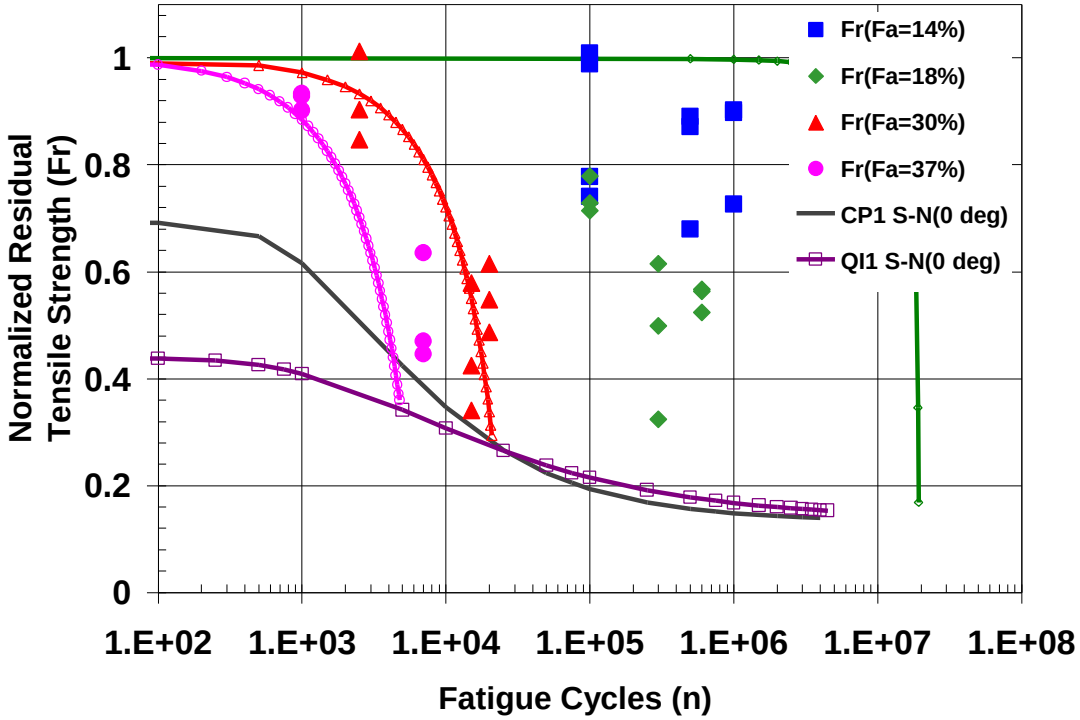

Figure 80: Prediction for CP1 from Quasi-static X_T & E of CP1 and E-Reduction from Estimate of CP1Quasi-static Secant Stiffness, & Fa-N of QI1.

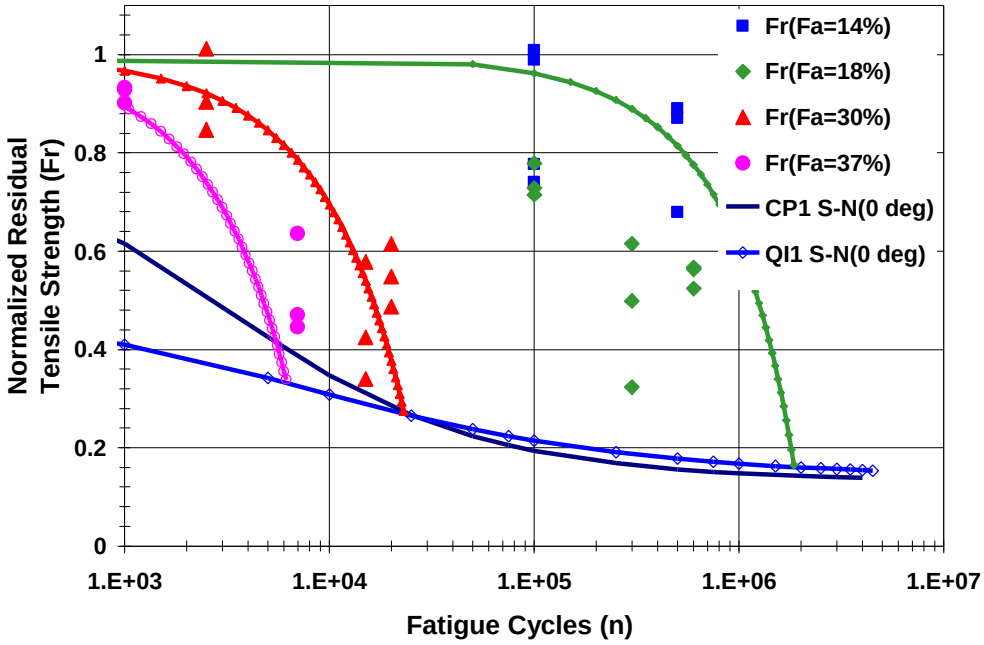

Figure 81: Residual Strength Prediction of CP1, Using Strength and Stiffness Values from Quasi-Static Data of CP1. E2 & G12 Reduction Curves are Estimated from CP1 and AP Fatigue Stiffness Reduction Curves, and Normalized S-N, Fa-N, from QI1.

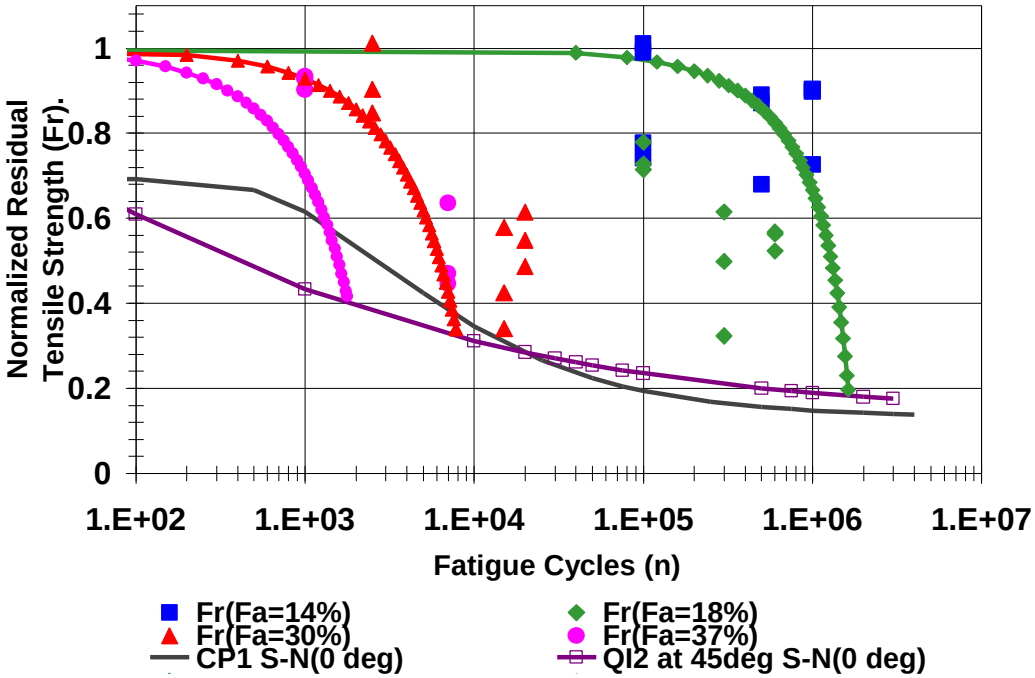

Figure 82: Residual Strength Prediction of CP1, Using Strength and Stiffness Values from Quasi-Static Data, Eoffaxis Stiffness Reduction Curves, and Normalized S-N, Fa-N from QI2 at 45 °.

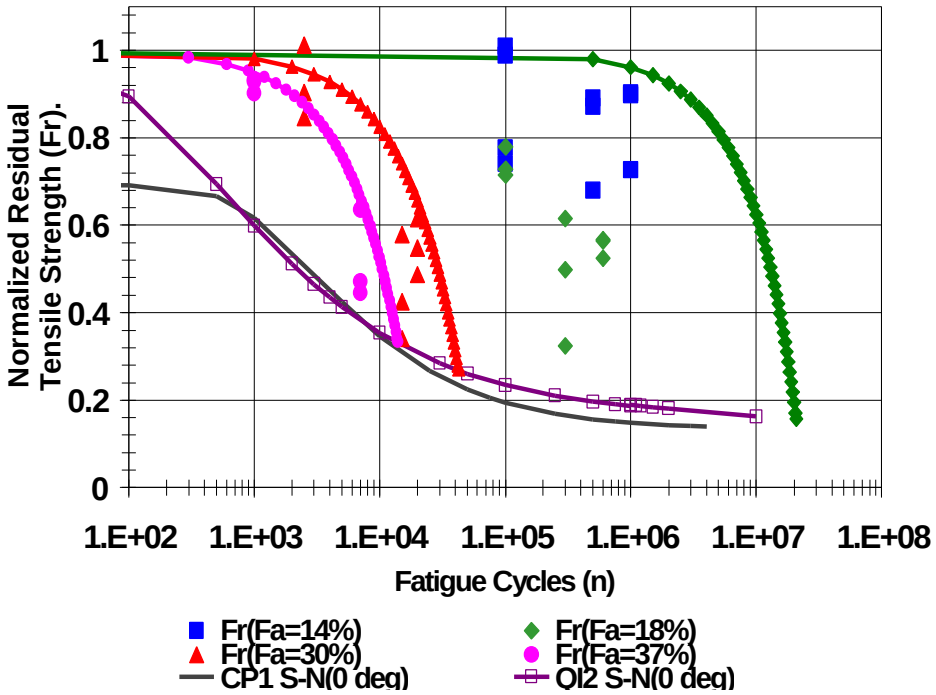

Figure 83: Residual Strength Prediction of CP1, Using Strength and Stiffness Values from Quasi-Static Data, Eoffaxis Stiffness Reduction Curves, and Normalized S-N, Fa-N from QI2.

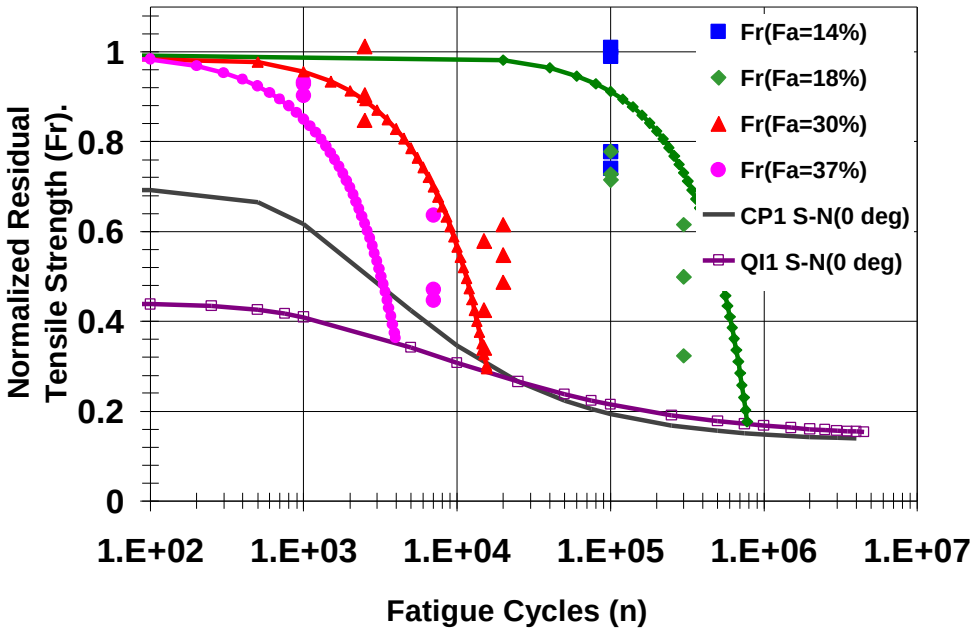

Figure 84: Residual Strength Prediction of CP1, Using Strength and Stiffness Values from Quasi-Static Data of CP1. Eoffaxis Stiffness Reduction Curves, and Normalized S-N, Fa-N from QI1.

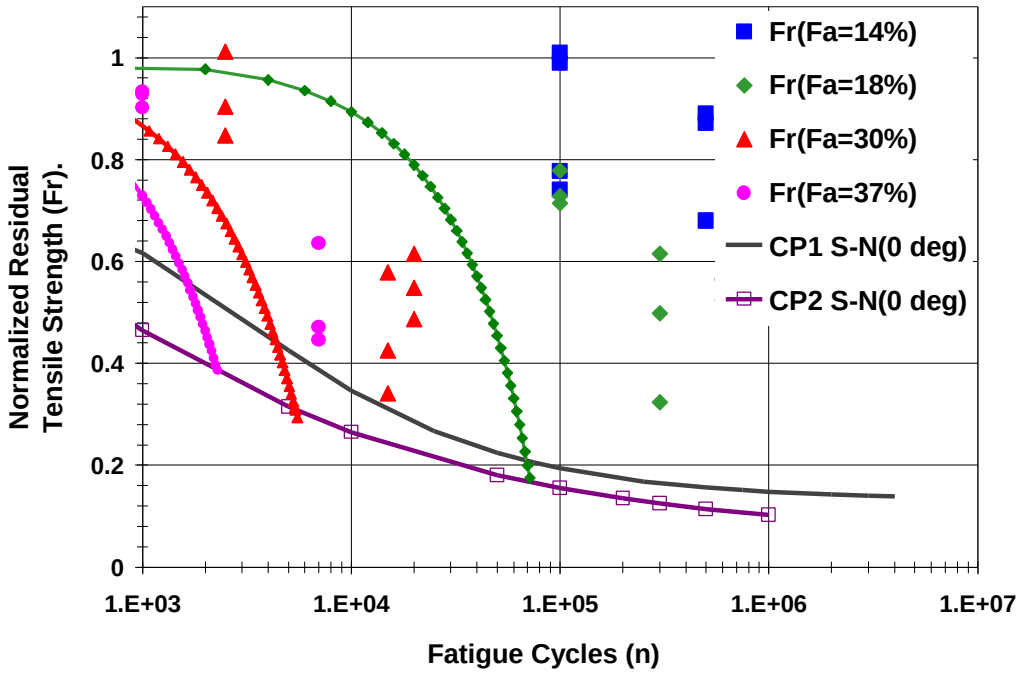

Figure 85: Residual Strength Prediction of CP1, Using Strength and Stiffness Values from Quasi-Static Data of CP2. Eoffaxis Stiffness Reduction Curves, and Normalized S-N, Fa-N from CP2.

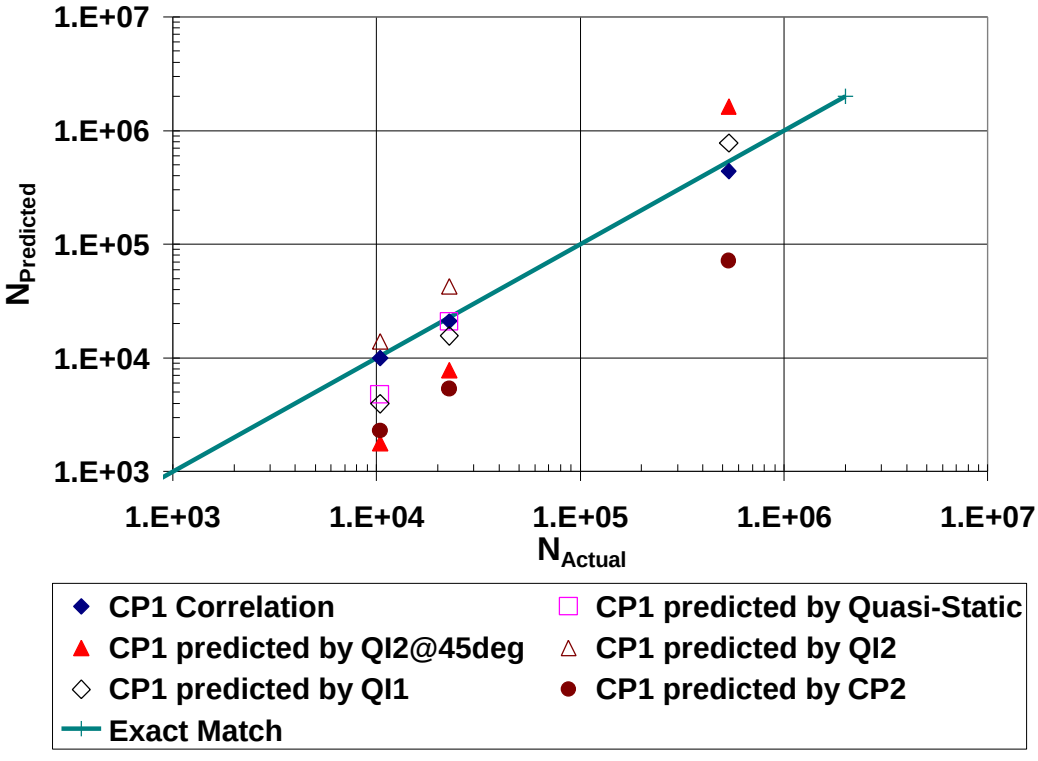

Figure 86: CP1 Life Correlation and Predictions $N_{Predicted} - N_{Actual}$

QI1 Remaining Strength Analysis

The correlation of the quasi-isotropic QI1 laminate, $(90,0,\ 2(\pm 45),\ 0,90)_{2T}$, Figure 87, most accurately fit the residual strength data. Following the correlation, was the prediction using QI1's strength, X_i, and stiffness, E_i, the fatigue stiffness reduction curve E_2 from CP2 and G_{12} from angled ply laminate, AP, and the normalized S-N curve from QI1 laminate shown in Figure 90. Figure 89 represents the exact prediction of Figure 90 with the substitution of CP1 for CP2 fatigue stiffness reduction. Comparing these two graphs shows the effect of a higher stiffness reduction curve, CP1 as seen in Table 9. The next best prediction is seen in Figure 91, QI1 prediction using strength, X_i, and stiffness, E_i, the stiffness reduction curve, and the normalized S-N curve from CP1 laminate. The quasi-static secant stiffness prediction was high in this case seen in Figure 88. Figure 95 shows the predicted verses actual fatigue life for each correlation and prediction.

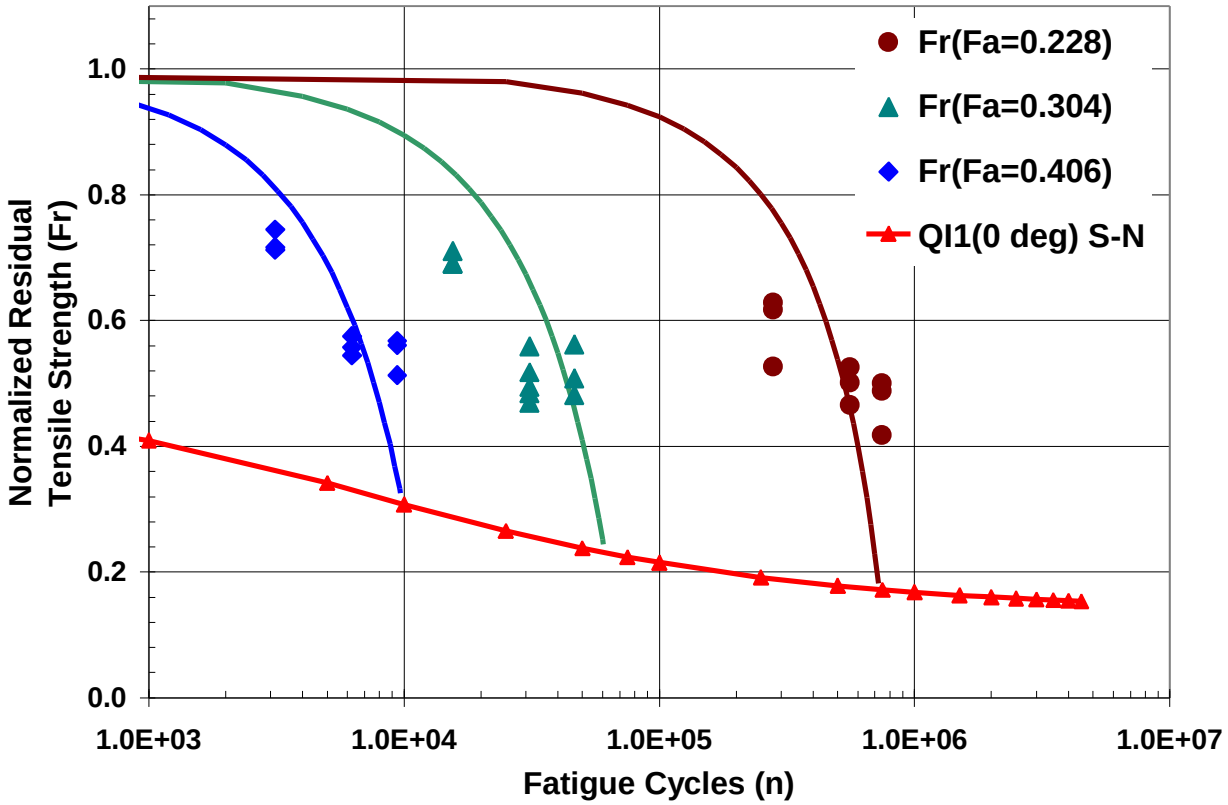

Figure 87: Remaining Strength <u>Correlation</u> for QI1 Using S-N, X_i, E_i, & Stiffness Reduction from QI1 Laminate.

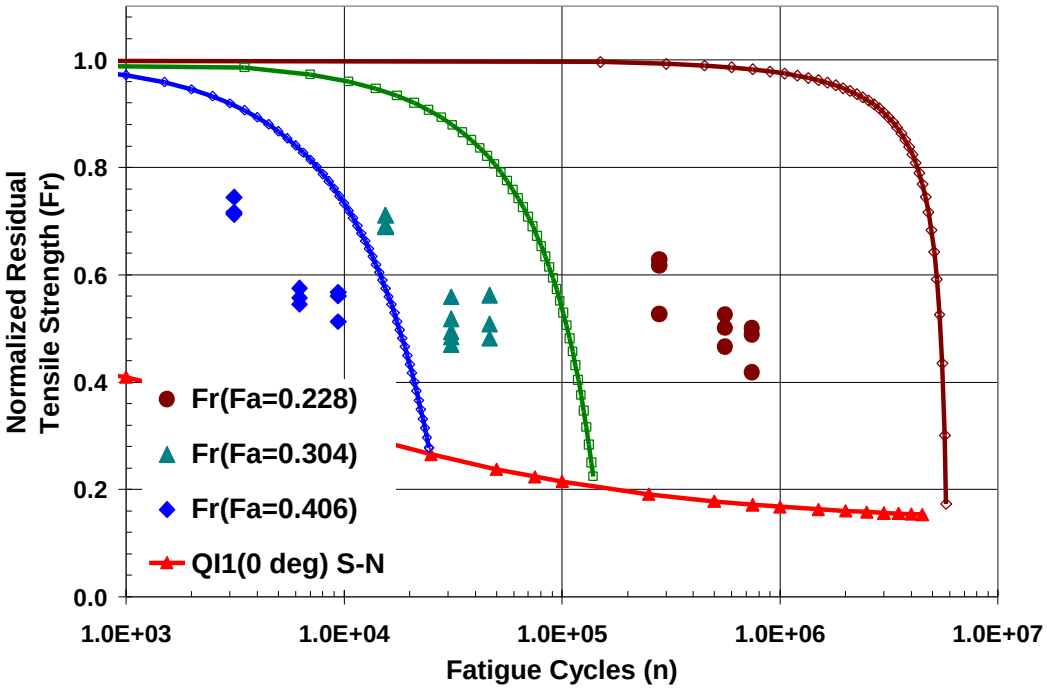

Figure 88: Residual Strength Prediction of QI1 Using Strength and Stiffness Values from Quasi-Static Data and Stiffness Reduction Estimated from Quasi-Static Secant Stiffness at Applied Fa and at Ultimate Failure.

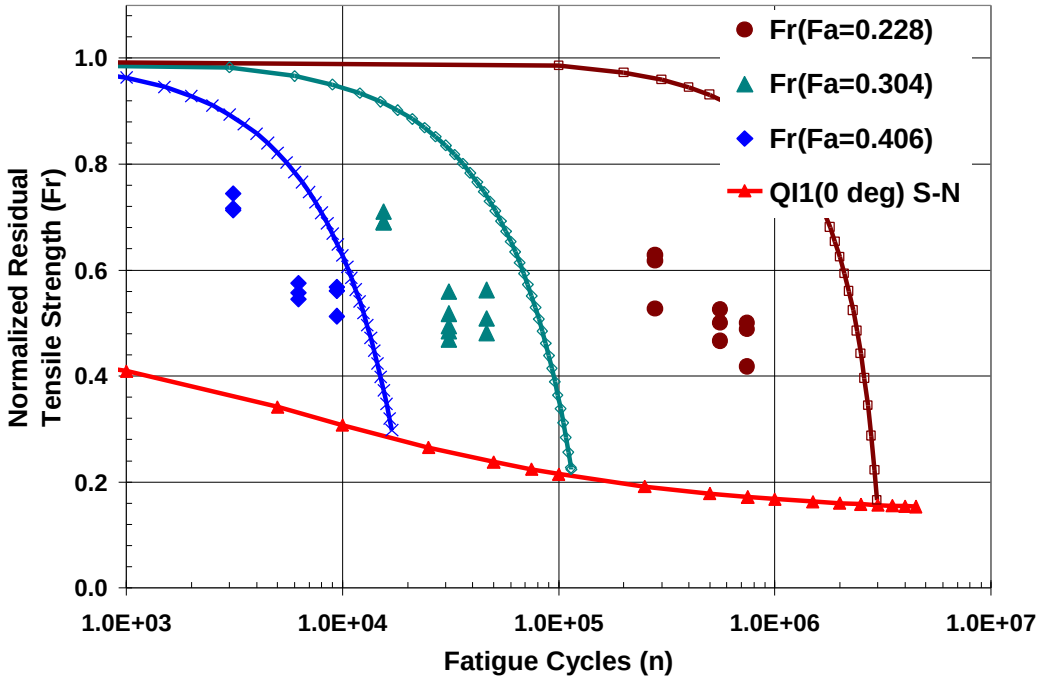

Figure 89: Residual Strength Prediction of QI1 Using Strength and Stiffness Values from Quasi-Static Data of QI1, E2 & G12 Reduction Curves Estimated from CP1 and AP Fatigue Stiffness Reduction Curves, and Normalized S-N, Fa-N, from QI1.

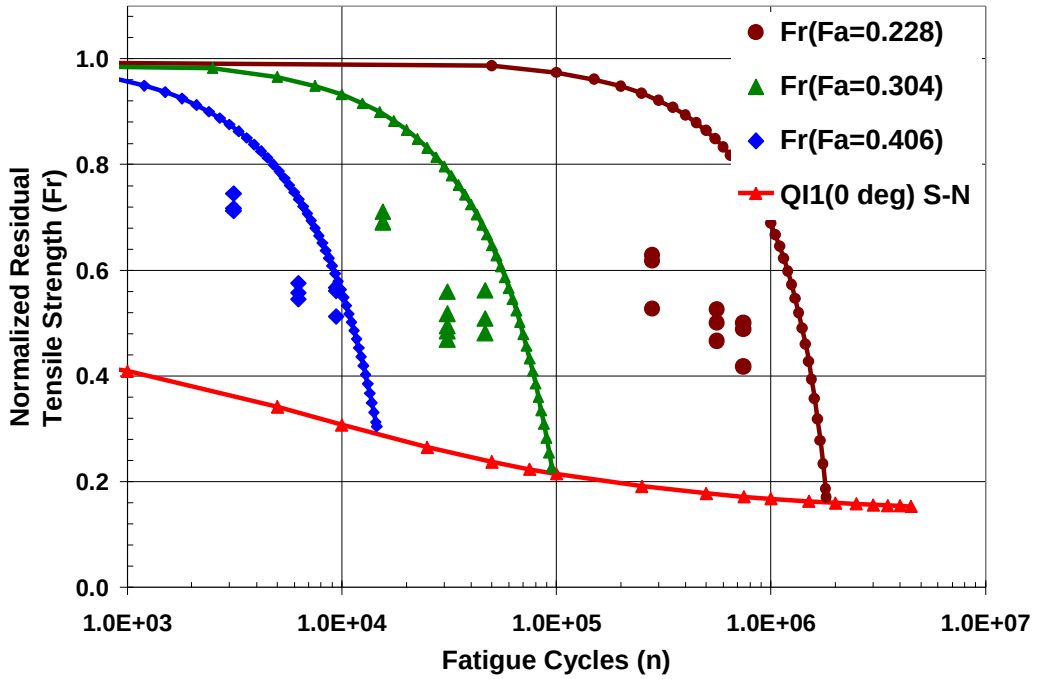

Figure 90: Residual Strength Prediction of QI1 Using Strength and Stiffness Values from Quasi-Static Data of QI1, E2 & G12 Reduction Curves Estimated from CP2 and AP Fatigue Stiffness Reduction Curves, and Normalized S-N, Fa-N, from QI1.

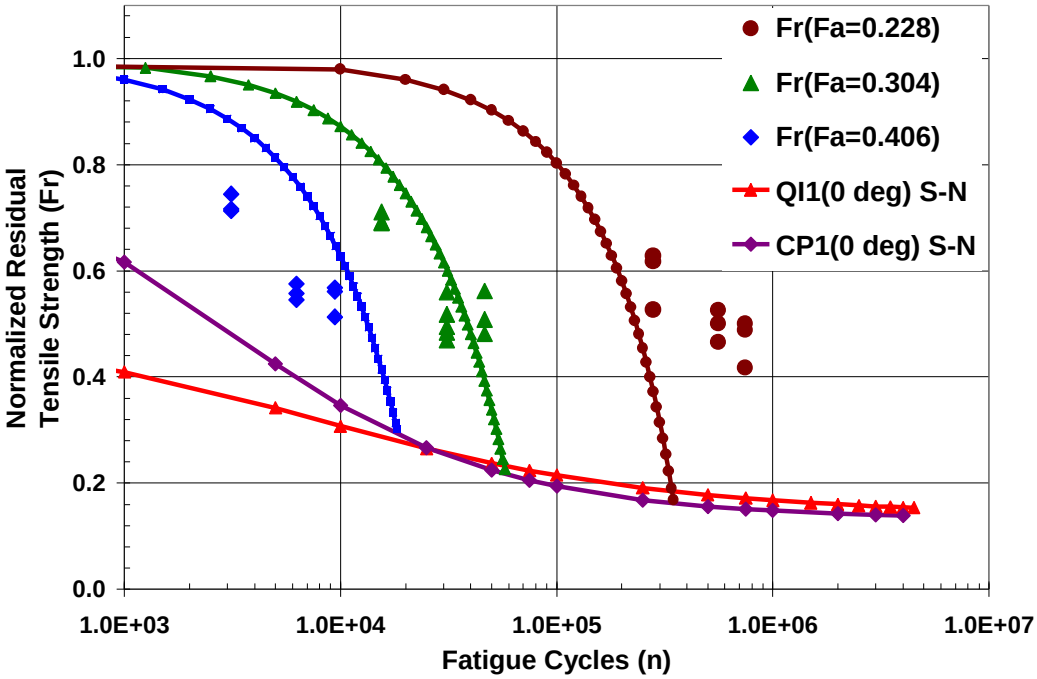

Figure 91: Residual Strength Prediction of QI1 Using Quasi-static Strength and Stiffness Values, Fatigue Stiffness Reduction Curve, and Normalized S-N, Fa-N curve from CP1 Laminate.

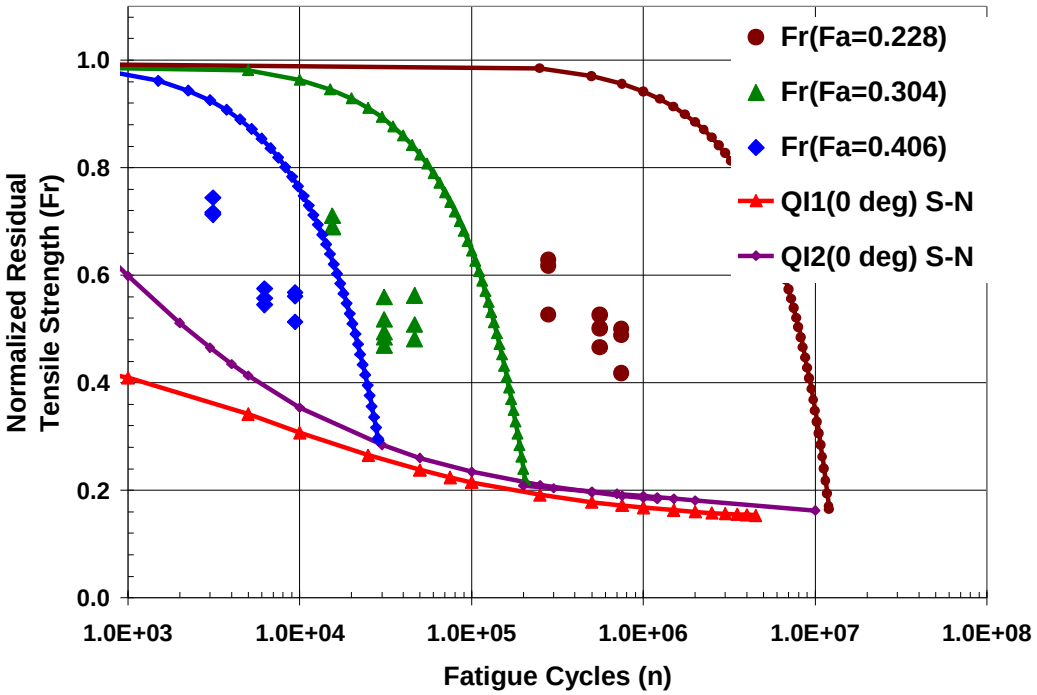

Figure 92: Residual Strength Prediction of QI1 Using Quasi-static Strength and Stiffness Values, Fatigue Stiffness Reduction Curve, and Normalized S-N, Fa-N curve from QI2 Laminate.

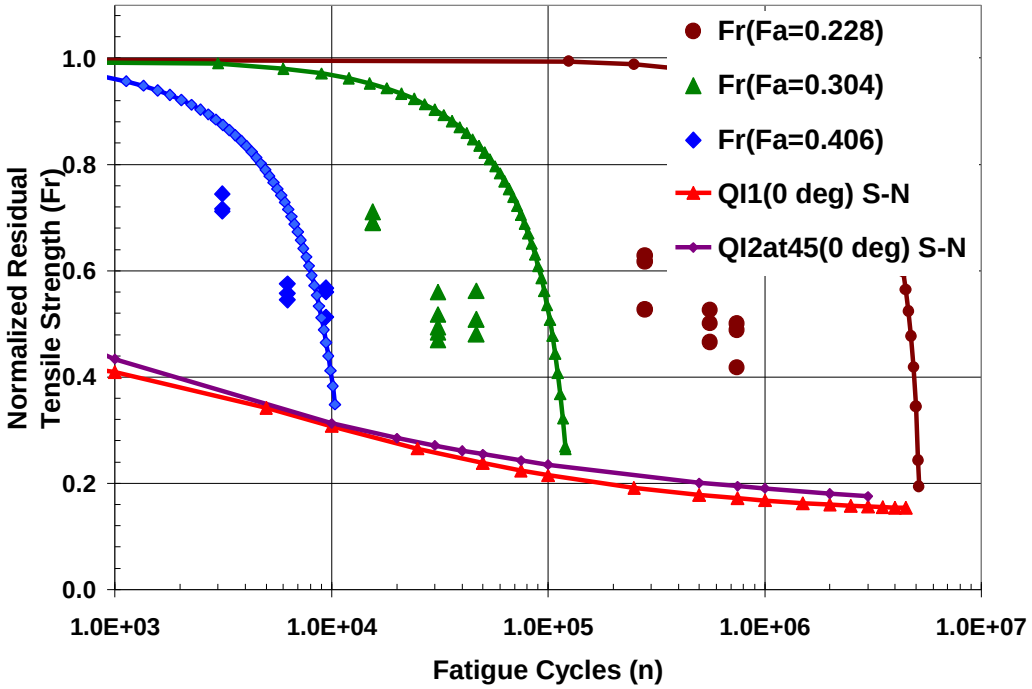

Figure 93: Residual Strength Prediction of QI1 Using Quasi-static Strength and Stiffness Values, Fatigue Stiffness Reduction Curve, and Normalized S-N, Fa-N curve from QI2 at 45 ° Laminate.

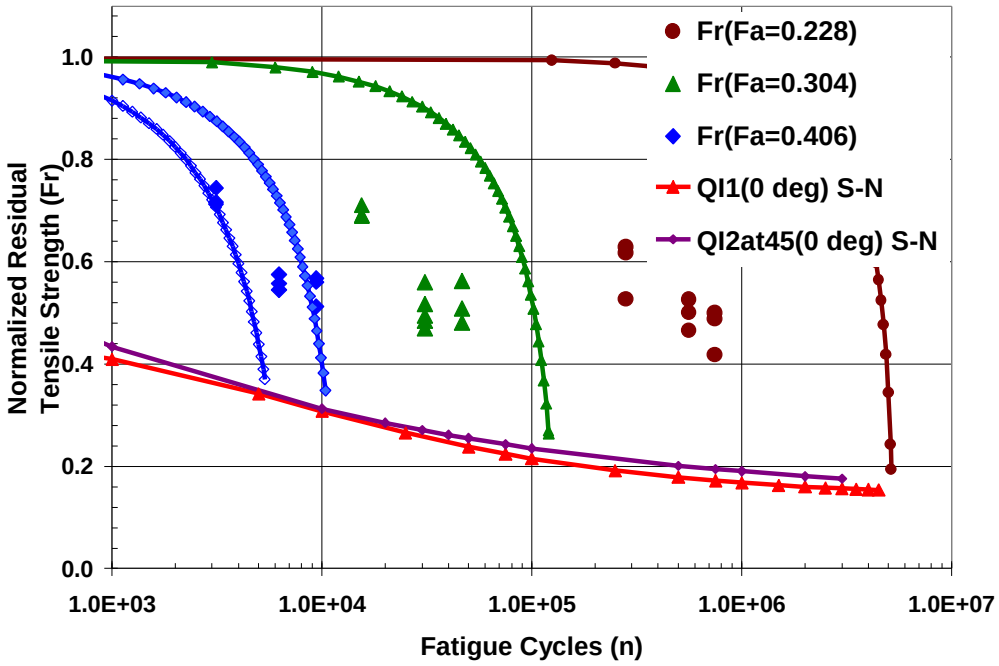

Figure 94: Residual Strength Prediction of QI1 Using Quasi-static Strength and Stiffness Values, Fatigue Stiffness Reduction Curve, and Normalized S-N, Fa-N curve from QI2 at 45 ° Laminate. The Fr(Fa=0.406) was predicted with the two Stiffness Reduction Curves shown in Figure 50.

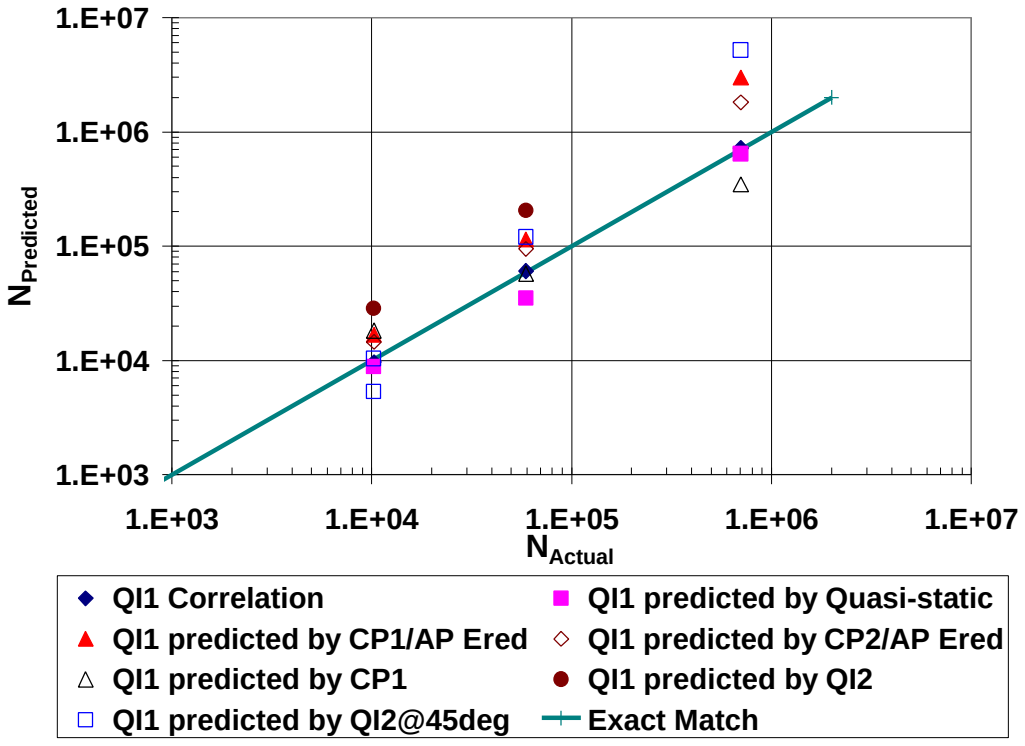

Figure 95: QI1 Life Correlation and Predictions $N_{Predicted} - N_{Actual}$

QI2 Remaining Strength Analysis

The correlation of the quasi-isotropic QI2 laminate$(0,90,\pm 45,0,90)2_T$, Figure 96, most accurately fit the residual strength data. Following the correlation, was the prediction using QI2's strength, X_i, and stiffness, E_i, the fatigue stiffness reduction curve E_2 from CP1 and G_{12} from angled ply laminate, AP, and the normalized S-N curve from QI1 laminate shown in Figure 98. The S-N curve of QI2 is slightly higher than QI1 as seen in Figure 73. The next best prediction is seen in Figure 99, prediction using strength, X_i, and stiffness, E_i, the stiffness reduction curve, and the normalized S-N curve all from CP1 laminate. The quasi-static secant stiffness prediction was high in this case. Figure 100 shows the predicted verses actual fatigue life for each correlation and prediction.

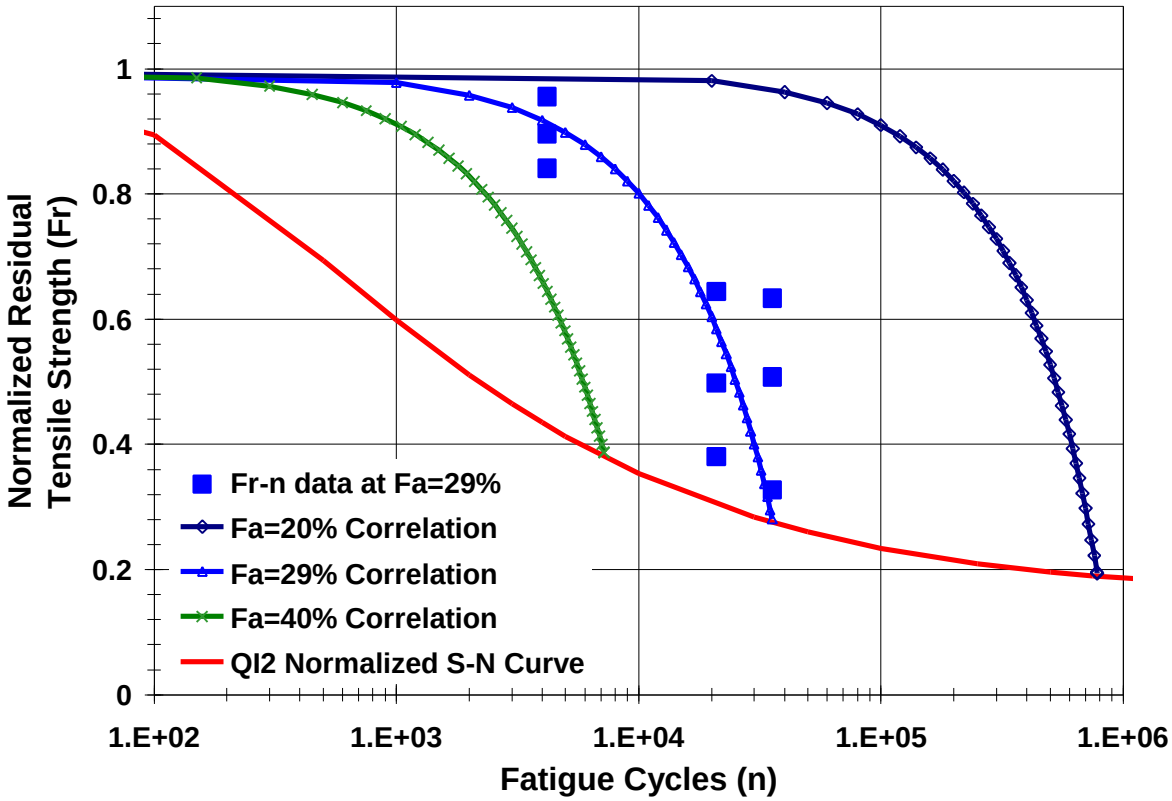

Figure 96: Remaining Strength Correlation for QI2 Using S-N, X_i, E_i, & Stiffness Reduction from QI2 Laminate.

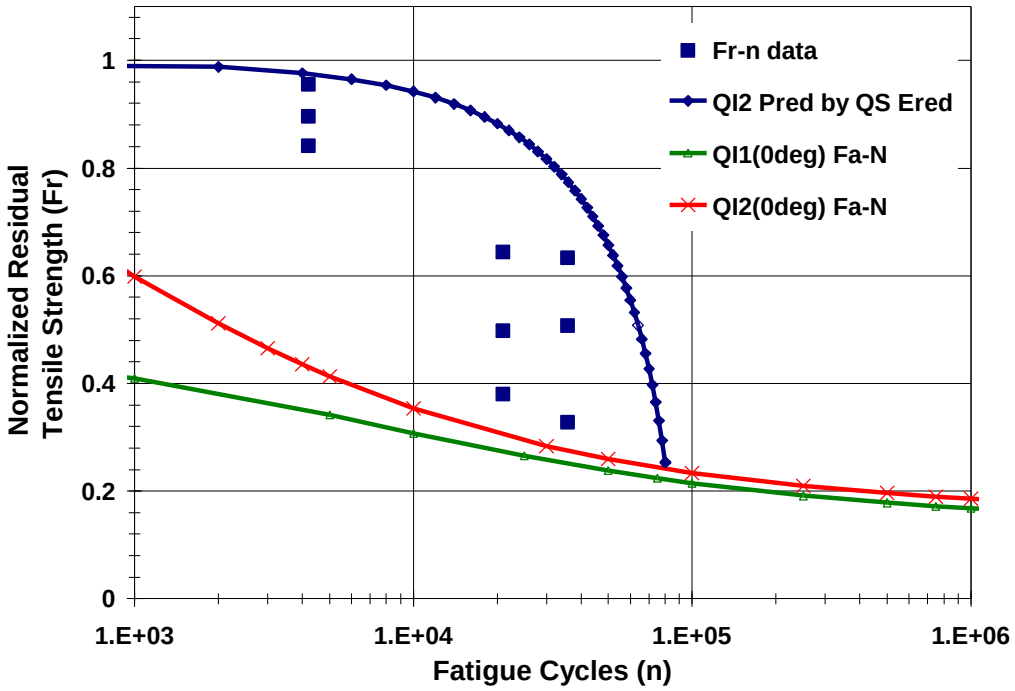

Figure 97: Residual Strength Prediction of QI2 Using Strength and Stiffness Values from Quasi-Static Data and Stiffness Reduction Estimated from Quasi-Static Secant Stiffness at Applied Fa and at Ultimate Failure.

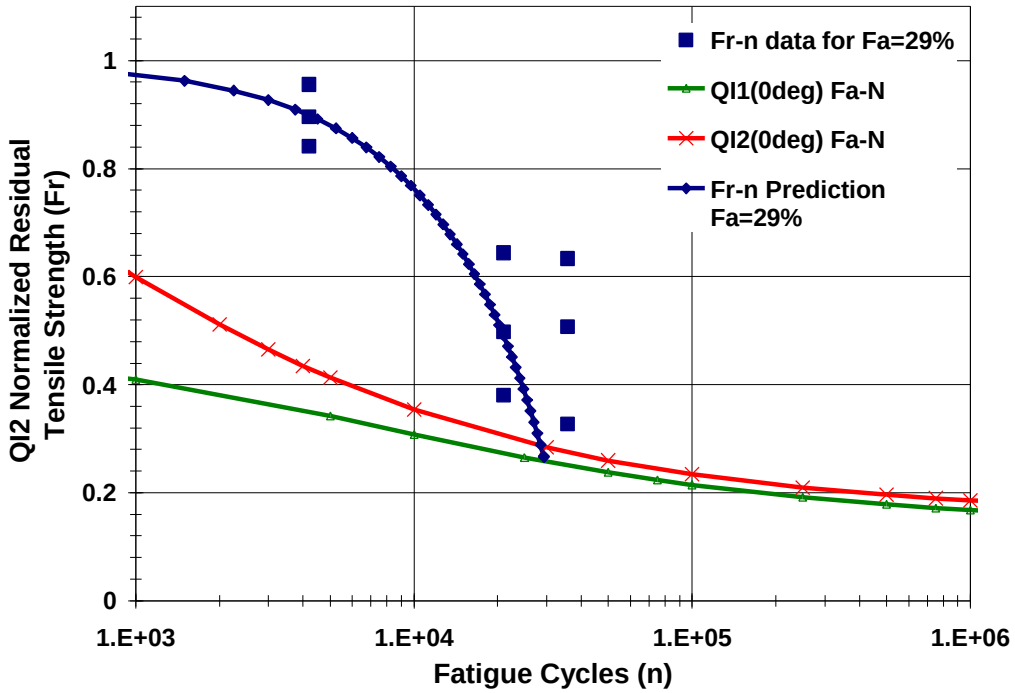

Figure 98: Residual Strength Prediction of QI2 Using Strength and Stiffness Values from Quasi-Static Data of QI2, E2 & G12 Reduction Curves Estimated from CP1 and AP Fatigue Stiffness Reduction Curves, and Normalized S-N, Fa-N, from QI1 Laminate.

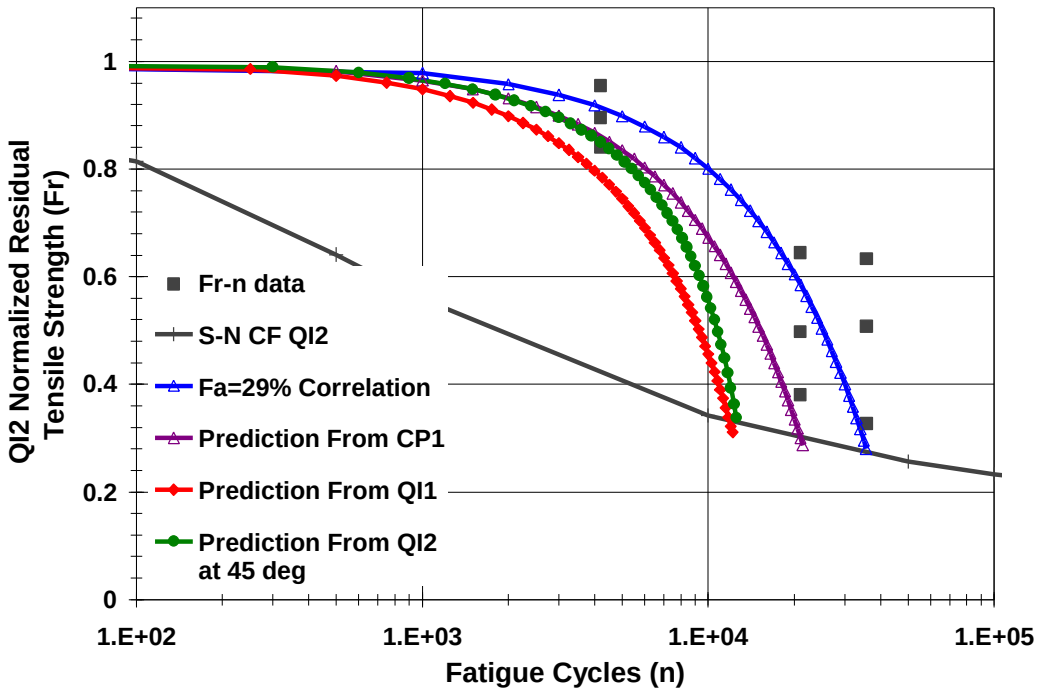

Figure 99: Residual Strength Prediction of QI2 and Stiffness Values, Fatigue Stiffness Reduction Curve, and Normalized S-N, Fa-N curve from CP1, QI1, and, QI2 at 45 ° Laminates.

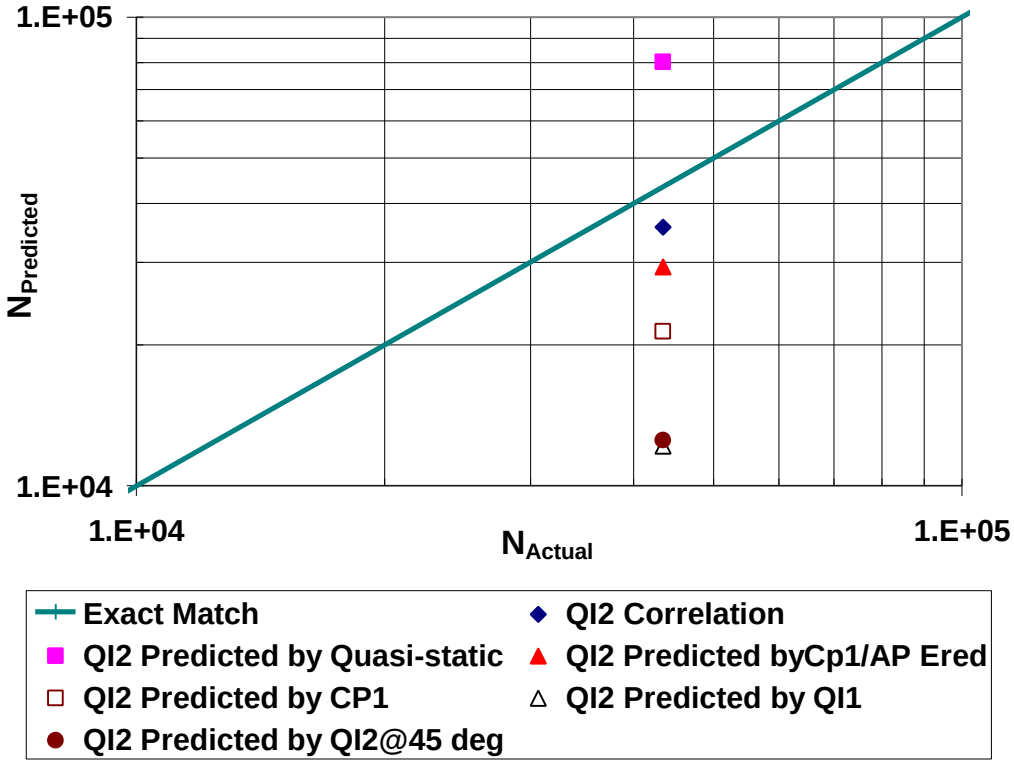

Figure 100: QI2 Life Correlation and Predictions $N_{Predicted} - N_{Actual}$

Summary of Results and Discussion: Residual Strength and Life Analysis

This form of residual strength analysis considered the composite laminate composed of a critical element and sub-critical elements. For a quasi-isotropic composite laminate, the 0° plies to the applied load are the critical element for when the 0° plies fail the laminate fails. The subcritical elements are the plies off-axis to the applied load These would be the angle and transverse plies, which suffer large reductions in stiffness through microcracking and delamination; thus, throughout the life of the laminate, the off-axis plies continually reduce in stiffness, and shift load to the critical element. Considering Equation 26, the residual strength analysis is shown to be dependent upon the critical element's S-N, the sub-critical element's stiffness reduction, the critical element's residual strength shape factor, J, and the ply level quasi-static strength and stiffness as shown in Figure 49.

To perform this analysis, the following assumptions were made.

1. Laminate stiffness reduction is assumed to occur only in the off-axis plies. The off-axis stiffness, E_2 and G_{12}, are determined from the measured laminate stiffness reduction curves. This is accomplished using simple rule-of-mixtures mechanics-of-materials approach. Assuming that stiffness of the 0° plies is constant and that transverse plies reduce in an elastic-plastic manner, the off-axis stiffness reduction may be approximated for cross-ply laminates. An added assumption for quasi-isotropic laminates is required; assuming that G_{12} can be represented in fatigue by the quasi-static stress/strain curve of the angle-ply laminate, designated AP in Table 2, off-axis stiffness reduction may be estimated. This is perhaps the least accurate assumption, since there is fiber undulation in the 0° direction, which would allow stiffness reduction of the critical element.
2. In estimating the S(0°)-N curve of the critical element from the measure laminate S-N curve, it is assumed, that in load control, the average normalized applied stress to the critical element, Fa(0°), can represent the actual situation where gradual increase in applied stress occurs due to the stiffness reduction of the off-axis plies.
3. It is assumed that the residual strength shape factor "J" obtained from laminate remaining strength testing is the same for the critical element of the laminate. This is a good assumption, since the ultimate strength of the laminate is controlled by the strength of the critical element, the 0° plies. This also has the added benefit that this method includes any processing defects and laminate effects, which lower the residual strength such as fiber undulation.
4. The "J" value for the critical element was determined from curve fits of Equation 25 to residual strength laminate data. This reveals the final assumption that the Fa(0°) of the critical element and the N fatigue life at that Fa(0°) is constant thus assuming that the average value of Fa(0°) can be used to represent applied stress on the critical element over its entire life.

Since the measured fatigue data was taken at the laminate level, the off-axis stiffness reduction and the critical element's S-N curve were estimated or extracted using the above assumptions. Utilizing rule-of-mixture mechanics-of-materials approach the stiffness of the off-axis plies was calculated per Equation 28 and corrected for Poisson's effect with classical laminate theory, CLT. Extraction of the critical element's S-N curve was necessary since fatigue testing was load controlled. The applied stress to the critical element increased as the stiffness reduced in the sub-critical elements. The critical element's S-N curve was extracted from laminate's S-N curve at each load level of the S-N curve by applying the extracted off-axis

stiffness reduction curve at that load level in CLT to the laminate. The critical element's stress increase was averaged over it entire life. This also implies another assumption, this increase in stress of the critical element over if life can be represented by this average value.

The variation in S-N curves of the vinyl ester/E-glass pultruded laminates shown in Figure 73 reveals the effects of stacking sequence, ply thickness, fiber undulation caused by transverse fiber bundle size associated with the tricot stitch effects. There is at maximum a 10% variation in normalized fatigue strength, Fa(0°) for these laminates tested. More importantly, there is only ½ decade difference of fatigue cyclic life at higher fatigue stress level Fa(0°)= 33%, but a 1-½ decade difference at fatigue stress level Fa(0°)=18%. As seen in the comparisons of S-N curves for cross-ply and woven laminates, the tested pultruded vinyl ester/E-glass laminates were lower than other published cross-ply data and approximately equal to 181style E-glass woven fabric laminate as shown in Figure 74. This lower life is in large part due to the fiber undulation created by the non-woven NCF tricot stitch E-glass fabric and the low matrix failure strain as discussed in section entitled "Physical Description of As-Pultruded Laminates". The cross-ply laminate, designated as CP2 in Table 2, is shown to have the lowest S-N curve, which can be explained by it having the largest fiber undulation in the pultruded and applied load direction. This can translate into poor predictions if the correct S-N curve is not chosen.

Fatigue stiffness reduction is the second major factor in residual strength and life prediction. It is strongly affected by stacking sequence, ply thickness, fiber, matrix and interface strength and stiffness. Microcracking and delamination are the major forms causing stiffness reduction. As Table 9 shows, there is a great variability in stiffness reduction. An estimate of the fatigue stiffness reduction from quasi-static stress/strain data is shown in Figure 54, 58, 61, and 64; they are shown to be conservative which yield shorter life predictions.

Quasi-static strength and stiffness are the third major contributor to residual strength and life predictions. As seen in Table 5 and Table 6, the strength and stiffness values for these pultruded vinyl ester/E-glass laminates vary considerably, and even the same cross-ply laminate, designated as CP1 in Table 2, when tested in the transverse direction yielded only 55% of the axial ply strength.

The final variable in the residual strength analysis is the residual strength shape factor, J, described in Equation 26, which has been determined to be constant for all currently tested laminates. Figure 74 shows the effect of more damage resistance laminates with Adams cross-ply laminates possessing a residual strength curve shape parameter of J = 7.5 while all pultruded vinyl ester/E-glass laminates were best represented by J = 0.95, exhibiting a lower damage tolerant laminate.

Four basic residual strength analyses were performed for each laminate shown in Table 10.

1. A correlation, C1, using the laminates own quasi-static strength and stiffness, extracted S-N(0°) curve, off-axis fatigue stiffness reduction curve, and the residual strength shape factor, to correlate the residual strength theory of Reifsnider [04] to the measured data.
2. The second analysis, P1, utilized the average extracted S-N(0°) curve, taken to be QI1, an off-axis fatigue stiffness reduction curve estimated from the quasi-static stress/strain curve, the average residual strength shape factor, J, and the strength and stiffness of the predicted laminate to estimate the residual strength and life of each laminate.

3. The third analysis, P2, utilized the fatigue stiffness reduction obtained from fatigue of cross-ply and angle-ply laminates to represent the stiffness reduction of E_2 and G_{12} respectively in the off-axis plies, the average S(0°)-N curve, average "J" value, and strength and stiffness of the predicted laminate.
4. The final analysis, P3, used the extracted S(0°)-N curve, the off-axis fatigue stiffness reduction curve and the quasi-static strength and stiffness of one laminate to blindly predict the other laminates without regard to the differences between the laminates.

The residual strength and life analysis has been shown to depend greatly on the quasi-static strength and stiffness, the S(0°)-N, the off-axis stiffness reduction, and the residual strength shape factor, J, chosen for the analysis. The correlation, C1, has been shown to yield the most accurate results; thus reinforcing the validity of the assumptions and methodology. This correlation would be required for qualification of products, which are fatigue sensitive. For companies which manufacture many products with the same base fiber and resin system, one thorough fatigue test program defining the S-N, fatigue stiffness reduction, and the residual strength curves, would suffice for all like laminates fabricated in the same manner. Only stress analysis due to the geometry and loading changes would be required; repeatedly, utilizing the fatigue data to predict residual strength and life for new products. If there are changes in the laminate stacking sequence, simple quasi-static tests may be performed to determine an approximate off-axis stiffness reduction and to compare the quasi-static strength and stiffness to the originally laminate which was fatigue tested. If base materials change such as the fiber or resin type or the type of preprocessing that the fiber undergoes such as stitching, this would required quasi-static evaluation and limited fatigue testing to determine variation from original laminate. In addition, trade studies and preliminary designs may not require correlation but predictions from similar laminate fatigue data may be acceptable. The analysis P1 through P3 from Table 10 would be used to satisfy the requirements for the above scenarios.

The most accurate prediction was the prediction P2 from Table 10. The quasi-static strength and stiffness of the laminate being predicted, the average S(0°)-N, and the off-axis fatigue stiffness reduction obtained from extraction of fatigue data of cross-ply and angle-ply laminates which represented the stiffness reduction of E_2 and G_{12}, respectively, and the average residual strength shape factor, J, were used to predict the laminate residual strength behavior. P3 prediction was generally the worst prediction since the quasi-static strength and stiffness, the S-N curve of the 0° plies and the off-axis stiffness reduction of one laminate were applied to another laminate without regard to the type of laminate being predicted. The off-axis stiffness reduction has been shown to be greatly dependent upon the stacking sequence, ply thickness, and matrix strength and stiffness for quasi-isotropic laminates as can be seen shown in Table 9. The S(0°)-N curve and the quasi-static strength and stiffness are strongly dependent upon the fiber undulation as shown in Table 5, Table 6, and Figure 73. Prediction, P4 from Table 10, generally, over estimated the stiffness reduction thus the predicted life was lower except for the laminates, which had lower S(0°)-N curves than the average QI1 S(0°)-N curve used. Most all analysis were shown to better predict low cycle/high stress but deviated when predicting high cycle/low stress conditions; the fatigue life taken at the fatigue stress level from the S(0°)-N curve has been shown to range over 1.5 decades of cyclic life when comparing all laminates' S(0°)-N curves tested from this research as shown in Figure 73.

Conclusions: Fatigue Analysis of CRTM Pultruded Vinyl Ester/E-Glass Laminates

Fatigue of continuous fiber reinforced polymer (CFRP) laminated composites has a variety of failure mechanisms which include microcracking in the plies off-axis to load, delamination between plies, matrix microcracking perpendicular to the load in the on-axis plies, and ultimate fiber failure of the plies parallel to the load application. The residual strength and life predictions for laminated composites are shown to depend strongly upon four parameters:

- the quasi-static strength and stiffness,
- the S-N curve,
- the residual strength curve shape, and
- the stiffness reduction of the laminate in question.

The quasi-static strength and stiffness, S-N, and residual strength are functions of the critical element of the laminate, which are the 0° plies to the applied load. The critical element is the portion of the laminate, which when fails, the laminate will fail. When failure occurs in the subcritical elements, the ±45° and 90° plies to the applied load, ultimate failure does not occur. As these subcritical elements degrade in the form of microcracking and delamination their stiffness is reduced and the applied load is shifted continually higher to the 0° critical element. The reduction of the laminate stiffness during fatigue occurs mainly in the subcritical element degradation, which is depended upon fiber and matrix properties, cure shrinkage induced residual strain, ply thickness, and ply stacking sequence. Laminate stiffness reduction was obtained from strain-cycle data from the S-N evaluation, and subcritical element or off-axis stiffness reduction was extracted using a simple mechanics-of-materials approach.

Quasi-static strength and stiffness, the S-N curve, and the residual strength curve shape were compared with values found in literature to determine the ranking of these CRTM pultruded vinyl ester/E-glass non-woven NCF fabric laminated composites. The first of these parameters, the quasi-static strength and stiffness are shown in Figure 42 and were found to mainly depend upon the brittle nature of the matrix and the fiber undulation induced by the non-woven tricot stitched fabric. Literature has shown epoxy/E-glass laminates with failure strains from 2.1 to 2.9% and polyester laminates ranging from 1.3 to 2.3%. This vinyl ester matrix had 1.9% failure strain, and the specimens loaded along the pultrusion direction had 1.91% to 2.08% average ultimate failure strain. Specimens loaded transverse to the pultrusion direction had average ultimate failure strain as low as 1.29%. Fiber undulation was responsible for this 10% variation in strain/strength for laminates loaded along the pultrusion axis and when loaded transverse to the pultrusion axis, a maximum of 44% reduction in strain/strength compared with axial values. The tricot stitch of the non-woven NCF E-glass fabric gathered the axial fiber parallel to the pultrusion axis in bundles leaving gaps of approximately ¼ to ½ the fiber bundle width between axial fiber bundles as shown in Figure 6. The tricot stitch also gathered the fiber transverse to the pultrusion axis with approximately a gap one-tenth the width of the transverse fiber bundle. The fiber undulation in the plies off-axis to the pultrusion had substantial out-of-plane fiber undulation while the axial plies aligned to the pultrusion direction had only slight undulation.

The S-N performance and the residual strength performance were also compared with values found in literature. S-N curves of these CRTM pultruded laminates were found to be much lower than unidirectional and cross-ply laminates, and nearly equivalent with woven fabric epoxy laminates as seen in Figure 73 and Figure 74. Residual strength curves of various epoxy fiber composites are shown in Figure 48, revealing that E-glass is less damage resistant than

Kevlar, and Carbon fiber composites. Residual strength from these pultruded vinyl ester laminates was compared with values found in literature as shown in Figure 76. This reveals that these pultruded laminates are even less damage resistant than the epoxy E-glass laminates found in literature.

Strength and stiffness, S-N performance, and residual strength curve shape of the critical element and the off-axis fatigue stiffness reduction of the subcritical elements were extracted from measured laminate data. From these extracted properties, a correlation and various predictions, based upon Reifsnider's residual strength and life theory outlined in Figure 49, were made to determine the best method to predict residual strength and life of these pultruded vinyl ester E-glass laminates. The best predictions were found to use:

- the quasi-static strength and stiffness from the laminate being predicted,
- the average S-N curve,
- the average residual strength curve shape factor, and
- the off-axis fatigue stiffness reduction separated into E_2 and G_{12} taken from the fatigue data of the cross-ply and angle-ply laminates respectively.

The worst predictions resulted from the blind application of one laminate's quasi-static and fatigue properties to predict another.

Future Work

Future research should included:

- Fatigue evaluation of pultruded laminates loaded transverse to pultrusion axis.
- Analytical or FEA modeling the effect of fiber undulation, and matrix properties including residual stresses on the strength and stiffness of the pultruded laminates. This will allow sensitivity studies to determine the optimized design of the pultruded laminates.

REFERENCES

[01] Wilson Brian A., Pultrusion, Handbook of Composites, Peters, S. T., Editor, 1998. 1

[02] Lesko, J., Cousins, T., Case S., Gomez, J., and Massarelli, P., Assessing Durability of Composite Structural Systems Through Laboratory & Field Evaluations of the Tom's Creek Bridge, selected for presentation at the Transportation Research Board, January 1999. 3

[03] Mandell, J. F., Chapter 4: Fatigue Behavior of Fibre-Resin Composites, Developments in Reinforced Plastics-2, Pritchard, G., Ed., Applied Science Publishers, London, 1982, p .67-107. 4

[04] Reifsnider, Kenneth L., Durability and Damage Tolerance: Testing, Simulation, and Other Virtual Realities, Composite Materials: Testing and Design, Thirteenth Volume, ASTM STP 1242, Hooper, S. J., Ed., American Society for Testing and Materials, 1997, pp. 45-59. 5

[05] Sumerak, Joseph E., the Pultrusion Process for Continuous automated Manufacture of Engineered composite Profiles, Composites Engineering Handbook, Mallick P. K., 1997. 5

[06] Gibson Ronald F., Principles of Composite Material Mechanics, McGraw-Hill, Inc., 1994. 6

[07] Chou Tsu-Wei, Microstructural Design of Fiber Composites, Cambridge University Press, 1992. 6

[08] Hopkins Dale A. and Chamis Christos C., A Unique Set of Micromechanics Equations for High-Temperature Metal Matrix Composites, ASTM STP 964, 1988, pp.159-176. 7

[09] Chamis Christos C., Simplified Composite Micromechanics for Predicting Microstresses, 41st Annual Conf. Reinforced Plastics/Composites Inst., SPI, Jan. 27-31, 1986. 7

[10] Reifsnider, K., and Case, S., Strength and Durability of Composite Materials Class Notes, Virginia Polytechnic and State University, 1997. 7

[11] Nielsen, Lawrence E. and Landel, Robert F., Mechanical Properties of Polymers and Composites, 2nd Edition, 1994. 8

[12] Jones F. R., Micromechanics and Properties of Fibre Composites, Middleton D. H., Editor, Composite Materials in Aircraft Structures, 1990. 8

[13] Manders Peter W. and Chou Tsu-Wei, Variability of Carbon and Glass Fibers, and Strength of Aligned Composites, Journal of Reinforced Plastics and Composites, Vol. 2 , Jan 1983. 8

[14] Swanson, Stephen R., Chapter 23: Design Methodology and Practice, Ed. Mallick, P. K., Composite Engineering Handbook,1997. 10

[15] Zweben C., Size Effect in Composite Materials and Structures: Basic Concepts and Design Considerations, NASA Workshop and Scaling Effects in Composite Materials and Structures, NASA Langley Research Center, Hampton, VA, Nov. 15-16, 1993/ 10

[16] Cohen, D., Application of Reliability and Fiber Probabilistic Strength Distribution Concepts to Composite Vessel Burst Strength Design, Journal of Composite. Materials. 26:1984-2014, 1992. 10

[17] Klett, M. W. and Martine E. A., Mechanical Property Relationships of Pultruded Fiber Glass Reinforced Plastic (FRP) Unidirectional Composites, Advanced Composite Materials: New Developments and Applications Conf. Proc., Detroit, Michigan USA, Sept. 30, 1991. 10

[18] Saidpour, S. H. and Richardson M. O. W., Glass Fibre Coating for Optimum Mechanical Properties of Vinyl Ester Composites Part A, Composites, 28A, 1997, pp. 971-975. 10

[19] Hahn, H.T. and Tsai, S. W., On the Behavior of Composite Laminates After Initial Failures, Journal of Composites, 1975, pp. 296-304. 11

[20] Bailey, J. E. and Parvizi A., On Fibre Debonding Effects and the Mechanism of Transverse-Ply Failure in Cross-Ply Laminates of Glass Fibre/Thermoset Composites, Journal of Materials Science, Vol. 16, 1981, pp. 649-659. 11

[21] Bailey, J. E., Curtis, P. T., and Parvizi A., On the Transverse Cracking and Longitudinal Splitting Behaviour of Glass and Carbon Fibre Reinforced Epoxy Cross Ply Laminates and the Effects of Poisson and Thermally Generated Strain, Proc. Royal Society of London, Series A, 366, 1979, pp. 599-623. 11

[22] Clements, L. L., and Moore, R. L., Composites Properties for E-glass Fibres in a Room Temperature Curable Epoxy Matrix, Composites, April, 1978, pp.93-99. 11

[23] Mooney, Rodney D. and McGarry Frederick J., Resin-Glass bond Study, Proceedings from Society of the Plastics Industry 1959, Vol. 14, Section 12-E. 11

[24] Adams Donald F. and Doner Douglas R., Transverse Normal Loading of a Unidirectional Composite, Journal of Composite Materials,1967, pp.152-64. 13

[25] Naik, Rajiv A. and Crews John H. Jr., Micromechanical Analysis of Fiber-Matrix Interface Stresses Under Thermomechanical Loadings, ASTM STP 1206, Camponeschi, E. T. Jr. ,Editor ,1993. 14

[26] Jones, F. R. , Wheatley A. R. and Bailey J. E., The Effect of Thermal Strains on the Microcracking and Stress Corrosion Behaviour of GRP, Composite Structures 1st International Conference, 1981, pp.415-428. 14
[27] Garrett K. W. and Bailey J. E., Multiple Transverse Fracture in 90 degree cross-ply Laminates of a Glass Fibre-Reinforced Polyester, Journal of Materials Science, Vol.12, 1977, pp.157-168. 15
[28] Highsmith Alton, L., Stinchcomb Wayne W., and Reifsnider Kenneth L., Stiffness Reduction Resulting From Transverse Cracking in Fiber-Reinfoced Composite Laminates, Thesis, ESM, Virginia Polytechnic Institute and State University,1981. 15
[29] Nairn J. A. and Hu S., Chapter 6 ,Matrix Microcracking, Editor, Talreja, R., Damage Mechanics of Composite Materials, 1994. 15
[30] Herakovich Carl T., Mechanics of Fibrous Composites, John Wiley and Sons, Inc, 1998. 15
[31] Swanson S. R., Biaxial Failure Criteria for Toughened Resin Carbon/Epoxy Laminates, Proc. Am. Soc. for Composites 7th Tech. Conf. on Composite Materials, Pennsylvania State Univ., Oct. 13-15, 1992, pp. 1075-1083. 15
[32] Swanson, S.R., Messick, M. J., and Tian, Z., Journal of Composite Materials, Vol. 21, July, 1987, pp. 619-630. 16
[33] Hart-Smith L. J., A Re-Examination of the Analysis of In-Plane Matrix Failures in Fibrous Composite Laminates, Composites Science and Technology, 56, 1997, pp. 107-121. 16
[34] Hart-Smith, L. J., The Role of Biaxial stresses in discrimination Between Meaningful and Illusory Composite Failure Theories, Composite Structures, 25, 1993, pp. 3-20. 16
[35] Hart-Smith, L. J., A Scientific Approach to Composite Laminate Strength Prediction, Composite Materials: Testing and Design, Tenth Volume, ASTM STP 1120, Grimes, Glenn, Ed., American Society for Testing and Materials, Philadelphia, 1992, pp. 142-169. 16
[36] Burts, Ellen, and Verghese, Nakhil, Non-published Research, Virginia Polytechnic Institute and State University ,1998. 31
[37] Bibo, G. A., Hogg. P. J., and Kemp M., Mechanical Characterisation of Glass- and Carbon-Fibre-Reinforced Composites Made with Non-Crimp Fabrics, Composite Science and Technology, 57, 1997, pp.1221-1241. 48
[38] Mallick P. K., Fiber-Reinforced Composites Materials, Manufacturing, and, Design, Marcel Dekker, Inc., 1993. 52
[39] Rotem Assa and Hashin Zvi, Fatigue Failure of Angle Ply Laminates, AIAA Journal, Vol. 14, no. 7, p. 868-872. 54
[40] Lorenzo, Luis and Hahn, H. Thomas, Fatigue Failure Mechanisms in Unidirectional Composites, Composite Materials: Fatigue and Fracture, ASTM STP 907, 1984, pp.210-232. 54
[41] Kim, Hong C. and Ebert Lynn J, Axial Fatigue Failure Sequence and Mechanisms in Unidirectional Fiberglas Composites, Journal of Composite Materials, Vol. 12, April, 1978. 55
[42] Agarwal B. D., Dally James W., Prediction of Low-Cycle Fatigue Behavior of GRRP: an Experimental Approach, Journal of Materials Science, Vol. 10, 1975, p193-199. 56
[43] Mandell John F. and Meier Urs, Effects of stress Ratio, Frequency, and Loading Time on the Tensile Fatigue of Glass-Reinforced Epoxy, ASTM STP 813, Long Term Behavior of Composites, O'Brien T. K., Ed.,1983, pp.55-77. 56
[44] Shokrieh M. M. and Lessard L. B., Multiaxial Fatigue Behaviour of Unidirectional Plies Based on Uniaxial Fatigue Experiments-I. Modeling, International Journal of Fatigue, Vol. 19, No.3, pp.201-207,1997. 58
[45] Adams, T., Dickson R. F., Jones, C. J., Reiter H., and Harris B., A Power Law Fatigue Damage Model for Fibre-Reinforced Plastic Laminates, Proceedings of the Institute of Mechanical Engineers Part C: Mechanical Engineering Science, Vol. 200, No. C3, 1986. 59
[46] Case, S. W., Lesko, J. J., Cousins, T. E., Development of a Life Prediction Scheme for the Assessment of Fatigue Performance of Composite Infrastructures, CDCC'98, First International Conference on Durability of Composites for Construction (Delta Hotel, Sherbrooke, Quebec, Canada), August 5-7, 1998. 59
[47] Broutman, L. J., and Sahu, S., A New Theory to Predict Cumulative Fatigue Damage in Fiberglass Reinforced Plastics, Composite Materials: Testing and Design (Second Conference), ASTM STP 497, American Society for testing and Materials, 1972, pp. 170-188. 61
[48] Morrell, Melissa, Verghese, N., Phifer, S., Haramis J., and Lesko, J., Correlation of Crack density and Residual Strength and Stiffness of Saturated Vinyl Ester E-Glass Composite, Internal Document, ESM, Material Response Group, Summer, 1998. 77

Vita : Stephan Paul Phifer

The author graduated from Tennessee Technological University with a B.S. in Mechanical Engineering degree in 1986; during which he co-oped at E. I. DuPont's x-ray manufacturing plant in Brevard, North Carolina, where he worked in the Finishing Area where the film was slit, inspected, chopped, and packaged. He worked from 1986 to 1996 with Texas Instruments, Defense Systems, Antenna and Nonmetallics Department where he designed composite products and processes for military applications. Autoclave molding, resin transfer molding, RTM, compression molding, prototyping, preform development, bonding and composite machining were areas of greatest effort. He is currently seeking a Masters and Ph.D. in Engineering Science and Mechanics Department at Virginia Polytechnic Institute and State University.